Stress-Induced Transcription Factors and Their Role in RNA Disruption in Ovarian Cancer Cells

By

Melissa Kay

A thesis submitted in partial fulfillment
of the requirements for the degree of
Master of Science (MSc) in Biology

Presented to the School of Graduate Studies
Laurentian University
Sudbury, Ontario, Canada

THESIS DEFENCE COMMITTEE/COMITÉ DE SOUTENANCE DE THÈSE
Laurentian Université/Université Laurentienne
Office of Graduate Studies/Bureau des études supérieures

Title of Thesis Titre de la thèse	Stress-Induced Transcription Factors and Their Role in RNA Disruption in Ovarian Cancer Cells
Name of Candidate Nom du candidat	Kay, Melissa Marie
Degree Diplôme	Master of Science
Department/Program Département/Programme	Biology
Date of Defence Date de la soutenance	mai 20, 2021

APPROVED/APPROUVÉ

Thesis Examiners/Examinateurs de thèse:

Dr. Amadeo M. Parissenti
(Co-Supervisor/Co-directeur(trice) de thèse)

Dr. Tom Kovala
(Co-Supervisor/Co-directeur(trice) de thèse)

Dr. Kabwe Nkongolo
(Committee member/Membre du comité)

Dr. Carita Lanner
(Committee member/Membre du comité)

Approved for the Office of Graduate Studies
Approuvé pour le Bureau des études supérieures
Dr. Tammy Eger
Madame Tammy Eger
VP Research
Vice-rectrice à la recherche

Dr. Rachid Mazroui VP Research
(External Examiner/Examinateur externe)

ACCESSIBILITY CLAUSE AND PERMISSION TO USE

Acknowledgements

I would like to start off by giving my largest thanks to Dr. Amadeo Parissenti and Dr. Tom Kovala for co-supervising me on this project. An equally special thanks to Dr. Carita Lanner for working closely and providing guidance throughout the project as well. I would also like to extend a thanks to Dr. Kabwe Nkongolo, a member of my supervisory committee. Thank you to Laurentian University, Health Sciences North Research Institute, Northern Cancer Foundation, Northern Ontario School of Medicine and Rna Diagnostics Inc for providing the space, tools, and funding necessary to complete this project. I would like to extend a special thanks to Dr. Baoqing Guo, Dr. Twinkle Masilamani, and Dr. Renee St. Onge for their help with lab skills, moral support, and statistics. I would like to take this opportunity to thank Avery Newman-Simmons and Carly Zulich for their work and contribution to this project. As well, I would like to thank the other Masters students in the Parissenti research group for our time spent in the lab, it was nice knowing we were all in it together. Last but certainly not least, I would like to thank some of the friends and family who I could not have done this without. I want to thank my parents for their continued and unending support in whatever I pursue even if they do not understand what it is that I do exactly. I could not have done it without my own personal wake-up call service from my mom on those early mornings. I would like to thank some of my fellow M.Sc. Biology friends Katie Mitchell, Jade Dawson, Saskia Hart, and Robyn Rumney for being there when the days were tough, and when times were good. I would like to thank Mandy Durkin for her professional support, scientific direction, and our coffee fueled friendship.

Abstract

When cancer patients respond positively to chemotherapy treatment, their tumour ribosomal RNA (rRNA) is degraded, which has been termed RNA Disruption. The RNA disruption assay (RDA) has been developed to quantify RNA disruption as an RNA disruption index (RDI), which is the mass ratio of degraded to intact rRNAs. The underlying mechanism(s) for RNA disruption remain unclear. RNA disruption occurs *in vivo* and *in vitro* in response to various cellular stressors, including many structurally and mechanistically distinct chemotherapy drugs. Therefore, there must be a common pathway or mechanism occurring in each of these cases. Transcription factors are good upstream targets to begin elucidating a potential pathway or mechanism for RNA disruption, since they are major regulators of gene expression. The goal of this study was to: (i) identify transcription factors that are activated in response to treatment with agents known to induce RNA disruption, (ii) create enriched cytoplasmic and nuclear extracts from treated and untreated A2780 ovarian tumour cells, (iii) assess the relationship between stress-induced RNA disruption and activation/altered localization of stress-induced transcription factors in relation to RNA disruption. A2780 cells were treated with docetaxel or left untreated as a control for 8 hours, and nuclear extracts from these cells were prepared. The activation of a wide variety of known transcription factors in these extracts were analyzed using transcription factor activation profiling plate arrays. The activation was measured based on their ability to bind specific DNA sequences resulting in luminescence. Using a variety of criteria ranging from statistical significance to relevance to stress in the literature, a few transcription factors of interest were chosen: TFEB, TFE3, Nrf2, and YY1. Cytoplasmic and nuclear extracts were then made from A2780 cells after treatment with doxorubicin, docetaxel, thapsigargin, and starvation for 0, 2, 16, or 24 hours. The amount of RNA disruption was then assessed by RDA 72 hours

after treatment with the same stressors. Treatment with doxorubicin, docetaxel, thapsigargin, and starvation resulted in significant change in RDI compared to control cells. Nrf2 was found localized in the nucleus with or without treatment. Thus, Nrf2 appeared to be constitutively activated in A2780 ovarian cancer cells, perhaps due to its role in cell survival. This study corroborates the results of another study (Investigating the Relationship Between the Activation of Transcription Factor Nrf-2 and Ribosomal RNA Degradation Upon Exposure to Various Cellular Stressors, Carly Zulich, 2020) and eliminates Nrf2 as a potential transcription factor associated with the activation of RNA disruption. Contrary to expected findings, there appear to be higher levels of TFEB and TFE3 in both the cytoplasm and nucleus of the untreated and DMSO vehicle control than cells treated with chemotherapy or other cellular stressors. Future studies could investigate the potential of other transcription factors as targets for elucidating the mechanism(s) for RNA disruption.

Key Words

Transcription Factor, Ovarian cancer, YY1, TFEB, TFE3, Nrf2, RNA Disruption, Docetaxel, Doxorubicin, Thapsigargin, Starvation

Abbreviations

i. Transcription Factors

AP-1	Activator protein 1 (JUN/FOS)
AP-2	Activator protein 2
AP-3	AP3 protein
AP-4	AP4 protein
AR	Androgen receptor
ATF2	Activating transcription factor 2
ATF3	Activating transcription factor 3
ATF4	Activating transcription factor 4
ATF6	Activating transcription factor 6
Brn-3	Brain-specific homeobox (POU4F1)
CAR	Constitutive active/androstane receptor
CBF/NFY	CCAAT-binding factor/nuclear transcription factor Y
CDP	CCAAT displacement protein
C/EBP	CCAAT/enhancer-binding proteins
CHOP	C/EBP Homologous protein
COUP-TF	Chicken Ovalbumin Upstream Promoter (NR2F2)
CREB	cAMP responsive element binding protein 1
E2F1	E2 promoter binding factor 1
EGR	Early growth response
ELK	ETS domain-containing protein Elk-1
ER	Estrogen receptor
Ets	v-ets erythroblastosis virus E26 oncogene homolog 1
FAST-1	Forkhead box H1

FOXA1	Forkhead box A1
FoxC1	Forkhead box C1
FOXD3	Forkhead box D3
FOXG1	Forkhead box G1
FOXO1	Forkhead box O1
FOXO3	Forkhead box O3
FREAC2	Forkhead-related activator 2
GAS/ISR	IFN-stimulated response element
GATA	GATA-binding family
Gfi-1	Growth factor independent 1 transcription
Gli-1	GLI zinc finger transcription factor
GR/PR	Glucocorticoid receptor/Progesterone receptor
HEN	Helix-loop-helix protein
HIF	Hypoxia-Inducible Factor
HNF-1	Hepatocyte nuclear factor 1
HNF4	Hepatocyte nuclear factor 4
HOX4C	HOX4C homeobox
HoxA-5	Homeobox A5
HSF	Heat shock transcription factor 1
IRF	Interferon regulatory factor
KLF4	Kruppel-like factor 4
MEF1	Myocyte enhancer factor 1
MEF2	Myocyte enhancer factor 2
Myb	V-myb myeloblastosis viral oncogene homolog
Myc-Ma	V-myc myelocytomatosis viral oncogene homolog
MyoD	Myogenic differentiation 1 protein
MZF	Myeloid zinc finger
NF-1	Nuclear factor 1
NF-E2	Nuclear factor-erythroid 2

NFAT	Nuclear factor of activated T-cells
NFκB	Nuclear factor kappa B
Nkx2-5	Homeobox protein Nkx-2.5
Nkx3-5	Homeobox protein Nkx 3.5
NRF1	Nuclear respiratory factor 1
NRF2/ARE	Nuclear factor erythroid 2-related factor 2/antioxidant response element
Oct-1	Octamer-binding transcription factor 1
OCT4	Octamer-binding transcription factor 4
p53	Tumor protein p53
Pax-5	Paired box 5
Pax2	Pair box-2 protein
Pax3	Pair box-3 protein
Pax8	Pair box-8 protein
Pbx-1	Pre-B cell leukemia transcription factor 1
PGC-1α	Peroxisome proliferator-activated receptor gamma coactivator 1-alpha
Pit	Pituitary specific transcription factor 1
PLAG1	Pleiomorphic adenoma gene 1
PIT1	POU class 1 homeobox 1
PPAR	Peroxisome proliferator-activated receptor
Prox1	Prospero homeobox 1
PXR	Pregnane X receptor
Rb	Retinoblastoma control element
RUNX	Runt-related transcription factor 1
ROR	Retinoic acid receptor-related orphan
RXR	Retinoid X receptor
SATB	Special AT-Rich sequence-binding protein 1
SF-1	Steroidogenic factor 1

SMAD	Sma (c. elegans) or Mad (mothers against decapentaplegic) (drosophila)
SMUC	Snail-related transcription factor Smuc Snail-related gene from murine skeletal muscle cells
Snail	Snail 1 zinc finger protein
SOX2	Sex Determining Region Y (SRY)-Box 2
SOX9	SRY-Box transcription factor 9
SOX18	SRY-Box transcription factor 18
Sp1	Specificity protein 1
SREBP1	Sterol regulatory element-binding protein 1
SRF	Serum response factor
SRY	Sex determining region Y
STAT1	Signal transducer and activator of transcription 1
STAT3	Signal transducer and activator of transcription 3
STAT4	Signal transducer and activator of transcription 4
STAT5	Signal transducer and activator of transcription 5
STAT6	Signal transducer and activator of transcription 6
TCF/LEF	T-cell factor/lymphoid enhancer factor
TFIID	TATA box binding protein
TFE3	Transcription factor binding to IGHM
TFEB	Transcription factor EB
TR	Thyroid hormone receptor
USF-1	Upstream transcription factor 1
VDR	Vitamin D receptor
WT1	Wilms tumor 1 suppressor protein 1
XBP1	X-box binding protein 1
YY1	Yin Yang 1

ii. **Other**

AAV	Adeno-associated virus
ABC	ATP Binding Cassette
ARE	Antioxidant Response Element
ATG	Autophagy related proteins
ATP	Adenosine Triphosphate
Bcl-2	B-cell lymphoma 2
bHLH	Basic Helix-Loop-Helix
bHLH-LZ	bHLH/Leucine Zipper
bZIP	Basic Leucine Zipper
CLEAR	Coordinated Lysosomal Expression and Regulation
CNC	Cap 'n' Collar
CRE	cAMP Response Element
Cul3	Cullin-3
DFS	Disease-Free Survival
DMSO	Dimethyl Sulfoxide
DOX	Doxorubicin
DXL	Docetaxel
eIF2α	Eukaryotic Initiation Factor 2 α
eIF3f	Eukaryotic initiation factor 3 subunit f
ER	Endoplasmic Reticulum
ERAD	ER-Associated Degradation
ERK2	Extracellular Signal-Regulated Kinase
ERSE	ER Stress response element
ETC	Electron Transport Chain
Fadd	Fas-associated death domain
FBS	Fetal Bovine Serum
GAPDH	Glyceraldehyde 3-Phosphate Dehydrogenase
GCLC	Glutamate-Cysteine Ligase Catalytic

GST	Glutathione S-Transferase
hnRNPk	Heterogeneous nuclear ribonucleoprotein K
HRP	Horseradish Peroxidase
IRE1α	Inositol Requiring Enzyme 1 α
IBS	Irritable bowel syndrome
Keap1	Kelch-like ECH-associated protein 1
MDR	Multi Drug Resistance
MEF	Mouse Embryonic Fibroblasts
MiT/TFE	Micropthalmia-transcription factor E
MPTP	Mitochondrial Permeability Transition Pore
MRP	Multi-Drug Resistance-Associated Protein
mtDNA	Mitochondrial DNA
mTOR	Mammalian Target of Rapamycin
NQO1	NADPH-quinone oxidoreductase
NHR	Nuclear Hormone Receptor
NRD	Non-Functional RNA Decay
PARP	Poly ADP-Ribose Polymerase
pCR	Pathological Complete Response
PE	Phosphatidylethanolamine
PERK	Double Stranded RNA dependent Protein Kinase (PKR)-like ER kinase
PBS	Phosphate Buffer Saline
Pgp	P-glycoprotein
Rag	Ras-related GTP-binding
Rbx	RING-box-based
RDA	RNA Disruption Assay
RDI	RNA Disruption Index
RIN	RNA Integrity Number
RLU	Relative Light Unit
RNA	Ribonucleic Acid

ROS	Reactive Oxygen Species
rRNA	Ribosomal RNA
S1P	Serine Protease Site-1
S2P	Metalloprotease site-2 protease
SE	Standard Error
SERCA	Sarco-ER Ca^{2+}-ATPase
sMAF	Small masculoaponeurotic fibrosarcoma
SRE	Sterol Regulatory Element
TAX	Paclitaxel
TNF	Tumor Necrosis Factor
Tpg	Thapsigargin
TRAIL	TNF-related apoptosis inducing ligand
TRADD	TNF-receptor-associated death domain
uORF	Upstream open reading frame
UPR	Unfolded Protein Response
VEGF	Vascular Endothelial Growth Factor

Table of Contents

List of Figures

List of Tables

1.0 Introduction

1.1 Cancer

Cancer is the leading cause of death in Canada and it has been estimated that roughly half of all Canadians will develop cancer in their lifetime [1]. It is expected that there will be 225,800 new cases of diagnosed cancer, and 83,300 cancer-related deaths in Canada in 2020 [1]. For these reasons, cancer puts a significant burden on the health care system. The cost of providing healthcare for cancer related issues more than doubled between 2005 and 2012, from $2.9 billion to $7.5 billion respectively [1]. In addition, significant amounts of funding are applied to cancer research to find new treatments and to better understand the biology of cancer. There remain some cancers that have not slowed in progression of number of cases and deaths, such as pancreatic cancer, which shows that continued research is required [1].

There are several hallmarks that cancer cells have in common, which account for their diversity and complexity. These traits set apart normal cells from tumorigenic cells. These hallmarks include resisting cell death, evading growth suppressors, sustaining proliferative signaling, inducing angiogenesis, activating invasion and metastasis, and enabling replicative immortality [2]. In addition, avoiding immune destruction, genomic instability, tumor-promoting inflammation, and deregulated cellular energetics are also hallmarks of tumour cells [2].

1.1.1 Ovarian Cancer

It is estimated there will be 3,100 new cases of ovarian cancer and 1,950 deaths caused by ovarian cancer in Canada in 2020 [1]. Despite the low incidence rates of ovarian cancer, it has the highest mortality rate among cancers of the reproductive system [3]. In the United States, the leading cause of death caused by gynecologic malignancies is epithelial ovarian cancer [4]. A

large factor in the rate of mortality, as well as 5-year survival, is the stage of cancer at diagnosis. Women with advanced-stage ovarian cancer often die within 5 years due to chemoresistant recurrent disease [4]. Ovarian cancer has very few early symptoms and patients can be asymptomatic early in the disease [5]. Symptoms can be mistaken for irritable bowel syndrome, and include pelvic pain, abdominal pain, bloating, loss of appetite, diarrhea, vomiting, fatigue, burning during urination, and back pain [6]. Unfortunately, many of these symptoms are non-specific, which often leads to a misdiagnosis or a late-stage diagnosis [7]. Due to the common late-stage diagnosis of ovarian cancer, it has been named the "silent killer" [3, 7, 8]. The cancer is often metastatic at the time of diagnosis, which is generally late-stage [4, 9]. The 5-year survival for advanced disease is between 20 and 25%, with an initial response to chemotherapy, but recurrence and resistance is common [4, 10-12]. Nevertheless, ovarian cancer can be quite easy to treat when found and diagnosed in stage I or II, since the tumor is confined to the ovary, with a 5-year survival of 90% [7-9, 12]. However, early-stage diagnosis only accounts for 20% of ovarian cancer diagnoses [8-10]. In stage 1, the cancer is restricted to the ovaries, stage 2 the cancer has metastasized to the pelvic organs, stage 3 the cancer has metastasized to the abdomen, and stage 4 is when the cancer has left the peritoneal cavity [8].

1.1.2 Treatment

The first steps taken when ovarian cancer is suspected is an exploratory laparotomy in order to confirm the histology, stage of tumor, and to surgically remove tumour (debulk) [6, 12]. Tumor debulking or cytoreduction has been shown to be advantageous to survival in advanced-stage disease since as early as 1934 [6]. Effective cytoreduction is defined as residual disease less than 1 cm or no visible residual disease [6]. To this day, cytoreduction remains a staple in

ovarian cancer treatment, which is not as common in other cancers [8, 11-13]. Unlike malignancies in other cancers, cytoreduction of malignant ovarian cancer has been shown to improve patient survival [13].

The systemic treatment of ovarian cancer depends on the stage and grade of the tumor. Adjuvant chemotherapy is not recommended in patients with well-differentiated, low-grade, stage I disease, since cytoreduction is sufficient in more than 90% of patients who achieve long-term survival (>10 years) [5, 6, 8, 12, 13]. The original chemotherapy treatment plan involved drugs termed alkylating agents; however, the use of platinum-based chemotherapy drugs was introduced in 1976, cisplatin-based combination treatment throughout 1984 and 1986, and the addition of the taxane paclitaxel in 1993 [12, 14]. Currently, high-grade stage I and stage II tumors are treated with cisplatin or carboplatin [5, 6]. Up to 60% of early-stage disease will not have a recurrence if properly monitored, but there is a lack of biomarkers available to identify patients who will benefit from chemotherapy [6, 13].

Patients who do not respond to initial treatment or have recurrence after response to initial treatment are eligible for a second-line of treatment [5, 6]. Recurrence can be measured by an ovarian tumour cell antigen found in the serum of ovarian cancer patients (CA-125), which usually appears in the serum 3-4 months before clinical presentation [5]. The length of disease-free time after treatment with platinating agents can categorize the patients into platinum-sensitive and platinum-resistant disease [5, 11, 12]. Platinum-resistant disease is defined as recurrence within 6 months of the last platinum treatment [5, 13]. However, the issue remains that even in chemosensitive tumors, there is a lack of cure using the established treatments. Furthermore there is no agreed upon effective follow-up treatment plan for resistant tumors [11,

13]. There are discrepancies in the literature, whether or not these patients should undergo a second surgery either after initial chemotherapy response, after recurrence, or at all [5].

1.2 Taxanes

Taxanes are antineoplastic chemotherapy drugs derived from the plants in the *Taxus* genus [15]. Paclitaxel was derived in 1971 from the bark of *Taxus brevifolia*, a Pacific yew tree [15-17]. Paclitaxel has been used effectively in breast, ovarian, head and neck, and lung cancer malignancies [15]. Docetaxel (DXL) is derived from the needles of *Taxus baccata* and is a semisynthetic analogue of paclitaxel developed in the 1980s [14-16]. DXL has been significantly effective in breast, ovarian, head and neck, gastric and lung cancers [15]. Paclitaxel and DXL have similar toxic side effects.

1.2.1 Mechanisms of Taxane Action

High concentrations of paclitaxel result in the stable formation of microtubule bundles, which interrupts normal polymerization and depolymerization of microtubules, whereas low concentrations suppress the dynamics of microtubules rather than causing stable formations [18]. Paclitaxel and DXL interfere with cell division through the same binding site on the β-subunit of tubulin [14, 15, 17, 19]. Microtubules are heterodimers composed of polymerized α and β tubulin subunits that form tubulin dimers with microtubule-associated proteins [16, 20]. Microtubules are an important part of the cytoskeleton and play a role in cell division, cell shape, transcription factor trafficking, and vesicle transport [20-22]. Their role in cell division for separating chromosomes during mitosis is their most well-known function [22]. Microtubules are dynamic

and therefore unstable, with tubulins being polymerized and microtubules being depolymerized constantly, and they exist in equilibrium [16, 21].

The binding of taxane to tubulin subunits results in the formation of stable, non-functional microtubules that cannot depolymerize, resulting in inhibition of dynamic microtubules and cell cycle arrest [14, 15, 19, 21, 22]. Paclitaxel specifically interferes with the cell cycle at the G_2/M-phase junction, and DXL interferes primarily in the S-phase, resulting in cell cycle arrest due to mitosis inhibition [16, 19]. This difference in cell cycle phase is due to differences in affinity for the β-subunit of tubulin; DXL has a greater affinity for β-tubulin than paclitaxel [16]. DXL targets centrosome organization, and paclitaxel causes damage by affecting the mitotic spindle [16]. Uncontrolled cell division is a hallmark of many cancers; therefore, targeting microtubules could slow progression [20]. The cell cycle arrest eventually leads to cell death by apoptosis through the mitochondrial pathway [17, 22].

Toxicities associated with paclitaxel treatment are neutropenia (bone marrow suppression), anaphylaxis, neuropathy, myalgias, hypersensitivity reactions, arthralgia, fatigue, alopecia, nausea, vomiting, stomatitis/mucositis, cardiac toxicity, and diarrhea [15, 16, 19, 23]. The neurotoxicity and neutropenia are side effects that are ultimately dose-limiting [21]. Paclitaxel phase I trials were delayed due to high incidence of hypersensitivity reactions in patients, such as rash, facial flushing, pruritus, urticaria, fever, and angioedema [15]. Premedication with histamine antagonists and corticosteroids has prevented hypersensitivity reactions caused by paclitaxel [15, 19, 23]. In addition to the toxicities observed with paclitaxel, DXL toxicities include: fluid retention, cutaneous eruption, and nail changes [15, 16]. However, cardiac toxicity was not observed with DXL as in the case with paclitaxel [15]. Premedication

with corticosteroids has reduced the severity of fluid retention associated with DXL treatment [19, 23]. Both taxanes are able to induce apoptosis, and have anti-angiogenic properties [19].

The pharmacological activity of DXL differs from paclitaxel in a few ways: DXL has a longer plasma half-life, greater intracellular retention than paclitaxel, a stronger promoter of tubulin polymerization *in vitro*, and DXL shows a greater activity in some tumour models [14, 19]. Cells uptake DXL more readily and have a slower efflux of DXL, leading to longer intracellular retention times, which could explain why there is incomplete cross-resistance between the two taxanes [16].

DXL was also found to be about 2 times more cytotoxic than paclitaxel, and 1000 times more cytotoxic than cisplatin or etoposide in ovarian cancer cell lines [14, 21, 24, 25]. In addition, DXL has been shown to act synergistically with platinum agents *in vitro*, and to have potent cytotoxic activity in platinum-resistant ovarian cancer cell lines [14].

The gene for the antiapoptotic oncoprotein B-cell CLL/lymphoma 2 (Bcl-2) is overexpressed in several solid tumours [16, 22]. DXL induces Bcl-2 phosphorylation, which inhibits its function, and therefore results in apoptosis [21, 22]. DXL is able to do so at concentrations 100 times less than paclitaxel [21].

1.2.4 Mechanism of Taxane Resistance

Resistance can be *de novo* or acquired [17]. *De novo* resistance is an inherent insensitivity to the drug, whereas acquired resistance is a result of the development of resistant populations in response to taxane treatment [17]. Acquired tumor resistance to treatment can be attributed to: protein isoform modifications, alterations in drug efflux mechanisms, or apoptotic modulation [17].

Taxane resistance research has largely centered around drug efflux proteins [17]. These are proteins that are known to limit drug efficacy by detection and removal of excessive concentrations of substrates and toxins intra- and extracellularly [17]. Resistance to anti-tubulin agents is best described as the multidrug resistance (MDR) phenotype, which is mediated by the ATP-binding cassette (ABC) transport protein P-glycoprotein (Pgp) encoded by the *MDR-1* gene [16, 17, 22, 26, 27]. Transfection experiments have shown that an increased expression of *MDR-1* is sufficient to cause MDR [27]. ABC proteins protect the cells under normal conditions, by moving toxins outside of the cells [26]. The multidrug resistance protein Mrp1 is an ABC transporter involved in the exclusion of phase II metabolites [28]. Overexpression of this protein is common in cancer [26]. As the phenotype suggests, this mechanism of resistance creates a cross-resistance to structurally unrelated cytotoxic agents [17]. For example, DXL is still effective in paclitaxel-resistant tumors, such as breast, ovarian and lung cancers [16].

Mutations that affect the tubulin binding site for taxanes represent another important mechanism of resistance [22]. Differences in the specificity of tubulin binding sites could account for the lack of cross-resistance between taxanes and other microtubule-stabilising agents [22]. An additional mechanism of resistance is the alteration of protein expression. Taxanes bind β-tubulin, and taxane-resistant cancer cell lines have shown loss of β-II-tubulin and overexpression of β-III-tubulin [26].

Efforts to overcome taxane resistance include novel formulations of taxanes, such as nanoparticle albumin-bound paclitaxel, which has been shown to increase response rates and is better tolerated than Cremophor-based paclitaxel [26].

1.3 Anthracyclines

The anthracyclines are a group of antibiotics (such as doxorubicin, daunomycin, and rubidazone) with antitumor properties [27, 29]. Doxorubicin (DOX) and daunomycin were isolated from *Streptomyces* spp. in the 1960s [30]. DOX is commonly used in breast, lung, ovary, and soft tissue sarcoma malignancies [27, 30]. Toxicities associated with anthracyclines include cardiotoxicity which often results in the need for dose reductions in patients [31, 32]. There are many proposed mechanisms of action for the cardiotoxicity associated with anthracyclines. Most proposed mechanisms involve the mechanisms of action of anthracyclines but fail to explain why these would cause preferential cardiotoxicity.

1.3.1 Mechanism of Anthracycline Action

Anthracyclines cause toxicities and cytostatic effects through: intercalation within DNA and formation of complexes with iron (causing inhibition of both DNA replication and RNA polymerase II), generation of free radicals (causing DNA damage or lipid peroxidation), covalent DNA binding and alkylation, DNA cross-linking, interference with DNA unwinding, DNA strand separation, helicase activity, direct membrane damage due to lipid oxidation, and inhibition of topoisomerase II, and ultimately induction of apoptosis [27, 32, 33].

Anthracyclines form covalent complexes between topoisomerase II and DNA, which inhibits the resealing of DNA breaks [30]. The complexes that anthracyclines form with iron lead to errors in transcription and replication, as well as the formation of reactive oxygen species (ROS) [33]. ROS can cause damage to proteins, lipids, and DNA [33]. DOX and daunomycin assert their effects by intercalating within DNA, which results in an inhibition of DNA synthesis due to the two strands being unable to separate in preparation for replication [29]. The cause of

cell death appears to be the inhibition of topoisomerase II [27]. Anthracyclines covalently bind to DNA-topoisomerase II complexes to inhibit the enzyme's activity, which is to rejoin the two strands of DNA, therefore resulting in DNA double-strand breaks [27].

1.3.2 Mechanism of Anthracycline Resistance

The MDR phenotype is also suggested to be a part of anthracycline resistance mechanisms [27]. Non-Pgp-mediated MDR, changes in intracellular distribution of drug, increased glutathione S-transferase (GST) content and detoxification mechanisms, alterations in TOPO II, and increased DNA repair are additional resistance mechanisms against anthracyclines [27]. As previously mentioned, cells can become resistant to several cytotoxic agents through drug efflux caused by Pgp [27]. This protein is commonly overexpressed in chemoresistant tumors.

Several cell lines have shown an MDR phenotype without Pgp overexpression, but with overexpression of multidrug resistance-associated protein (MRP) (a family member of ABC), LRP56, and P95 [27]. LRP56 is a glycoprotein found in several lung cancer cell lines [27]. P95 is a membrane transporter that has been identified in the MCF-7 DOX-resistant cell line [27]. In resistant cells, the intracellular anthracycline distribution changes from mostly nuclear in wildtype cells to mainly cytoplasmic localized in acidic vesicles or the membranes of vesicles [27].

Topoisomerase II is an important nuclear enzyme that relaxes DNA molecules in an ATP-dependent manner [27]. There are two isoforms of topoisomerase II. Topoisomerase IIα is the smaller isoform, while topoisomerase IIβ is larger [27]. Topoisomerase IIα is highly expressed during S-phase, but decreases as cell growth plateaus, whereas topoisomerase IIβ is

expressed highly during cell plateau phase, but is low during rapid cell proliferation [27]. Alterations in the topoisomerase IIα gene, the enzyme target of the anthracyclines, can contribute to anthracycline resistance, including downregulation of expression or mutations resulting in altered protein function or binding [26, 27].

Cells can adapt to DNA damage through increased DNA repair mechanisms and tolerance to damage [27]. Types of DNA repair include: reversal of damage, excision of damage, and post-replication repair [27]. Resistance to alkylating agents has been shown to be associated with increased DNA repair in many anthracycline-resistant cell lines [27]. Combination treatment of anthracyclines with DNA repair inhibitors can be used to circumvent resistance caused by increased DNA repair mechanisms [27].

Due to these resistance mechanisms especially across multiple drugs, it is imperative to find biomarkers that assess patient response and efficacy of the treatment.

1.4 Response to Treatment

During the CAN-NCIC-MA22 clinical trial, patients with locally advanced or inflammatory breast cancer were treated with various doses of epirubicin (an anthracycline) and DXL (a taxane) at 2 or 3 week intervals [34]. Tumour core biopsies were taken pre-, during, and post-treatment for the first 50 patients enrolled in the trial [35]. RNA integrity was assessed in each sample using the RNA Integrity Number (RIN) [35]. The RIN categorizes RNA quality from 1 to 10, with 1 being highly degraded and 10 being completely intact RNA [36]. A low mid-treatment RIN was observed to be associated with a pathological complete response (pCR) post-treatment [35]. Moreover, it was observed that the tumour RNA in highly responding tumours exhibited unique and aberrant bands between the 28S and 18S in the electropherograms

and resulted in an “n/a” RIN value, which is indicative of a highly degraded sample or a sample with an aberrant RNA banding pattern [35, 37].

This unique and aberrant banding was later termed RNA disruption, and the RNA disruption assay (RDA) was subsequently developed, which uses a proprietary algorithm to quantify the magnitude of disruption as an RNA Disruption Index (RDI) [35]. The RDI value is obtained through an algorithm expressing the mass ratio of disrupted RNA to normal RNA [35]. The RDI value increases as the aberrant RNA disruption band intensities increase and the band intensities of the 28S and 18S rRNAs decrease [35]. Patients who did not achieve pCR but had a high level of RNA disruption had an equivalent disease-free survival (DFS) compared to those who did achieve pCR [35]. This is evidence that tumour RDA assessment on-treatment could be a better chemoresponse biomarker than pCR, which is assessed post-treatment. Moreover, RDA could predict pCR after neoadjuvant chemotherapy in patients with HER2+ breast cancer after 1 cycle of chemotherapy [38].

The benefits of RDA include identifying non-responding patients early in treatment, such that these patients could be provided with early access to alternate treatments that may work and improve their survival [35]. This approach would also spare patients the toxic side effects of the ineffective chemotherapy regimen [35]. The exact mechanism of RNA disruption remains unknown. However, understanding the pathways involved could provide more, and potentially better, targets for increased treatment response or additional biomarkers. One of these potential targets for determining the mechanism(s) involved in RNA disruption are stress-induced transcription factors. Stress-induced transcription factors are a good target due to their upstream role in inducing and moderating cellular stress pathways in response to cellular stressors. Transcription factors can play a role in multiple cellular stress pathways at once, which can also

include changing the cellular outcomes (i.e. changing from autophagy to apoptosis). Therefore, stress-induced transcription factors could provide insight into the pathways and mechanisms involved in RNA disruption, which is a cellular response to various cellular stressors.

1.5 Stress-Induced Transcription Factors

The expression of genes is primarily controlled by regulating their transcription through the binding of specific proteins called transcription factors to particular DNA sequences in the regulatory elements within the promoters of those genes [39]. Transcription factors are critical in the regulation of cell function through activation or repression of specific genes, which are necessary for growth, development, and differentiation [40]. However, the activity of these factors must also be regulated in order for transcription to occur in response to a specific stimulus at the correct time [41]. Transcription factor activation can be achieved through conformational changes through ligand binding, disruption of an inhibitory protein-protein interaction, and protein modifications [41]. Transcription factors can be categorized into families, which are based on the protein structure used for DNA binding [39]. The major families are the C_2H_2-zinc finger, Homeodomain, basic helix-loop-helix (bHLH), basic leucine zipper (bZIP), and nuclear hormone receptor (NHR) families [42].

The dysregulation of transcription factors has been seen in disease development and progression. When a transcription factor or the DNA binding sequence of a transcription factor contains non-functional mutations, this usually results in the underexpression of a specific gene resulting in disease [39]. Alternatively, when transcription factor activity becomes dysregulated, transcription factors can be activated at the wrong time, which can lead to overexpression of the genes they regulate [39]. Overexpression or overactivity of transcription factors has been identified in human cancers, which aid in cell survival, overgrowth, and metastatic behaviour of

the cancer cells [43]. Their role in the activation of specific genes and in stress pathways could provide an interesting target for the elucidation of novel pathways associated with RNA disruption.

1.5.1 Transcription factors EB and E3 (TFEB and TFE3)

Transcription factor EB (TFEB) was first identified for its ability to bind the adenoviral major late promoter in human B-cells [44]. TFEB belongs to subfamily micropthalmia-transcription factor E (MiT/TFE), which includes TFE3, TFEC, and MITF [44, 45]. This subfamily belongs to the family of basic helix-loop-helix/leucine zipper (bHLH-LZ) transcription factors [46-48]. TFEB is considered a master regulator of lysosomal biogenesis and was the first in the MiTF/TFE family to be identified [45]. When binding to DNA, the subfamily of MiT/TFE form homodimers or heterodimers with each other, but not with members of the larger bHLH-LZ family of transcription factors [47]. All the members of MiT/TFE have an identical basic region that binds the DNA, but TFEC does not share the same activation domain as the others and appears to be the most divergent of the subfamily [47]. The DNA target sequences for this group of transcription factors was found to overlap with the Coordinated Lysosomal Expression and Regulation (CLEAR) motif, which is found in the promoter region of at least 96 lysosomal genes [44, 49, 50]. CLEAR elements are 10-base pair motifs (GTCACGTGAC) found in the promoter region of lysosomal and autophagic genes, such as *LAMP1* and *UVRAG* respectively [45-48, 51]. It was found that TFEB specifically targets CLEAR elements and upregulates essential genes for lysosomal biogenesis and function [44, 45, 47, 48]. TFE3 has been shown to also bind CLEAR elements to activate lysosomal biogenesis and autophagy [45].

TFEB regulates autophagy through its autophagic and lysosomal gene targets. TFEB overexpression in HeLa cells activated transcription of lysosomal transmembrane proteins, lysosomal hydrolases, and a significant increase in the number of lysosomes present [50]. Settembre *et al.* (2011) further confirmed this in HeLa cells, and saw an increase in autophagosome and autophagic activity with TFEB overexpression [49, 52]. This overexpression resulted in increased bulk autophagy degradation of long-lived proteins, lipids and damaged mitochondria [47, 52]. Knockdown of TFEB resulted in inhibition of autophagy and decreased numbers of autophagosomes [44, 49, 52]. Martina *et al.* (2012) found that mutations in ARPE-19 human retinal epithelial cells at the codon for the phosphorylation site of TFEB (S211) resulted in the accumulation of TFEB in the nucleus, and increased transcription of autophagic and lysosomal genes, independent of the mammalian target of rapamycin (mTOR) [48]. These mutations also resulted in a significant increase in cellular autophagosomes [48].

There are two important serine residues, whose phosphorylation results in the protein staying in the cytoplasm and remaining inactive. Under nutrient-rich conditions, TFEB is phosphorylated by mTOR at S211, which promotes the binding of the cytoplasmic retention protein/chaperone, YWHA protein 14-3-3 [46-48]. YWHA proteins are involved in regulating nutrient-sensing pathways and the nuclear transport of several transcription factors [48]. It is thought that YWHA binding on 14-3-3 masks the nuclear localization signal of TFEB [47]. When there is nutrient deprivation, mTOR is no longer active, resulting in the dissociation of TFEB and 14-3-3 and the translocation of TFEB into the nucleus [45, 46, 48]. There is a release of lysosomal calcium ions during nutrient deprivation, which activates the phosphatase calcineurin, which dephosphorylates TFEB [45, 47]. It is possible that calcium release from other compartments, such as the ER, could lead to calcineurin-mediated activation of these

transcription factors [45]. In addition to being phosphorylated by mTOR, TFEB is phosphorylated at serine 142 by extracellular signal-regulated kinase (ERK2, also MAPK1) which keeps it inactive in the cytoplasm [44, 47-49]. ERK1/2 is activated by growth factors [44]. Settembre *et al.* (2011) found that this was the main regulator of TFEB localization [52]. However, Peña-Llopis *et al.* (2011) did not find that a mutation at this residue had an effect on the localization of TFEB [53]. Phosphorylation at serine 142 had no effect on 14-3-3 expression or activity [48]. Dephosphorylation of TFEB caused by nutrient starvation results in TFEB translocation to the nucleus to upregulate target genes [44]. TFEB translocation is sensitive to nutrient and growth factors [49]. TFEB promotes the transcription of genes associated with cell adaptation and survival, such as autophagic, metabolic and lysosomal genes [46]. Many of the factors that regulate TFEB activation, such as the lysosome and lysosomal calcium ion channel, are regulated by TFEB transcriptionally, which indicates that the lysosome adaptation to environment is regulated through multiple feedback loops [47].

TFE3 also regulates lysosomal biogenesis and autophagy [46]. There appears to be a redundancy in the function of TFEB and TFE3 in certain cell types, as they share the binding of CLEAR elements, response to nutrient levels, and the ability to induce lysosomal biogenesis and autophagy [46]. TFE3 is also regulated by nutrient availability, mTOR activity, and binding to Ras-related GTP-binding (Rag) GTPases and 14-3-3 [47]. Ragulator is a lysosomal surface-associated pentameric protein complex that relays amino acid availability information through its modulation of Rag GTPases [45]. Rag GTPases recruit mTOR to the surface of the lysosome under nutrient-rich conditions, and mTOR is activated by the small GTPase Rheb [45, 47]. These Rags also recruit TFEB and TFE3 to the lysosomal surface, where they can be phosphorylated by mTOR [45, 47]. There is a coordinated, Rag-mediated recruitment of mTOR and its substrates to

the lysosome providing spatiotemporal regulation of mTOR and the subsequent phosphorylation and inhibition of TFE3 and TFEB [45].

mTOR phosphorylates TFE3 at S321 and it is also retained in the cytosol by 14-3-3 [45, 51]. Martina *et al.* (2014) showed that TFE3 is able to increase the number of lysosomes independently of TFEB, as this was seen in TFEB depleted cells in both HeLa and ARPE-19 [45, 54]. When there is no nutrient deprivation, TFEB and TFE3 are both in the cytoplasm, but rapidly translocate to the nucleus after starvation and dissociation from 14-3-3 to upregulate multiple genes [45]. Under starvation conditions, the inactivation of mTOR allows for TFEB and TFE3 translocation that mediate lysosomal biogenesis, autophagy induction, and expression of critical mitochondrial and metabolic regulators [51].

1.5.2 NF-E2 Related Factor2 (Nrf2)

The transcription factor nuclear factor erythroid-2-related factor 2 (Nrf2) is responsible for activating the antioxidant response in cells and is closely regulated by Kelch-like ECH-associated protein 1 (Keap1) [55, 56]. Nrf2 is a ubiquitously expressed member of the cap 'n' collar (CNC) subfamily of bZip transcription factors [28, 55-58]. Other transcription factors in this family are p45, NF-E2, Nrf1, and Nrf3 [28, 57]. There are 7 highly conserved domains (Neh 1-7) distributed along the *Nrf2* gene [55, 56]. Neh1 displays specificity for DNA binding, and allows for the binding to small masculoaponeurotic fibrosarcoma (sMAF) proteins and ubiquitin-conjugating enzyme E2E3 to form a nuclear complex [56]. The Neh2 domain possesses the DLG and ETGE motifs that allow for Keap Kelch domain binding in negative regulation of Nrf2 [56]. Neh2 also mediates electrophilic sensitivity and stabilization of Nrf2 [28]. Neh4 and Neh5 are two activation domains and bind to the coactivator cAMP-response-element-binding-protein

(CBP) independently, and the simultaneous binding of both synergistically activate Nrf2 target genes [28]. Neh6 is essential for Keap1-independent degradation of Nrf2 [28, 56].

Under basal conditions, Nrf2 is negatively regulated by Keap1 in the cytoplasm through interaction with the BTB domain on Keap1 [59]. Keap1 is a Kelch protein and a substrate-specific adaptor for the Cullin-3 (Cul3) RING-box-based (Rbx) E3-ligase ubiquitin complex [55-57, 60]. Keap1 is a thiol-rich protein with five reactive cysteine residues, which can be modified in response to electrophiles, oxidative stress, and xenobiotics, acting as a sensor [28]. Two of these cysteines are critical for Nrf2 repression, and their modification inhibits the ability of Keap1 to ubiquitinate and degrade Nrf2 [28, 56]. Keap1 constantly targets Nrf2 for ubiquitin degradation by 26S proteasome in order to keep Nrf2 levels low [55-58].

Upon activation, Nrf2 translocates to the nucleus and forms a heterodimer with sMAF proteins through the Neh1 domain. The heterodimer formation facilitates Nrf2 binding to the antioxidant response element (ARE) in the promoter region of target genes [28, 55-58]. The ARE motif is a common regulatory element found in the promoter region of many phase II detoxifying enzyme genes and drug transporters, such as ABCG2, MRP3, MRP4, and GST [28, 59]. Other target genes include phase I enzymes (NQO1, NQO2, HO-1), metabolic (G6PD, TKT, PPARγ) molecular chaperones, antiapoptotic proteins (Bcl-2), DNA repair enzymes, and anti-inflammatory response proteins [56-58]. The products of these genes are able to reduce reactive compounds to less toxic intermediates and increase cell repair to fix any damage that may have occurred [58]. Nrf2 targets genes are involved in metabolism, intracellular redox-balancing, apoptosis, and autophagy [55].

The Nrf2-mediated antioxidant response is one of the major cellular defenses against endogenous and exogenous xenobiotics, and oxidative and electrophilic stress [55, 56]. The

antioxidant response more specifically protects the cell through restoring redox homeostasis, efficient metabolism and efflux of xenobiotics, removal of damaged proteins, and preventing cell death [57]. Nrf2 is responsible for the inducible and basal expression of proteins involved in drug metabolism, oxidative stress response, and cytoprotection [58]. Nrf2 has been associated with differentiation, proliferation, growth, apoptosis, and has been suggested to have evolved from an original role in haematopoiesis [58]. Nrf2 is generally described as a cytoprotective transcription factor and tumour suppressor [55]. However, this benefit to cell survival is not only seen in normal cells, but also cancer cells [55]. The antioxidant role of Nrf2 may help prevent cancer, but when cancer is present it may favour tumour survival through protection from oxidative stress, chemotherapy, or radiotherapy [55]. Nrf2 appears to play a dual role in cancer, and its role is dependent on the stage of tumorigenesis [57].

1.5.3 Yin Yang 1 (YY1)

Yin Yang 1 (YY1) is a ubiquitously expressed multifunctional zinc-finger transcription factor member of the Polycomb Group protein family [4, 40, 61, 62]. This protein family plays an important role in hematopoiesis and cell cycle control [61]. The gene is highly conserved among species [4, 40, 61]. *YY1* null mice embryos did not survive beyond the blastula stage, and heterozygotes survived but had significant growth retardation and neurological defects [40, 63]. Its ubiquitous expression suggests important roles in cellular stability and normal functioning [40]. YY1 has a role in transcriptional regulation, cell proliferation and differentiation, cellular movement, cell morphology, cell-to-cell adhesion, chromatin remodeling, and apoptosis [61-63].

YY1 was discovered through studies of the adeno-associated virus (AAV) P5 promoter region and its activation by E1A gene products [40]. E1A is a protein that activates the AAV P5

promoter, which has been repeatedly shown to associate with and modulate YY1 [40, 61]. In the presence of E1A, YY1-mediated activation of transcription takes place [40, 61]. In the absence of E1A, YY1 become a transcriptional repressor [40, 61]. The ability to activate or repress transcription is where the name of the transcription factor came from. Unlike other transcription factors, YY1 has the ability to activate or repress transcription, modulate the function of other proteins, and affect chromatin structure in addition to initiating transcription [4, 40]. The activation or repression of gene expression depends on the cofactors it recruits [63].

The YY1 protein contains four C_2H_2-type zinc-finger motifs with two specific domains that characterize its function as an activator or repressor [40, 61]. The N-terminus region has two acidic regions and acts as an activation domain (a.a. 43-53), followed by a glycine-rich domain [40, 63]. The C-terminus region has repression activity (a.a. 298-397), with two other repression domains within the zinc-finger motifs and the glycine-rich area between amino acids 157-201 [40, 63].

Overall, the function of YY1 in transcription is context-specific and requires interactions with many cellular factors [61]. YY1 can assert many functions including transcriptional initiation, activation, including repression which lead to the regulation of normal cell growth and survival [61].

An individual transcription factor can play many roles in various cellular signaling pathway, including stress response and cellular homeostasis. Transcription factors can initiate specific cellular pathways and push towards new ones depending on the stress, such as the change from autophagy to apoptosis after prolonged stress.

1.6 Cellular Stress Signaling Pathways

Cells respond to assaults through signalling cascades resulting in the upregulation of certain genes and downregulation of others depending on the circumstance. These pathways can range from adaptation to the stressor through defense mechanisms to initiating programmed cell death. Many of the pathways and pathway components are conserved across species, due to their importance in the cell's survival and outcome. There are a variety of stresses that the cell can face, and there are a variety of pathways that are able help the cell adapt or eliminate the stress with some overlap occurring between pathways [64].

Cancer cells often display antiapoptotic characteristics, including overexpression of antiapoptotic proteins, which contributes to cancer cell survival and evasion of apoptosis in spite of stressors [65]. Apoptosis evasion can also be achieved through the downregulation of proapoptotic proteins [65]. The tumor microenvironment is stressful as well, due to poor vascularization, which can result in stressors such as low oxygen, nutrient depletion, and pH changes [64]. Despite these stresses, cancer cells are able to overcome them through adaptation and specific advantageous mutations resulting in their continued growth and survival.

Ultimately, the cells will try to adapt and overcome the stress through prosurvival and antiapoptotic pathways. However, if the stress is prolonged or too large of a burden, the cell will activate proapoptotic proteins and pathways resulting in programmed cell death [64].

1.6.1 Autophagy

Autophagy is a highly conserved biological process that involves catabolic lysosomal degradation and recycling of intracellular cytoplasmic components, involved in the maintenance of cell homeostasis [66-68]. Autophagy maintains cell metabolism and starvation adaptation

through the lysosomal degradation of misfolded or aggregated proteins and damaged organelles to recycle metabolites including amino acids, fatty acids, and nucleotides [46, 69].

The role of autophagy is mainly protective and adaptive in response to enhanced cellular stress [67]. It has many roles in intracellular clearance, development, anti-aging, elimination of microorganisms, cell death, tumour suppression, and antigen presentation [70]. Autophagy is also associated with prevention of diseases, such as the removal of mutant protein aggregates, as in the case of the mutant protein huntingtin in Huntington's disease, a neurodegenerative disorder [71, 72]. Autophagy also plays a role in response to invasion by viral and bacterial pathogens [66, 71].

Most of the early studies delineating the mechanisms regulating autophagy were done in *Saccharomyces cerevisiae*, and later confirmed in mammals with a high degree of similarity [72, 73]. Autophagy has been observed in plants, worms, and slime mould, with conservation of genes throughout [72]. It is a highly conserved pathway, but there are some differences and some aspects of the mammalian autophagy pathway are still not understood [72].

There are different types of autophagy such as: macroautophagy, microautophagy, chaperone-mediated autophagy, ribophagy, and mitophagy [70, 72, 74, 75]. Microautophagy involves the direct sequestration of cellular components through invaginations in the lysosomal membrane [75]. Chaperone-mediated autophagy has proteins directly fed into lysosomes through a protein translocation pathway [75]. Ribophagy and mitophagy is the clearance and degradation of ribosomes and mitochondria, respectively. Macroautophagy (simply referred to as autophagy from this point forward) sequesters the cellular components for degradation through autophagosomes and presents them for lysosomal degradation [75].

Autophagy can be classified as induced-autophagy and basal-autophagy. Induced-autophagy is initiated by starvation, hypoxia, endoplasmic reticulum (ER) stress, a pathogen infection, and growth factor withdrawal and results in protein turnover producing amino acids and other macromolecules [70, 75]. In contrast, basal-autophagy is the constant turnover of cytoplasmic components to maintain cellular homeostasis [70, 75]. Basal autophagy acts as a quality control system for organelles and proteins, preventing the accumulation of damaged organelles or aggregate proteins [66]. Cells must maintain a constitutive basal level of autophagy to maintain cell homeostasis [45].

1.6.1.1 Mammalian target of rapamycin (mTOR)

Autophagy is mainly, but not exclusively, regulated by mTOR [66]. mTOR is a highly conserved serine/threonine kinase, which inhibits autophagy when there is nutrient availability [46, 67]. Levels of amino acids, insulin signaling, ROS, calcium, growth factor receptor signalling, hypoxia, and cellular ATP levels all act to regulate mTOR activity [70, 72]. There are mTOR-independent pathways for autophagy, although they are not well understood [70].

1.6.1.2 Nutrient-Rich Conditions

Under nutrient-rich conditions, mTOR is recruited to and activated on the lysosomal membrane by small Rag GTPases and activated through the GTPase Rheb, where it inhibits autophagy through phosphorylation of Atg proteins [45, 47, 72]. mTOR is activated on the surface of lysosomal membranes, which is perhaps why lysosomes are implicated in nutrient sensing [51]. The whole process of autophagy is modulated by over 30 autophagy-related genes (*ATG*) and their Atg proteins in response to nutrient availability and inhibition through mTOR

[66, 68]. mTOR directly phosphorylates the Atg13-Atg1 complex (Atg1 is also ULK1/2 in humans) and is also bound to ULK1 [48, 75].

1.6.1.3 Nutrient-Poor Conditions

When nutrients become depleted, mTOR is released from the lysosomal surface and becomes inactive, leading to autophagy induction [45, 47]. Under nutrient-poor conditions, mTOR is inhibited and dissociates from ULK1, which initiates autophagy [67]. Once autophagy is initiated, the process can be classified into several steps: nucleation, elongation, closure, maturation, and degradation [67, 70, 72].

The first step is phagophore formation or nucleation [66] . The phagophore is an early, semi-circle, lipid bilayer form of an autophagosome membrane [66, 70, 75]. The origin of the phagophore lipid bilayer remains controversial, but it theorized to derive from the ER, the trans-Golgi, and endosomes [72].

Elongation involves two ubiquitin-like conjugation steps [73]. Atg7 (E1-like ubiquitin activating enzyme) activates Atg12, which is then transferred to Atg10 (E2-like ubiquitin carrier protein), and links Atg12 to Atg5 [73]. Next, Atg8 (LC3 in humans) is proteolytically cleaved by Atg4, and then is conjugated with phosphatidyletanolamine (PE) on the membranes of autophagic vesicles [73]. Once cleaved and conjugated with PE, LC3 is designated LC3-II [73]. LC3-II is recruited by Atg12-Atg5, and distributed symmetrically on both sides of the autophagosome, which is believed to be the driving force of membrane curvature [72, 73].

Once the elongation of the phagophore is completed, and the cargo is membrane bound, the final vesicle is called an autophagosome. The autophagosome matures through fusion with a lysosome, creating an autophagolysosome, allowing for the inner components to be degraded

through lysosomal enzymes [70, 72]. There are over 50 lysosomal hydrolyzing enzymes that are capable of breaking down substrates in their acidic environment [46]. LC3-II can be released from the membrane or degraded along with the sequestered components [73]. Once the intracellular components have been degraded into monomeric units, they are transported back into the cytosol for reuse as building blocks or metabolic processes [70, 72]. Building blocks include fatty acids and amino acids, which are essential in maintaining ATP levels and synthesis of components required for cell survival [45].

Beclin 1 was originally identified as an interaction partner of Bcl-2, an anti-apoptotic protein, and that interaction that is reduced upon starvation by Jnk1-mediated phosphorylation of Bcl-2, freeing Beclin 1 to activate autophagy [70, 72]. The ER-targeted Bcl-2 appears to suppress autophagy, which could imply a dual role depending on subcellular localization: pro-survival at the mitochondria by inhibiting cytochrome c release, and anti-autophagy at the ER [70, 72]. Mono-allelic loss of the autophagy gene Beclin-1 (also known as ATG6) is found in high frequency in human breast, ovarian, and prostate cancers [66, 72]. There are many common upstream components and pathways between autophagy and apoptosis induced by ER stress [76]. Autophagy precedes apoptosis, and the two pathways are connected through inactivation of the other pathway's components [76]. Autophagy inactivates caspases therefore blocking apoptosis, and when apoptosis-activated caspases are activated they can cleave autophagy proteins [76].

Autophagy can be a tumor suppressing pathway, while the suppression of autophagy can lead to tumor development [69]. Knockdown of *beclin1* in mice lead to tumorigenesis, whereas its increased expression lead to the inhibition of human breast tumors in mouse models [69]. Consistent with this theory, genes that turn on autophagy are often mutated in human cancers,

and those that turn it off are activated [69]. Nevertheless, autophagy may confer an advantage to the cancer during times of nutrient and oxygen deprivation, allowing it to survive and degrade organelles during cancer treatments [69]. Most evidence indicates that autophagy aids in cell survival in tumors in response to metabolic stress *in vitro* and in hypoxic conditions *in vivo* [66]. Autophagy has been thought to prevent tumorigenesis by limiting necrosis and inflammation, inducing cell cycle arrest and preventing genome instability; autophagy has also been shown to be required for key aspects of the senescent cell phenotype, a dormant phagocytic cell type that is enriched in response to cancer treatments [72]. Such cells appear to be drug resistant and permit tumor cell to adapt to stressors [72].

1.6.2 Endoplasmic Reticulum (ER) Stress

The endoplasmic reticulum (ER) is an organelle responsible for the synthesis and maturation of proteins, lipid biosynthesis, carbohydrate metabolism and calcium storage [51, 68, 77]. The ER lumen is the main site of intracellular Ca^{2+} storage [73]. The movement of Ca^{2+} in and out of the ER mediates a variety of cellular responses and signalling, such as Ca^{2+}-mediated mitochondrial apoptosis [73]. The synthesis, folding and modification of proteins targeted to membranes or the secretory pathway takes place within the ER [78]. These newly synthesized proteins are assembled and folded with the assistance of chaperones and folding enzymes in the ER. They are then post-translationally modified and translocated to the Golgi apparatus, and finally to vesicles for secretion or display on the plasma membrane [73, 77]. The balance between protein synthesis and degradation is dynamic and essential for cell homeostasis [79].

When proteins are unable to fold correctly, an accumulation of unfolded or misfolded proteins occurs, causing ER stress [51, 73, 77]. The protein-folding capacity of the ER can be perturbed by environmental insult or when protein folding demands are strongly increased,

resulting in an accumulation of unfolded proteins in the ER [78]. The unfolded protein response (UPR) is the signalling cascade that is activated following ER stress [77, 78, 80]. The UPR promotes the upregulation of proteins involved in protein homeostasis, and attenuating protein translation and synthesis to limit the burden on the ER [73, 79].

The ubiquitin-dependent degradation of misfolded or unfolded proteins is an essential component of this response [79]. Lysosome-mediated degradation via autophagy is also induced by ER stress [73]. The ER associated degradation (ERAD) pathway degrades misfolded proteins during ER stress [79]. Unfolded proteins in the ER are retrotranslocated into the cytosol where they are ubiquitinated and degraded by the proteasome [73]. Autophagy can be activated when the ER is overwhelmed as a secondary response to degrade unfolded proteins and alleviate ER stress [73]. Fundamental pathways that are integral for the restoration of cellular homeostasis are the UPR, ERAD, autophagy, hypoxic signaling, and mitochondrial biogenesis pathways [68]. UPR dysfunction is implicated in many human diseases, including cancer, diabetes, neurodegeneration, ischemia, and infectious disease [68].

There are three ER-membrane associated proteins involved in sensing an accumulation of misfolded proteins and activating UPR: activating transcription factor 6 (ATF6), inositol-requiring enzyme 1 (IRE1), and double-stranded RNA dependent protein kinase (PKR)-like ER kinase (PERK) [51, 73, 77, 78, 80]. Each of these sensors sense ER stress through the luminal domain and a signal is transduced to the cytosol [78]. All of the initiators cooperate to upregulate chaperones for protein folding, and facilitate clearance of unfolded proteins from the ER [78].

IRE1 and ATF6 activation promotes expression of chaperones, which facilitate the restoration of proper protein folding within the ER [59]. PERK activation attenuates protein

translation via phosphorylation of eukaryotic initiation factor 2 α (eIF2α) [59]. PERK can also activate the prosurvival transcription factor Nrf2 through phosphorylation [59].

1.6.2.1 Double-stranded RNA dependent protein kinase (PKR)-like ER kinase (PERK)

Under normal conditions, the luminal domains of PERK and ATF6 are bound to binding immunoglobulin protein (BiP), an ER chaperone [73]. BiP keeps these proteins inactive, but upon ER stress BiP is released from these proteins to assist in protein folding [73].

Upon sensing ER stress by its luminal domain and BiP release, PERK becomes activated through oligomerization and autophosphorylation, through its cytosolic kinase domain [80]. Once activated, PERK phosphorylates eIF2α on serine 51, which attenuates protein translation selectively [77, 79, 80]. Attenuation of protein translation reduces the burden of stress in the ER by preventing new proteins from entering the ER compartment already under stress [51, 73].

Most mRNA translation is suppressed, although there is some preferential protein translation and upregulation that occurs, such as genes associated with UPR, specifically activating transcription 4 (ATF4) [51, 73, 77, 80]. ATF4 has cis-acting small upstream open reading frames (uORFs) in the 5'untranslated region (UTR), which repress translation, but they are bypassed during UPR stimulation of translation initiation [79]. General protein translation is inhibited, which enables dedicated translation of transcripts harboring an alternate open reading frame [68].

ATF4 has a short-half life and its transcript has low translation efficiency, resulting in low detection in cells under normal conditions [51]. ATF4 expression is upregulated in response to ER stress, low glucose, hypoxia, and amino acid depletion [80]. ATF4 is a transcription factor involved in cell survival by upregulating genes required for autophagy, redox homeostasis, and

amino acid import and synthesis [51]. ATF4 can play a role in tumour survival in hypoxic and nutrient-depleted areas by maintaining cell homeostasis, transcriptionally regulating amino acid biosynthesis, autophagy, redox balance, and angiogenesis [80].

PERK can also phosphorylate Nrf2 [73]. Upon phosphorylation, Nrf2 dissociates from its complex with Keap1 and translocates to the nucleus to promote expression of genes containing the ARE, which prevent oxidative stress through induction of antioxidant genes [73].

When ER stress is prolonged or too severe, ATF4 can also promote apoptosis through induction of C/EBP homologous protein (CHOP) [51]. CHOP is a transcription factor that inhibits Bcl-2 and induces pro-apoptotic BIM, thus triggering the activation of the mitochondria-dependent apoptotic pathway [51, 73]. CHOP also promotes GADD34 expression, which can dephosphorylate eIF2α which will allow protein translation to resume and sensitize cells to apoptotic signals [51].

A major regulator of protein translation and synthesis is the phosphorylation of eIF2α [78]. There are at least four kinases that act on eIF2α that respond to different stress conditions [78]. The phosphorylation of eIF2α under stress prevents the recycling of the eIF2α complex, which inhibits 43S translation initiation complex formation [78]. This allows for the downregulation of protein synthesis, even when there are ample nutrients and growth signals, but there is still stress within the cell as with UPR [78].

1.6.2.2 Activating transcription factor 6 (ATF6)

Upon sensing ER stress, and being released from BiP, ATF6 a transmembrane protein, translocates to the Golgi to be cleaved by two proteases [73]. Serine protease site-1 (S1P) cleaves the luminal domain, and metalloprotease site-2 protease (S2P) cleaves the N-terminal cytosolic

domain [73]. The cytosolic, cleaved N-terminal is released and translocates to the nucleus to function as transcription factor [73, 77]. Targets of ATF6 include the cAMP response element (CRE) and the ER stress response element (ERSE), which are in the promoter regions of CHOP, Grp94, XBP1, BiP, and other chaperones [73, 77]. ERSE can also be bound by mammalian transcription factors NF-Y and YY1 [81].

1.6.2.3 Inositol requiring enzyme 1 (IRE1)

IRE1 is highly conserved from yeast to mammals, with IRE1α a paralogue of IRE1 that is ubiquitously expressed [77]. IRE1α is a transmembrane protein that has sensory capabilities on the N-terminal luminal domain, and includes both endoribonuclease and kinase activities on the C-terminal cytosolic effector domain [73, 77].

Upon ER stress, IRE1α is activated in response to unfolded proteins binding directly to it, resulting in its oligomerization and autophosphorylation [73]. The endoribonuclease effector domain of IRE1α removes an intron within the *XBP1* primary transcript to produce a mature mRNA capable of being translated into a functional XBP1s protein [73, 77]. XBP1s translocates to the nucleus and binds to the promoter region of genes involved in restoring protein homeostasis, such as chaperones and components of the ERAD pathway [73, 77].

Ultimately, the UPR is a collection of intracellular signaling pathways that alleviate ER stress through increasing the expression of ER chaperones, attenuating protein translation, and transporting misfolded proteins out of the ER into the cytosol for ubiquitination and subsequent destruction by ERAD [73].

1.6.2.4 Thapsigargin (Tpg)

Thapsigargin (Tpg) is a natural compound known to induce ER stress *in vitro*. The *Thapsia* L. species is a plant that has been used medicinally for thousands of years [82]. Direct contact with the plant can result in skin irritation, caused by from potent histamine release [82, 83]. However, resin from the roots and stems of *Thapsia garganica* has been used medicinally as treatment of a number of diseases and illnesses such as lung disease, catarrh, fever, and a counter irritant to rheumatic pains [82]. *T. garganica* is the mother plant of thapsigargin, which is extracted from the roots and fruit of the plant [82]. Tpg is a naturally occurring sesquiterpene lactone found in *Thapsia garganica* [83-85]. Tpg was first found to cause a potent release of histamine in rat mast cells, in 1978 [83]. In 1990, the bioactivity of Tpg in mammalian cells was described as an irreversible inhibitor of calcium ion pumps, which in turn causes apoptosis [82, 84].

The movement of Ca^{2+}between the extracellular matrix and cytoplasm, the mitochondria and cytoplasm, or the ER and cytoplasm, is regulated by Ca^{2+} ATPase pumps, channels, exchangers, and electrophoretic uniports [86]. Ca^{2+} acts as an important messenger system through its localization and concentration [86]. Tpg is able to inhibit an ER Ca^{2+}-ATPase known as the Sarco-Endoplasmic Reticulum Ca^{2+} ATPase (SERCA) [86, 87]. This pump is responsible for pumping Ca^{2+} ions from the cytosol back into the intracellular membrane of the ER, or the sarcoplasmic reticulum [87]. However, for the purposes of this study, only the ER will be considered.

Tpg selectively binds to the transmembrane region of SERCA pumps, and inhibits the conformational change required for the pump to properly function and transport Ca^{2+} into the ER [87, 88]. The lipophilic nature of Tpg allows the molecule to diffuse into the cell membrane and

bind the SERCA pump [82, 89]. The pump is unable to bring the Ca^{2+}into the ER, and as a result the Ca^{2+}flows out of the ER and into the cytosol. The increased concentration of calcium ions in the cytoplasm opens the cell membrane channels, creating a further increase in calcium ions in the cytosol. The SERCA pump is unable to maintain low levels of calcium ions in the cytosol and a high concentration in the reticulum [87].

There is passive movement of the Ca^{2+} from the reticulum into the cytosol, which leads to an increase in calcium ion concentration [89]. This promotes a change in plasma membrane permeability that creates an influx of calcium ions from the extracellular fluid, which augments both ER and cytosolic Ca^{2+}concentrations [89]. Continued inhibition of the SERCA pump will deplete the calcium ion pool, which results in ER stress leading to induction of the UPR [88]. Ultimately, the prolonged inhibition of Ca^{2+} transport into the ER will lead to apoptosis in a cell proliferation-independent manner [89].

1.6.3 Mitochondrial Stress

The mitochondrion is a complex organelle, involved in energy metabolism, ATP production, and programmed cell death. Due to the importance of these functions, a precise coordination between the mitochondria and the rest of the cell is essential. Mitochondria are a major site of ROS production, which is a by-product of oxidative phosphorylation, but can be further increased by perturbations in the system [90]. Due to the high amount of basal ROS, mitochondria are often susceptible to DNA mutations and replication errors, which is made worse by the inferior DNA repair mechanisms. The most commonly inherited metabolic disorders are from defects in mitochondria, either encoded by the mitochondrial DNA (mtDNA) or nuclear DNA [91]. The high levels of ROS also create a harsh protein folding environment [90]. Mitochondrial stress can be identified through levels of ROS production, membrane

depolarization, levels of adenine nucleotides, fluxes in Ca^{2+}, secretion of proteins/peptides, and permeability transition pore opening [90]. Dysregulation of mitochondrial quality control has been implicated in pathological states and ageing [90]. Mitochondrial stress can result in cancer, cardiovascular disease, and diabetes [90].

Most of the genes that regulate function in the mitochondria are encoded in the nuclear DNA [92, 93]. Those proteins work in coordination with mitochondrially encoded proteins for maintenance and biogenesis of the mitoproteome [90]. mtDNA is double-stranded and circular, encoding 37 mitochondrial genes, and 13 polypeptides [90, 92]. As mentioned, mtDNA is highly susceptible to damage caused by ROS and inferior DNA repair machinery. Damage can include mutations in the mtDNA leading to defective oxidative phosphorylation and increased ROS [90]. mtDNA repair enzymes play an important role in responding to different stresses, with an increased activity of these enzymes protecting against oxidative stress-induced apoptosis [90].

Proteins encoded in the mtDNA are synthesized in the mitochondrial matrix, and folding of imported and mitochondrial proteins happens in the inner membrane with the help of resident chaperones [93]. Some mitochondrial chaperones include Hsp70 (isoform of BiP and Hsp72), Hsp60 (Cpn60), Cpn10, mtHsp70, mtGrpE, and mtDnaJ [92, 93]. These chaperones have homologues in *Escherichia coli* [92, 93] . The induction of Cpn60 and Cpn10 have been shown to be induced by heat shock, as well as by accumulation of protein aggregates in the mitochondria [92].

Oxidative phosphorylation involves the transport of electrons, from substrate oxidation, along the electron transport chain (ETC), along with proton pumping across the inner mitochondrial membrane creating a proton gradient. The electrons are carried on NAD+. The proton gradient and oxygen consumption are the driving forces of ATP production [90]. Since

ATP is a major output of oxidative phosphorylation, the level of ATP along with the ratio of ATP:adenine nucleotides are a signal of mitochondrial function [90]. NAD+ is also a signal of mitochondrial oxidative phosphorylation function [90].

Perturbations in oxidative phosphorylation can lead to reduced ATP production, changes in redox status, membrane depolarization, and excess ROS generation [90]. ROS are able to readily diffuse out of the mitochondrial membrane and act as signalling molecules. They are capable of activating redox-sensitive proteins, transcription factors and coactivators, inducing antioxidant responses in a negative feedback loop, and stimulate cellular adaptations to improve mitochondrial function including mitochondrial biogenesis [90]. Depolarization can act also as a signal of mitochondrial stress, promoting mitophagy and mitochondrial permeability transition pore (MPTP) opening [90].

1.6.4 Apoptosis

Necrosis is one type of cell death that occurs in response to chemical or mechanical injury and results in an inflammatory response [94]. Necrosis is defined by cellular swelling, membrane rupture and cellular bursting [94]. In contrast, apoptosis is a highly controlled form of cell death that is important in normal biological processes, such as normal cell turnover, tissue homeostasis, the immune system, embryonic development, metamorphosis and hormone-dependent atrophy, and chemical-induced cell death [95, 96]. Apoptosis can be triggered by DNA damage, deprivation of nutrients or oxygen, and viral infections [94]. Aberrant apoptosis also occurs in many diseases, such as neurodegenerative disease, ischaemic damage, autoimmune disorders, and cancer [95]. The concentration and length of exposure to a DNA-damaging agent often determines whether the cell dies from necrosis or apoptosis [94].

Apoptosis can be recognized through distinct morphological changes to the cell, as well as biochemical changes [95]. These morphological changes include nuclear chromatin condensation and fragmentation (pyknosis), compaction of cytoplasmic organelles and rearrangement, loss of cell-cell contact, dilatation of the endoplasmic reticulum, decrease in cell volume or cell shrinkage, and alterations to the plasma membrane including surface blebbings [95-98].

During the final stage of apoptosis, the surface blebbings result in the cell breaking into small membrane-bound fragments called apoptotic bodies, which can be recognized and phagocytosed by macrophages, so that unlike necrosis, no inflammatory response is elicited [95-97]. This fragmentation of cells occurs without leakage, and therefore does not induce an inflammatory response and cause injury to surrounding tissue [94].

Caspases are a family of intracellular cysteine proteases that cleave their substrates at specific, conserved aspartic acid (Asp) residues [97]. Caspases are synthesized as inactive proenzymes, which are activated by cleavage at their Asp residues, which are part of a proteolytic protease cascade [95, 97].

There are two mechanisms regulating apoptosis in cells that have been described in detail: the extrinsic and intrinsic pathways [97]. The first mechanism involves tumor necrosis factor (TNF) receptors and the other involves the mitochondria [97]. In the extrinsic pathway, the TNF family of receptors uses caspase-8 as its main effector enzyme [97]. Ligand binding to receptors such as Fas or TNF-related apoptosis inducing ligand (TRAIL) receptor, resulting in the recruitment of adaptor proteins, such as Fas-associated death domain (Fadd) or TNF receptor-associated death domain (TRADD), respectively, and activates pro-caspase-8 [97, 99]. The intrinsic pathway involves the mitochondria and caspase-9 as its main effector. Cytochrome

c is released from the mitochondria into the cytosol, which interacts with the caspase-activating protein Apaf-1 [97]. Apaf-1 is activated through binding of cytochrome c in the cytosol, which binds and cleaves pro-caspase-9, which in turn activates caspase-3 [97, 99]. Caspase-3 is responsible for cleaving kinases, DNA control proteins, cytoskeletal proteins, and endonuclease inhibitors [99]. This is a common endpoint pathway for both intrinsic and extrinsic pathways [99].

The mitochondria-dependent apoptosis pathway is governed by the Bcl-2 family of proteins, which contain both pro- and anti-apoptotic family proteins, and their relative amounts dictate the sensitivity of the cell to various apoptotic stimuli [97]. Variations in the amounts of these proteins are associated with pathological conditions, characterized by too much or too little cell death. Diseases associated with the dysregulation of the Bcl-2 family include: cancer, autoimmune disorders, immunodeficiency, and ischemia-reperfusion injury [97]. Bcl-2 and Bcl-XL proteins are antiapoptotic proteins and both are inappropriately overexpressed in many solid tumours, which contributes to resistance to chemotherapy- and radiation-induced apoptosis [97]. The Bax protein is pro-apoptotic and a tumour suppressor under normal conditions; however, loss-of-function mutations have been seen in human tumors [97].

1.7 Ribosomal RNA Biosynthesis and Degradation

Ribosomal RNA (rRNA) is an essential structural and catalytic component of the ribosome [100]. Ribosome biogenesis mainly takes place in a specialized compartment called the nucleolus [101]. Ribosomal biogenesis requires an enormous amount of energy; this, nevertheless, is required for continued protein biosynthesis within the cell [78]. Human ribosomes contain four RNA molecules, and two ribosomal subunits. The large subunit contains the 5S, 5.8S, and 28S ribosomal RNAs (rRNAs), and the small subunit contains the 18S rRNA

[37, 96]. The mature ribosomal subunits are very stable in the cytoplasm, and their rate of degradation is almost undetectable [102]. The 28S rRNA consists of highly conserved and divergent domains (D1 to D12) [98]. The divergent domains have no known function; however, there are certain subdomains that diverge faster than expected from random mutations, both in length and diversity. These domains make up almost half of the 28S rRNA in higher eukaryotes, but do not appear to be necessary for protein synthesis [98].

Intact rRNA is essential for the correct ribosomal function and cell survival [37]. The level of rRNA must be balanced through biosynthesis and degradation for cell homeostasis and function. An increase in rRNA caused by increased synthesis or decreased degradation can be oncogenic [100]. The degradation pathways for human rRNA during cellular processes, such as stress, cell cycle, and apoptosis, remain unclear [100].

rRNA accounts for 80-90% of the total RNA within a cell, and the synthesis of rRNA accounts for the majority of transcriptional activity in growing cells [78]. Pre-rRNA is transcribed by RNA polymerase I as a polycistronic mRNA, which encodes three out of the 4 rRNAs. Pre-rRNA is synthesized as 47S RNA, which is processed through several cleavages and modifications before assembling into the ribosomes [78, 102]. There are three main categories of RNA-degrading enzymes (termed ribonucleases or RNases): endonucleases that cleave RNA internally, 5’ exonucleases that hydrolyze RNA from the 5’end, and 3’exonucleases that hydrolyze RNA from the 3’end [102]. The pre-rRNA undergoes processing beginning with rapid endonuclease cleavage in the 5’ transcribed spacer region, followed by further cleavages external to or within the transcribed spacer region [78, 102].

DuRose *et al.* (2009) found pre-rRNA decreased rapidly after Tpg treatment and decreased 3-fold after two hours. In PERK-KO cells, the level of pre-rRNA did not change after

Tpg treatment for four hours. However, the levels of pre-rRNA in PERK-KO cells was similar to wildtype cells after 12 hours, but the cells were still viable [78]. In addition, cells treated with Tpg had decreased amounts of nuclear RNA, with the 28S and 18S rRNAs decreasing within an hour and further falling to barely detectable levels within three hours. The decrease in the 18S and 28S rRNAs is likely due to the lack of pre-rRNA available for processing within the nucleus [78].

There are different types of RNA granules in cells that are classified based on their composition, subcellular localization, cell origin, response to stimuli, dynamic behaviour, and their proposed function [103]. Some types of RNA granules include stress granules, P-bodies, germ granules, neuronal granules, and nuclear paraspeckles [103]. Stress granules and P-bodies are the most well studied and understood, and are associated with various diseases [103].

Stress granules are cytoplasmic, non-membranous structures composed of mRNAs and proteins, which include translation initiation factors (eIF2, eIF3, eIF4E, and eIF4G), 48S preinitiation complexes (small but not large ribosomal subunits), translationally stalled mRNAs, and RNA-binding proteins associated with RNA metabolism [103-105]. The 48S complexes are the core of stress granules, but mRNA-associated RNA-binding proteins are needed to mediate stress granule formation [103]. RNA provides the scaffolding for RNA-binding proteins to form protein-protein interactions required for the assembly of stress granules [106]. Some specific proteins involved in stress granule assembly are TIA1, G3BP1, and ATXN2 [106]. The protein and RNA composition of stress granules is in dynamic equilibrium with polysomes, and will stabilize and destabilize depending on the different drugs [104, 105].

Stress granules are not seen in cells under normal conditions, unlike other RNA granules. However, stress granules are rapidly assembled under stress conditions (~ 30 minutes) and

rapidly disperse after the stressor is removed [103, 105]. The stress granules form in response to signalling pathways, such as phosphorylation of eIF2α by stress-induced kinases, such as PERK, and through polysome disassembly [103-105]. When eIF2α is phosphorylated, there are lower levels of ternary complexes, which leads to inhibition of translation initiation, except for select mRNAs with uORFs in the 5'UTR, such as ATF4 [103]. Ribosomes already in the process of translation continue, run off the polysomes, resulting in translationally stalled 48S pre-initiation complexes that lack initiation factors [103]. Some of the mRNA derived from disassembled polysomes arranges into stress granules [104].

Stress granules are part of the integrated stress response and promote adaptation and survival during stress conditions [103]. Stress granules are interesting because they play a role in the stress response and gene regulation, and their formation can influence tumour progression and viral infection [106]. Stress granules recruit various signalling molecules in response to stress [103]. During stress, cells reallocate mRNA metabolism from encoding "housekeeping" proteins to the translation of mRNAs encoding chaperones and enzymes required for cellular repair [105].

One study found that stress granules were not degraded even after extensive treatment with RNase, which implies that this is not part of RNA disruption which can be induced through RNase treatment [106]. There is no evidence that rRNA is part of stress granules, which implies they are not part of RNA disruption, but the pathways associated with stress granules may impact RNA disruption induction.

1.7.1 RNA Degradation

There are many encoded RNases whose functions and targets overlap, as well as their targets. Such redundancy indicates a robustness and efficiency required for RNA degradation

pathways [102]. In addition to RNases, there are RNA helicases that translocate along nucleic acids and disrupt secondary structures and bound molecules. RNA helicases participate in pathways involved in RNA processing and degradation [102]. There are also chaperones that promote interactions with the RNA, which help to regulate the degradation of RNA [102].

There are different classes of RNA degradation, such as processing, regulated turnover of mRNAs and non-protein-coding RNAs, and quality control [102]. The regular and regulated turnover of mRNAs is one factor in the control of gene expression [102]. As well, the surveillance and identification of defective rRNA and rRNA complexes for degradation maintains the integrity and efficiency of the ribosome [102].

LaRiviere *et al.* (2006) created the term nonfunctional rRNA decay (NRD), which is a quality control mechanism in budding yeast that targets the RNA component in mature ribosomal subunits [107]. There are other known surveillance pathways, but NRD specifically acts on mature rRNAs, which may therefore be a major contributor to RNA disruption [107]. In yeast, there are two distinct pathways for NRD: mutated 18S rRNA in P bodies, and 25S (28S human equivalent) in perinuclear foci in the cytoplasm [100].

Wen *et al.* (2012) demonstrated that eukaryotic initiation factor 3 subunit f (eIF3f) directly interacted with heterogeneous nuclear ribonucleoprotein K (hnRNP K) to coordinate rRNA degradation. hnRNP K is an essential RNA and DNA binding protein, which dissociates from rRNA during stress allowing rRNA to be degraded [100]. eIF3f is a negative regulator of protein translation. The direct interaction of eIF3F with hnRNP K resulted in the dissociation from rRNA and a non-apoptotic rRNA decrease. However, eIF3f also interacted with hnRNP K during apoptosis [100].

The 28 rRNA and the associated proteins has been shown to be degraded in apoptotic cells induced by DOX treatment [108, 109]. Three ribosomal proteins were observed to be degraded in Jurkat cells, unlikely by caspases as they do not contain any of the sequences recognized by caspases [108]. A different ribosomal protein was seen to be degraded in a human breast carcinoma cell line, which may indicate cell-type specificity [108]. This event occurs at relatively early stages of apoptosis via both caspase-dependent and -independent mechanisms [108]. Interestingly, the decrease in protein translation was detected before the degradation of the ribosomal proteins, indicating their degradation is the cause of protein translation inhibition [108]. However, the degradation of the 28S rRNA occurred at the same time as the decrease in protein synthesis, indicating the ribosomal protein degradation is not as important as the structural changes for protein synthesis [96, 108]. The activation of nucleases leading to the degradation of DNA and RNA has been proposed to be an irreversible commitment step in the induction of apoptosis [96]. Another study used dexamethasone, anisomycin, and A23187 (a glucocorticoid and calcium ionphore), which all showed a similar pattern of 28S rRNA fragmentation [96].

Under starvation conditions, mature ribosomes can be sequestered by vacuoles and degraded in a process similar to autophagy termed ribophagy [102]. Ribosomes have been used as a marker of bulk, non-selective cytoplasmic degradation. They were among the first components detected inside the autophagosomes [110]. In ribophagy, the large and small ribosomal subunits and the ribosomal proteins are targeted for degradation independently. They are processed in the lysosomes during the ribophagy-mediated degradation, which may be a major source of amino acids and nucleotides [110]. It is possible that RNA disruption is part of some or none of these specific RNA degradation or cellular stress signalling pathways.

1.8 Study Design and Hypothesis

Due to the nature of transcription factors, such as their response to cellular stress and potential involvement in more than one signalling pathway, their activation could be an early event in the process of RNA disruption. I hypothesize that stress-induced transcription factors are activated (translocated) in A2780 cells after treatment with chemotherapy drugs and this is associated with the induction of RNA disruption induction downstream. I further hypothesize that their translocation to the nucleus precedes both RNA disruption and cell death.

Experimental objectives:

1) To identify stress-induced transcription factors that may be involved in the induction of RNA disruption through transcription factor profiling array plates and analysis of the results.
2) To obtain nuclear and cytoplasmic extracts from stressed and unstressed cells with minimal contamination with cytoplasmic proteins and nuclear proteins, respectively.
3) To monitor the kinetics of activation/translocation of specific stress-induced transcription factors in response to particular chemotherapy agents and stressors at specific timepoints
4) To determine whether there is a temporal association between the activation/translocation of specific stress-induced transcription factors and the induction of RNA disruption in cells when treated with particular chemotherapy agents and stressors, i.e. does translocation proceed, accompany, or follow RNA disruption.

2.0 Materials and Methods

2.1 Cell Culture

The human ovarian cancer cell line A2780 (ECACC 93112519) was obtained from the European Collection of Authenticated Cell Cultures (ECACC, Salisbury, UK). The A2780 cell line was cultured in RPMI-1640 medium containing 10% fetal bovine serum (FBS) and were incubated at 37°C with 5% CO_2. The cells were not grown to more than 70-80% confluency at any passage to ensure the cells were not stressed before the experiments began.

2.2 Assessment of Transcription Factors Induced Through DXL Treatment

2.2.1 Chemotherapy Agents and Treatments Used to Prepare Nuclear Extracts for the Transcription Factor Profiling Plate Arrays

Drugs known to induce RNA disruption as described previously by Narendrula *et al.* were used for the nuclear and cytoplasmic extracts [111]. Docetaxel (DXL) was used at a concentration of 0.2μM for the nuclear extracts used on the transcription factor array plates, as this was shown to produce optimal RNA disruption [111]. DXL was diluted 1000 times in 1X Phosphate Buffer Saline (PBS), and the appropriate volume was added to fresh media before adding to the cells 24 hours after plating. Cells were incubated in the DXL-treated media for 8 hours, to study the effect on a large variety of stress-induced transcription factors, and 48 hours to confirm RNA disruption in these cells. 1X PBS was made from 10X PBS (0.067M PO_4; GE Healthcare Life Sciences, Logan, Utah).

Docetaxel and doxorubicin were obtained from Health Sciences North Northeast Cancer Center pharmacy (Sudbury, Ontario).

2.2.2 Nuclear and Cytoplasmic Extractions Using Signosis Kits for Transcription Factor Profiling Plate Arrays

Initially, the nuclear and cytoplasmic extracts were made using the Nuclear Extraction Kit (SK-001, Signosis, Santa Clara, CA, USA). Cells were seeded at 2,000,000 cells on two 100mm plates per treatment at passage 8. Cells were treated 24 hours after plating with 0.2μM DXL alongside an untreated control. Cells were treated for 8 hours. Media and floating cells were collected from the plates and placed into a 15mL conical tube and centrifuged at 700 x g for 5 minutes. The supernatant was removed, and the pellet was resuspended with 1mL of cold 1X PBS and centrifuged at 700 x g for 5 minutes. The supernatant was removed with a pipette. Adhered cells on the plates were washed with 3mL of 1X PBS. Buffer I (proprietary hypotonic solution) was added to the pellets and the cells on the plates, which were placed on a shaking platform at 4°C for 15 minutes. Adhered cells were collected from the plates by scraping and combined with the pellet in a 2mL microcentrifuge tube. The tube was centrifuged at 12,000rpm for 5 minutes at 4°C. The supernatant (cytoplasmic extract) was collected and placed in a 1.5mL microcentrifuge tube. The cytoplasmic extract was stored at -80°C until further use. Buffer II (proprietary hypertonic solution) was added to the pellets, which were placed on a shaking platform at 4°C for 2 hours. The pellet was not resuspended, but the tube was tapped gently to mix. After 2 hours, the tubes were centrifuged at 12,000rpm for 5 minutes at 4°C. The supernatant (nuclear extract) was transferred to a 0.5mL microcentrifuge tube. The nuclear extract was stored at -80°C until further use.

Protein quantifications were done using the Bradford Assay. The Bradford reagent was made in-lab [112]. Protein quantifications were done in sextuplicate for accuracy. Further

confirmation of protein quantification accuracy was done by using a Coomassie stained 12% polyacrylamide gel.

Three nuclear and cytoplasmic biological replicate extracts were made. The nuclear extracts were used on the transcription factor profiling arrays.

2.2.3 Transcription Factor Activation Profiling Arrays

Transcription factor activation profiling array kits were purchased from Signosis (Santa Clara, CA, USA). Transcription factor arrays purchased were: ER Stress (UPR) TF Activation Profiling Plate Array (FA-1006), Mitochondrial UPR TF Activation Profiling Plate Array (FA-1010), and TF Activation Profiling Plate Array II (FA-1002).

The ER Stress UPR TF Activation Profiling Plate Array had 16 different transcription factors repeated six times on the 96-well plate. The Mitochondrial UPR TF Activation Profiling Plate Array had 16 different transcription factors repeated six times on the 96-well plate. The TF Activation Profiling Plate Array II had 96 different transcription factors on the 96-well plate with a second plate containing the same transcription factors to use as a control plate. There were 2 transcription factors that were the same between ER Stress Plate and Mitochondrial UPR plate: ATF4 and CHOP. There were 5 transcription factors that were the same between the ER Stress Plate and the TF II Plate: YY1, FOXO1, CBF, IRF, and HNF4. There were 7 transcription factors that were the same between Mitochondrial UPR and TF II: CEBP, E2F1, HIF, HSF, MEF2, NRF1, and SATB. There were 5 transcription factors that appeared on all 3 of the profiling plate arrays: XBP1, AP1, p53, NFκB, and NRF2. Therefore, there was a total of 104 transcription factors analyzed.

Before beginning, the Filter Binding Buffer, Filter Wash Buffer, and water were placed on ice for at least 10 minutes, and the TF Plate Hybridization Buffer and Hybridization Wash Buffer were placed in a water bath at 42°C for at least 30 minutes.

10µg of nuclear extract made using the Nuclear Extraction Kit from Signosis was mixed with 15µL of Transcription Factor Binding Buffer Mix, 3µL of Transcription Factor Probe Mix, and water up to a total volume of 30µL, which was incubated at room temperature for 30 minutes. 200µL of chilled Filter Binding Buffer was added to the filter of each of the isolation columns to equilibrate the column, which was centrifuged at 6000rpm for 1 minute and the flow-through discarded. The total 30µL of probe-nuclear extract mix was added to the columns and incubated on ice for 30 minutes. 500µL of Filter Wash Buffer was added to the columns and incubated for 3 minutes on ice. The columns were centrifuged at 6000rpm for 1 minute at 4°C and the flow through discarded. This was repeated 3 additional times. 50µL of Elution buffer was then added to the columns and incubated at room temperature for 5 minutes. The probe-transcription factor complex was eluted from the column into a 1.5mL microcentrifuge tube by centrifugation at 10,000rpm for 2 minutes at room temperature. The flow through was transferred to a PCR tube and denatured at 98°C for 5 minutes and immediately transferred to 200µL of cold water kept on ice. 2mL of warmed Transcription Factor Plate Hybridization Buffer was added to a dispensing reservoir and 200uL of the denatured probe mix was added to it. A multi-channel pipette was used to add 100µL of the mixture to the corresponding wells. The plate was sealed with an aluminum adhesive and kept in an incubator at 42°C overnight.

The next day the adhesive was removed, and the contents of the plate were expelled over a waste container. The plate was washed with 200µL of warmed Plate Hybridization Wash Buffer 3 times for 5 minutes with gentle shaking at each wash and complete removal from the

plate by tapping on paper towel. 200µL of Blocking Buffer was added to the plate for 5 minutes with gentle shaking and removed over a waste container. 20µL of Streptavidin-Horseradish Peroxidase (HRP) Conjugate was diluted in 10mL of Blocking Buffer. Finally, 95µL of diluted Streptavidin-HRP Conjugate was added to each well, and incubated at room temperature for 45 minutes with gentle shaking. The contents were removed, and the plate was washed with 200µL of Detection Wash Buffer 3 times for 5 minutes with gentle shaking at each wash, and decanted after each wash. 95µL of a proprietary Substrate Solution was added to each well and incubated for 1 minute. The luminescence was read using a Synergy H4 Hybrid Multi-Mode Microplate Reader (BioTek). The integration time was set to 1 second with no filter, and the luminescence was measured in relative light units (RLUs) at 5, 10, 15, and 20 minutes.

2.2.4 RNA Extraction

A2780 cells were plated at a seeding density of 150,000 cells on 60mm plates. Cells were treated 24h later with the stressor at the same dosage used for the nuclear and cytoplasmic extractions. RNA was extracted from the cells 48h later initially alongside the Signosis nuclear extractions used for the transcription factor profiling arrays.

Media was removed from the plates and placed in a corresponding 15mL conical tube. Adherent cells were washed with 2mL of 1X PBS and the wash was transferred into the corresponding 15mL tube. The tubes were spun at 500 x g for 5 minutes. 350µL of proprietary RLT buffer containing 0.01% β-mercaptoethanol was dispensed onto the adherent cells and the cells were scraped. Once the 15mL tubes were done centrifugation, the supernatant was removed, the pellets were washed in 5mL PBS, and centrifuged at 500 x g for 5 minutes. Once centrifugation was complete, the supernatant was removed. The scraped cells were transferred into the 15mL tube using a 21-gauge needle and 1mL syringe, and the solution was aspirated 5

times and transferred into a 1.5mL centrifuge tube. An equal volume of 70% ethanol to RLT buffer was added to the tube and mixed. 700µL of the solution was transferred onto a RNeasy spin column inside a 2mL collection column. The spin column and collection tube were spun at 12,000 x g for 15 seconds. This step was repeated if the volume of solution in the 1.5mL centrifuge tube exceeded 700µL. The flow-through was discarded. 700µL of proprietary RW1 buffer was added to the RNeasy spin column and centrifuged at 12,000 x g for 15 seconds. The flow-through was discarded. 500µL of proprietary RPE buffer was added to the spin column and centrifuged at 12,000 x g for 15 seconds. The flow-through was discarded. Another 500µL of RPE buffer was added to the spin column and centrifuged at 12,000 x g for 2 minutes. The RNeasy spin column was then placed on a new 2mL collection tube and centrifuged at 17,000 x g for 1 minute. The spin column was then placed on a RNase-free 1.5mL centrifuge tube, 35µL of RNase-free water was added to the spin column and centrifuged at 12,000 x g for 1 minute. The eluent was then placed back on the spin column and centrifuged at 17,000 x g for 1 minute. A 5µL aliquot was made for analysis on the Agilent 2100 Bioanalyzer using the Agilent RNA 6000 Nano Kit (Agilent Technologies, Santa Clara, California), which uses capillary electrophoresis to produce virtual gel images and electropherograms.

2.3 Translocation Kinetics of Specific Stress-Induced Transcription Factors

2.3.1 Chemotherapy Agents and Treatments Used to Prepare Nuclear Extracts for the Study of Translocation Kinetics of Stress-Induced Transcription Factors

In the studies involving the translocation kinetics of the transcription factors, thapsigargin, a chemical known to induce ER stress, was used at 0.5µM. This concentration was shown to induce some RNA disruption (unpublished data). Thapsigargin (T9033-1MG, Sigma-Aldrich, St. Louis, Missouri) is dissolved in DMSO to a 1mM stock concentration. Therefore, a

DMSO vehicle control was plated alongside the thapsigargin treated cells. Starvation was used as a stressor as well, using 15% media and 85% 1X PBS. Cells were incubated in thapsigargin and starvation conditions for 0, 2, and 16 hours, as Martina *et al.* showed similar conditions induce the translocation of TFEB and TFE3 at these times [51]. DOX was used at a concentration of 0.5μM, which was shown to cause some RNA disruption (unpublished data). DXL was used at the same concentration as previous experiments but was shown to cause less RNA disruption than previously seen. Cells were treated with DOX and DXL for 0, 16, and 24 hours. Adjacent RNA disruption assays with the same doses of stressors were treated for 72 hours.

2.3.2 Nuclear Fractionation Protocol Modified from Abcam for Western Blotting

After learning the Nuclear Extraction Kit did not generate the expected enrichment of cytoplasmic and nuclear extracts, a new protocol was developed from Abcam's Nuclear Fractionation protocol. Cells were seeded at 2,500,000 cells on three 100mm plates per treatment. Cells were treated 24 hours after plating. Cells were treated for 0h, 2h, and 16h for the thapsigargin and starvation treatments. Cells were treated for 0h, 16h, and 24h for the DXL and DOX treatments. Plates were placed on ice. Media and floating cells were removed from the plates. Adhered cells were washed with 5mL of 1X PBS. Buffer A (10mM HEPES, 1.5mM $MgCl_2$, 10mM KCl, 0.5mM DTT, 0.05% NP40, pH 7.9) was added to the adhered cells on the plate for 10 minutes on ice. Lysed cells were collected by scraping and centrifuged at 3000rpm for 10 minutes at 4°C. The supernatant (cytoplasmic portion) was removed and placed into a new tube. The pellet surface was washed three times using 100μL of Buffer A, then submerged in 400μL of Buffer A, and centrifuged again at 3000rpm for 10 minutes at 4°C. The wash supernatant was removed and discarded.

The pellet was resuspended in 400µL of Buffer B (5mM HEPES, 1.5mM $MgCl_2$, 0.2mM EDTA, 0.5mM DTT, 26% glycerol (v/v), pH 7.9) and a final concentration of 400mM NaCl to help lyse the membranes. The solution was then placed into a 7mL Dounce homogenizer and homogenized with 20 full strokes using pestle A on ice. The homogenate was left on ice for 30 minutes, after which the homogenate was spun at 21,100 x g for 20 minutes at 4°C. The supernatant (nuclear portion) was removed and placed into a new tube. The cytoplasmic and nuclear portions were both respun at 21,100 x g for 20 minutes at 4°C to ensure no cytoskeleton or membrane was remaining. The total volumes of each fraction were noted.

Protein quantifications were done using the Bradford assay.

The samples for western blotting were normalized according to their specific extraction volumes. There was generally about 2-fold more cytoplasmic fraction than the nuclear fraction. 30µg of quantified cytoplasmic protein was used, and roughly 2-fold less nuclear protein was used (specific to the volumes noted at each extraction). The difference in volume in the nuclear sample was supplemented with Buffer B, which is the buffer the nuclear sample was suspended in.

2.3.3 Time and Dosage Optimization Experiments

To determine the optimal timing and dosage for transcription factor translocation, cytoplasmic and nuclear extracts were made using the modified Abcam protocol. Cells were treated using doxorubicin at 0.1µM and 0.5µM for 0h, 0.5h, 2h and 6h. The cytoplasmic and nuclear extracts were assessed using Western blotting to ensure enriched extracts were being obtained. Histone H3 (Cell Signalling Technology, #9715) and GAPDH (Santa Cruz Biotechnology; sc-32233) were used as loading controls and to test how enriched the nuclear and

cytoplasmic extracts were, respectively. Transcription factor YY1 (Santa Cruz Biotechnology; H-10 sc-7341) was also used as a positive nuclear control due to complete localization in the nucleus, and more consistency than histone H3.

2.3.4 Western Blotting and Antibodies

4X Laemmli sample buffer (277.8mM Tris-HCl, 44.4% (v/v) glycerol, 4.4% SDS, 0.02% bromophenol blue) was added to each of the samples for a total concentration of 1X and boiled for 5 minutes. Samples were loaded into 10% SDS-PAGE gels and ran at 110V for an hour and a half. Proteins were transferred to 0.45µm nitrocellulose blotting membrane (GE Healthcare Life Sciences, Germany) at 12V for an hour and a half using a Bio-Rad Trans-Blot Semi-Dry Transfer Cell unit. Transfer of proteins was confirmed using Ponceau S. stain (0.1% Ponceau S (w/v), 1% acetic acid) and the stain was removed using 0.1% Tris-Buffer Saline (20mM Tris, 150mM NaCl) (TBS) with 0.1% Tween (TBST). Membranes were blocked in 5% milk in 0.1% TBST for 1 hour. After 1 hour, membranes were placed in 5mL of primary antibody overnight at 4°C with shaking. GAPDH (1:1000), H3 (1:1000), YY1 (1:200), Nrf2 (Santa Cruz Biotechnology; sc-365949), TFE3 (Sigma Atlas Antibodies; HPA023881) (1:700), TFEB (Abcam) (1:600).

The next day, the membranes were washed three times for 5 minutes using 0.1% TBST with shaking during each wash. Secondary HRP-conjugated antibody was added to the membranes for one hour. Anti-rabbit and anti-mouse were used at a dilution of 1:10,000 except for YY1 (rabbit; 1:3000) and TFE3 and TFEB (rabbit; 1:8000). Membranes were exposed using SuperSignal™ West Pico PLUS Chemiluminscent Substrate (Thermo Fisher, Cat.NO. 34080) and imaged using the Protein Simple GelDoc FluorChemQ software.

The densitometry values were obtained using the GelDoc FluorChemQ software.

2.3.5 RNA Extraction

In further studies, cells were plated for an RNA extraction concurrently with the cells plated for a nuclear extraction, and RNA was extracted 72h later as better RNA disruption was demonstrated at this timepoint. RNA extractions were done using the RNeasy Mini Kit (Qiagen Laboratories, Mississauga, Ontario).

2.4 Statistical Analyses

Statistical analyses were performed using GraphPad Prism 5 software or SPSS Statistics. A p value of <0.05 was considered significant. Significant differences were determined using paired T-tests or one-tailed T-tests.

3.0 Results

3.1 Identifying Stress-Induced Transcription Factors

3.1.1 DXL treatment caused significant RNA disruption at 48 hours

In order to confirm that the A2780 cells being used for the nuclear extractions, which would subsequently be used on the transcription factor profiling arrays, were able to induce RNA disruption, an RDA analysis was conducted on DXL-treated cells for 48 hours. Since changes in gene expression can take place earlier than their resulting biological effects, identical preparations of cells were treated for 8 hours for subsequent nuclear and cytoplasmic extract preparations. The cells treated for 48 hours exhibited RNA disruption (Figure 1A), as can be seen by the significant difference in cellular RDI values between treated and untreated cells (Figure 1B). The concentration used for the preparation of nuclear extracts was 0.2µM DXL; this concentration induced significant RNA disruption (*p* value of <0.01).

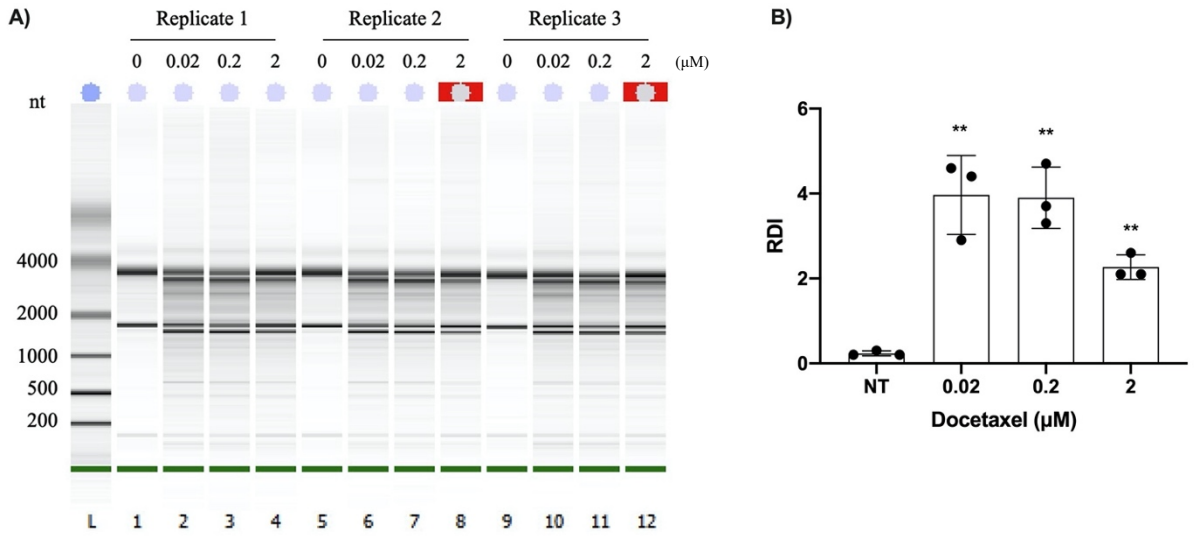

Figure 1. Effect of increasing doses of docetaxel (µM) on RNA disruption in A2780 ovarian cancer cells at 48 hours. (A) RNA gel image of three independent replicates treated with 0.02µM, 0.2µM, and 2µM docetaxel with a no treatment control. (B) RNA disruption index (RDI) analysis of three independent replicates. Error bars represent standard error. T-test, one-tailed (**p <0.01; n=3)

Table 1. Protein concentrations of nuclear extracts made using the Signosis protocol, as measured by the Bradford assay

	Nuclear Extract #1		Nuclear Extract #2		Nuclear Extract #3	
	NT	DXL	NT	DXL	NT	DXL
mg/mL	1.19 ± 0.05	1.02 ± 0.04	1.55 ± 0.14	1.17 ± 0.03	1.34 ± 0.05	1.48 ± 0.05

Note: Values denote mean ± SE

Table 2. Protein concentrations of cytoplasmic extracts made using the Signosis protocol, as measured by the Bradford assay

	Cytoplasmic Extract #1		Cytoplasmic Extract #2		Cytoplasmic Extract #3	
	NT	DXL	NT	DXL	NT	DXL
mg/mL	0.54 ± 0.01	0.71 ± 0.03	0.65 ± 0.03	0.67 ± 0.06	0.42 ± 0.16	0.29 ± 0.06

Note: Values denote mean ± SE

Since the cells showed RNA disruption, the nuclear and cytoplasmic extracts were quantified using a Bradford assay (Tables 1 and 2). The quantifications were performed using sextuplicate technical replicates. To confirm similar protein concentrations for the extracts and to compare their protein banding patterns, the 10µg protein samples were resolved by SDS gel electrophoresis and the gel stained with Coomassie Blue (Figure 2). The intensity and banding pattern were considered, as a different banding pattern of proteins would be expected between cytoplasmic and nuclear extracts. There appeared to be an increase in band intensity in replicate 3 of the cytoplasmic extracts (Figure 2B); however, only the nuclear extracts were used on the array plates, and they appeared uniform across all replicates (Figure 2A).

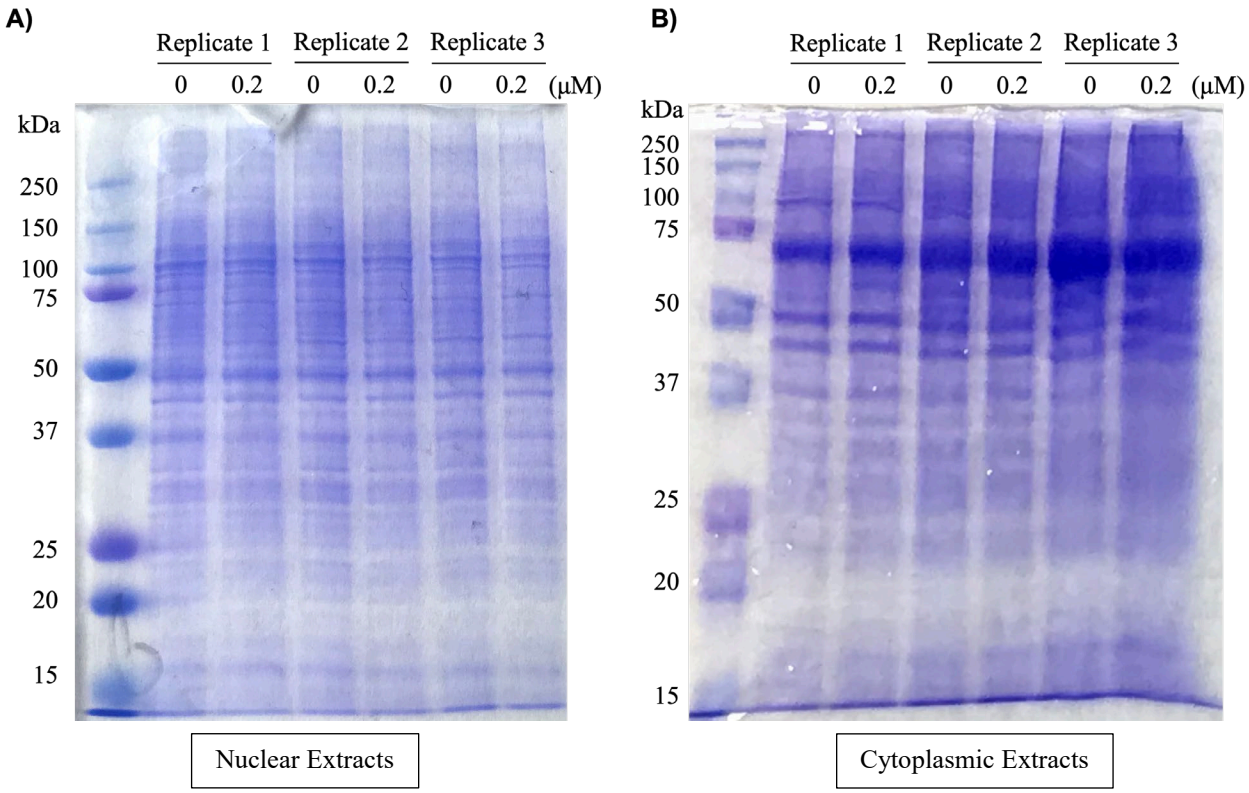

Figure 2. Coomassie blue stained gels of the nuclear and cytoplasmic proteins extracted using the Signosis Nuclear Extraction Kit on A2780 cells treated for 8 hours with 0.2μM DXL with a no treatment control (0μM). Protein quantifications from the Bradford assay and differences in protein (cytoplasmic versus nuclear) banding patterns were visually confirmed with these gels. A) 10μg of nuclear proteins as determined by Bradford assay. B) 10μg of cytoplasmic protein as determined by Bradford assay.

3.1.2 Transcription Factor Activation Profiling Plate Arrays

In order to determine transcription factors of interest that may play a role in RNA disruption, Signosis' Transcription Factor Activation Profiling Plate Arrays were used with the previously prepared nuclear extracts. There are many different transcription factors that can be activated by cellular stress, such as ER stress and mitochondrial stress. Two types of arrays used were associated with ER stress- and mitochondrial stress-induced transcription factors. A third type of array used contained 96 different transcription factors. The arrays measure transcription factor activity through their ability to bind specific sequences of DNA. Activated transcription factors, which are found in the nucleus, bind to DNA probes matching their binding sequences. The probes were denatured, and the amount of probe bound to the complimentary sequence on the array was deemed to be relative to the amount of activated transcription factor. In this study, nuclear extracts of A2780 cells treated with DXL or left untreated as a control were used on the arrays. This allowed for a direct comparison of the amount of activation of certain transcription factors between the DXL-treated and the untreated samples.

In total, with overlap between arrays, there were 104 transcription factors analyzed (see Appendix Table 6). There was a lot of variation between technical replicates on the same array plate, between the same types of arrays, as well as between different arrays. This created difficulties when analyzing the data and specific criteria were used to determine the best stress-induced transcription factors to investigate further.

3.1.2.1 Mitochondrial Stress Array Plate

Stress-induced transcription factors were investigated using nuclear extracts from cells treated with 0.2μM DXL for 8 hours or from untreated control cells. The first set of transcription factors investigated were associated with mitochondrial stress using Signosis' Mitochondrial

UPR TF Activation Profiling Plate Array (Figure 3). There were three biological replicates performed on one plate with technical replicates done on a second.

Due to the opposing patterns of DNA binding activity compared with the no treatment within the replicates, when the mean of the data was used there was a large standard error (SE) which resulted in large error bars (Figure 3G). There was no statistical significance among the biological replicates. E2F1 showed a slight decrease in activity compared to the no treatment, FOXO3 showed a decrease in activity compared to no treatment, Nrf2 had slightly increased activity although the strength of signal is weak, SATB had a slight decrease in activity, TFEB showed a slight increase in activity compared to no treatment, and XBP showed a slight increase in activity compared to no treatment (Figure 3G).

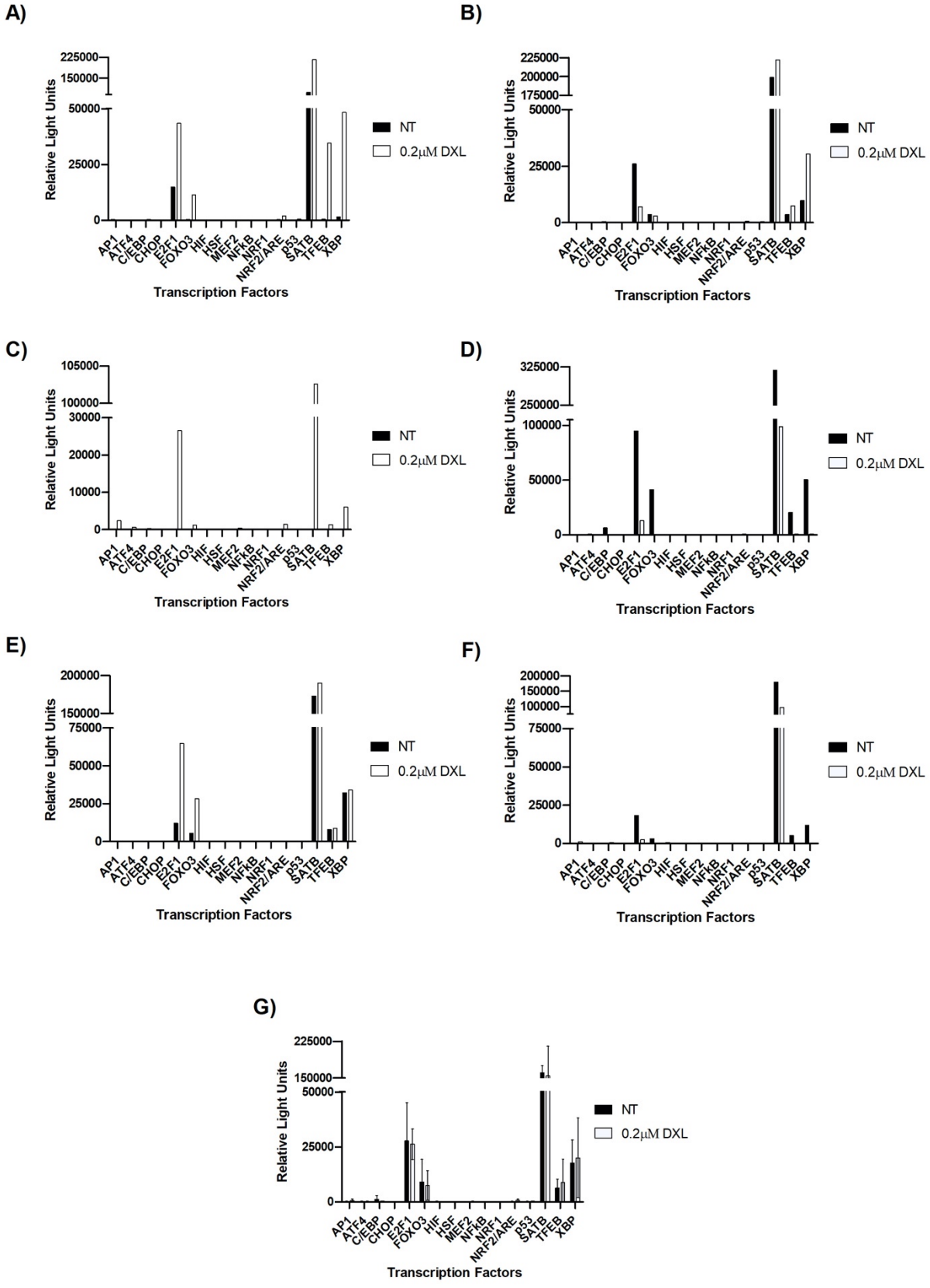
A)
B)
C)
D)
E)
F)
G)
Relative Light Units
Transcription Factors
NT
0.2μM DXL
AP1
ATF4
C/EBP
CHOP
E2F1
FOXO3
HIF
HSF
MEF2
NFkB
NRF1
NRF2/ARE
p53
SATB
TFEB
XBP

Figure 3. Comparison of activated transcription factors in A2780 cells either treated with 0.2μM DXL or untreated for 8 hours measured in relative light units (RLUs). Transcription factors are related to the mitochondrial unfolded protein response as determined by the Signosis Mitochondrial UPR Transcription Factor Profiling Array. A) and B) Nuclear extraction biological replicate 1 in technical replicates. C) and D) Nuclear extraction replicate 2 in technical replicates. E) and F) Nuclear extract replicate 3 in technical replicates. G) Mean of all three biological replicates. T-test with a Wilcoxon Signed Rank test was performed with no significance (n=3).

3.1.2.2 ER Stress Array Plate

The second set of transcription factors that were investigated were associated with ER stress and UPR using Signosis' ER Stress (UPR) TF Activation Profiling Plate Array (Figure 4). Three biological replicates were used on this plate, with no technical replicates.

Similar to the Mitochondrial UPR plate arrays, when the means of the data were used to display the data there were large error bars due to the opposing patterns of DNA binding activity between replicates (Figure 4D). The transcription factors XBP1, ATF4, ATF6, CBF/NFY, SREBP1, YY1, PGC-1α, ATF3, AP-1, p53, and NFκB had a decrease in activity compared to no treatment. The only transcription factor with moderate or strong signals that had an increase in activity was Nrf2 (Figure 4D).

A paired T-test and the non-parametric Wilcoxon Signed Rank test were performed, and there were no significant differences found in the data between the DXL treated and untreated samples.

CHOP and ATF4 appear on both Mitochondrial UPR and ER Stress plate arrays (Figure 3 and 4). CHOP only produced very weak signals in both arrays (Figure 3 and 4). ATF4 had a weak signal in biological replicate 2 on the Mitochondrial Stress plate (Figure 3C) and produced moderate signals in biological replicates 1 and 2 on the ER stress plate (Figure 4A and B). Using all replicates available between arrays and plates, another T-test was performed, and no significant differences were found between the DXL treated and untreated samples for these transcription factors.

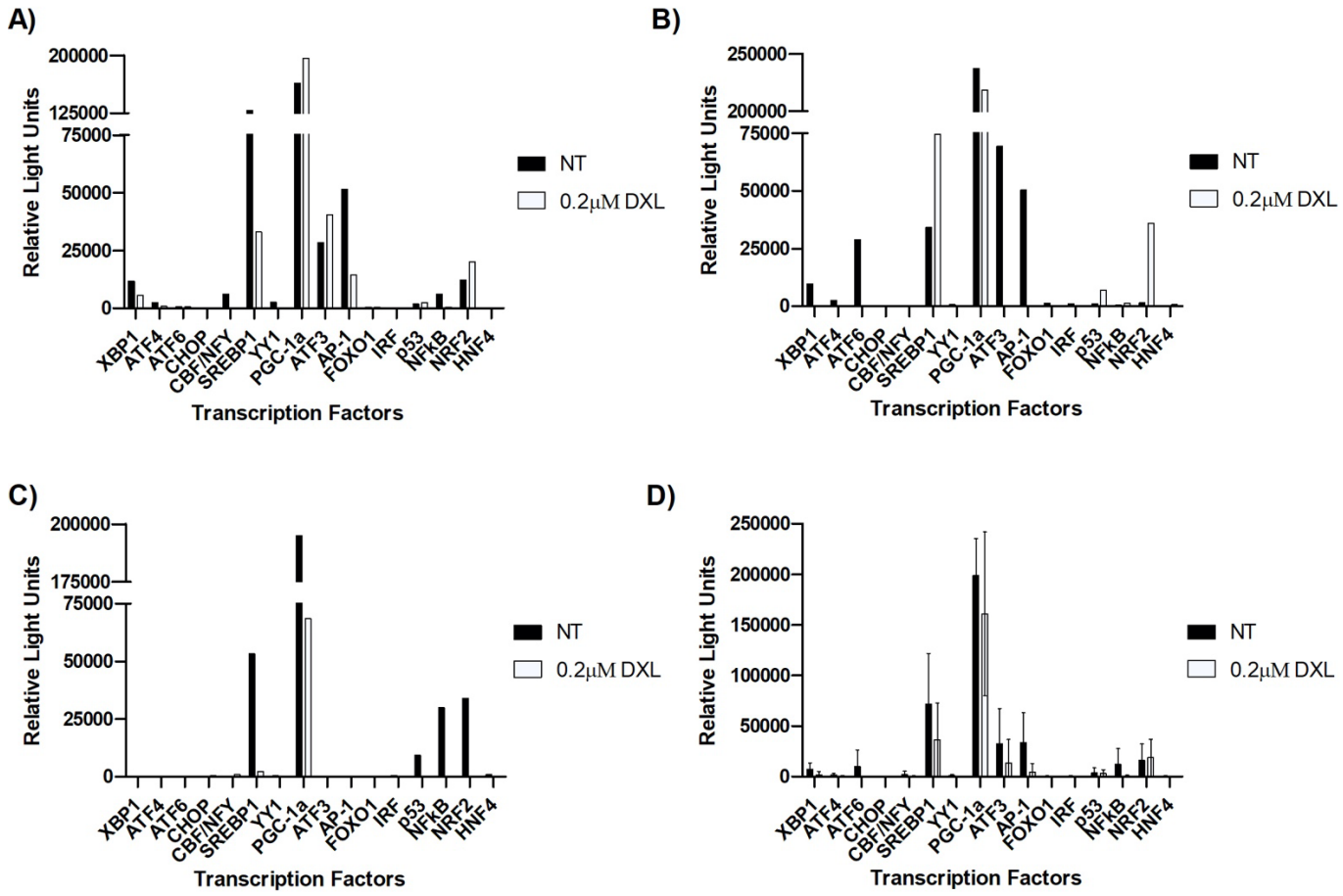

Figure 4. Comparison of activated transcription factors in A2780 cells either treated with 0.2μM DXL or untreated for 8 hours measured in relative light units (RLUs). Transcription factors are related to the ER stress response as determined by the Signosis ER Stress Transcription Factor Profiling Array. A) Nuclear extraction biological replicate 1. B) Nuclear extraction biological replicate 2. C) Nuclear extract biological replicate 3. D) Mean of all three biological replicates. T-test with a Wilcoxon Signed Rank test was performed with no significance (n=3).

3.1.2.3 TFII Array Plate

A set of 96-different transcription factors, some associated with known stress pathways, were also assessed for their activation by DXL in another transcription factor activity profiling array (Figure 5). Due to the variation seen between technical and biological replicates on the other arrays, only the first set of biological replicates was used for these plates using three technical replicates. This set of biological replicates was chosen as there seemed to be the most consistency between technical replicates for this set in the mitochondrial and ER stress arrays.

The definitions of strong, moderate and weak signals were redefined for the TFII array plates due to much weaker signals across all transcription factors compared to the mitochondrial and ER stress arrays. A strong signal was redefined as >1000 RLUs, a moderate signal was redefined as <1000 RLUs, and a weak signal was redefined as <200 RLUs.

When the mean of the technical replicates was used, there were similar issues with large error bars due to the opposing patterns of DNA binding activity of certain transcription factors compared to no treatment (Figure 5D). The transcription factors AP2, CAR, CREB, E2F-1, GR-PR, HIF, Myb, NFAT, NF-E2, Pax5, SRF, SATB1, STAT4, STAT5, TR, TFIID (Part I); AP3, AP4, FOXC1, FOXO1, FREAC2, Gfi-1, HNF, HSF, KLF4, Nkx3-5, OCT-1, Pax-2, RB, RNUX, and SMUC (Part II) had decreased activity compared to no treatment (Figure 5D). The transcription factors Brn-3, PPAR, PXR (Part I); COUP-TF, HOX4C, PIT1, PLAG1, ROR, RXR, SF-1, SOX9, VDR (Part II) had increased activity compared to no treatment (Figure 5D).

A T-test and Wilcoxon signed rank test were performed on the technical replicates. There were significant differences between the DXL treated and untreated samples for transcription factors CBF, PXR, SMAD, YY1 (Part I), MZF and MEF (Part II) (Figure 5D).

A)

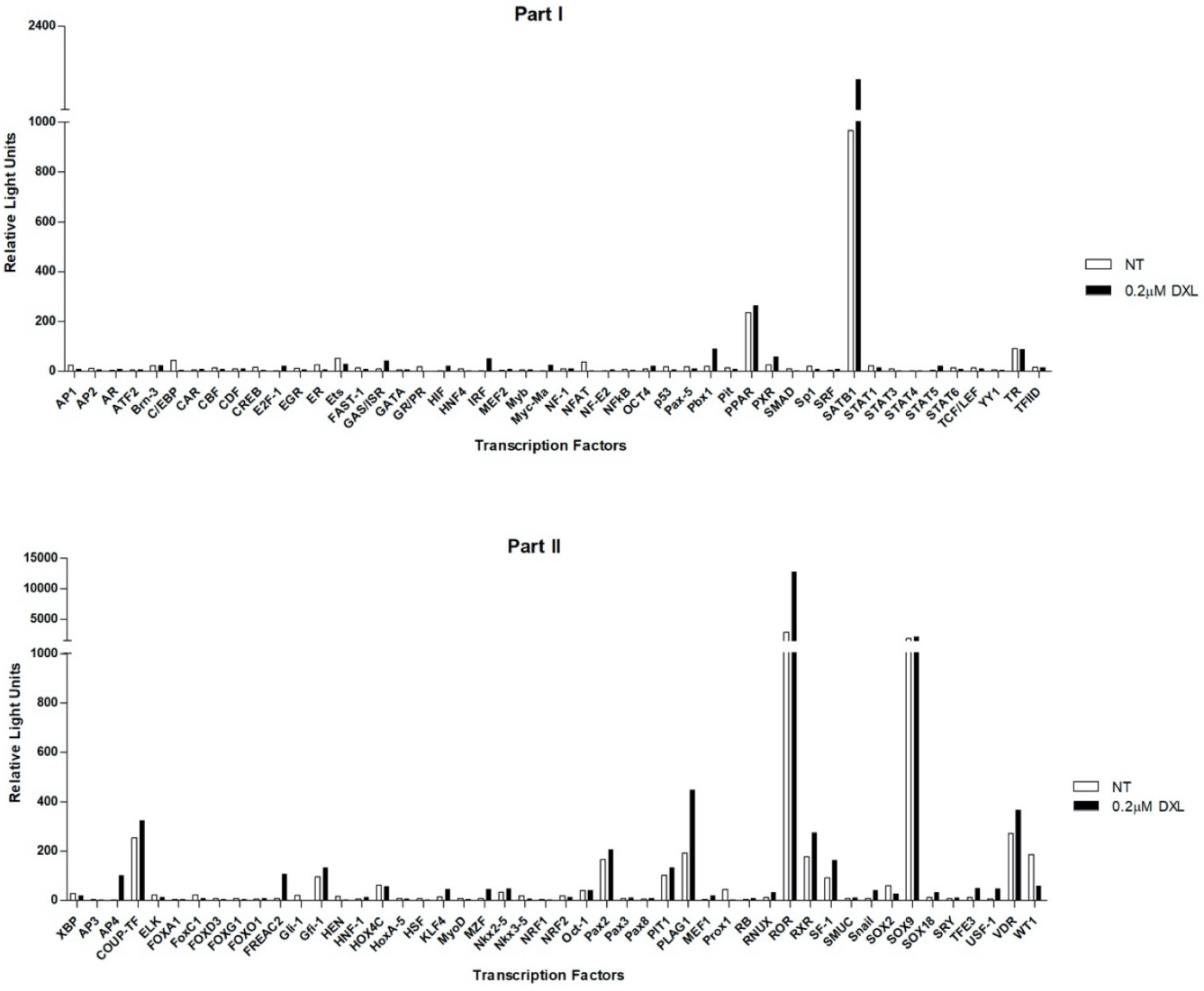
Part I
Relative Light Units
2400
1000
800
600
400
200
0
AP1 AP2 AR ATF2 Brn-3 C/EBP CAR CBF CDF CREB E2F-1 EGR ER Ets FAST-1 GAS/ISR GATA GR/PR HIF HNF4 IRF MEF2 Myb Myc-Ma NF-1 NFAT NF-E2 NFkB OCT4 p53 Pax-5 Pbx1 Pit PPAR PXR SMAD Sp1 SRF SATB1 STAT1 STAT3 STAT4 STAT5 STAT6 TCF/LEF YY1 TR TFIID
Transcription Factors
NT
0.2μM DXL
Part II
Relative Light Units
15000
10000
5000
1000
800
600
400
200
0
XBP AP3 AP4 COUP-TF ELK FOXA1 FoxC1 FOXD3 FOXG1 FOXO1 FREAC2 Gli-1 Gfi-1 HEN HNF-1 HOX4C HoxA-5 HSF KLF4 MyoD MZF Nkx2-5 Nkx3-5 NRF1 NRF2 Oct-1 Pax2 Pax3 Pax8 PIT1 PLAG1 MEF1 Prox1 RB RNUX ROR RXR SF-1 SMUC Snail SOX2 SOX9 SOX18 SRY TFE3 USF-1 VDR WT1
Transcription Factors
NT
0.2μM DXL

B)

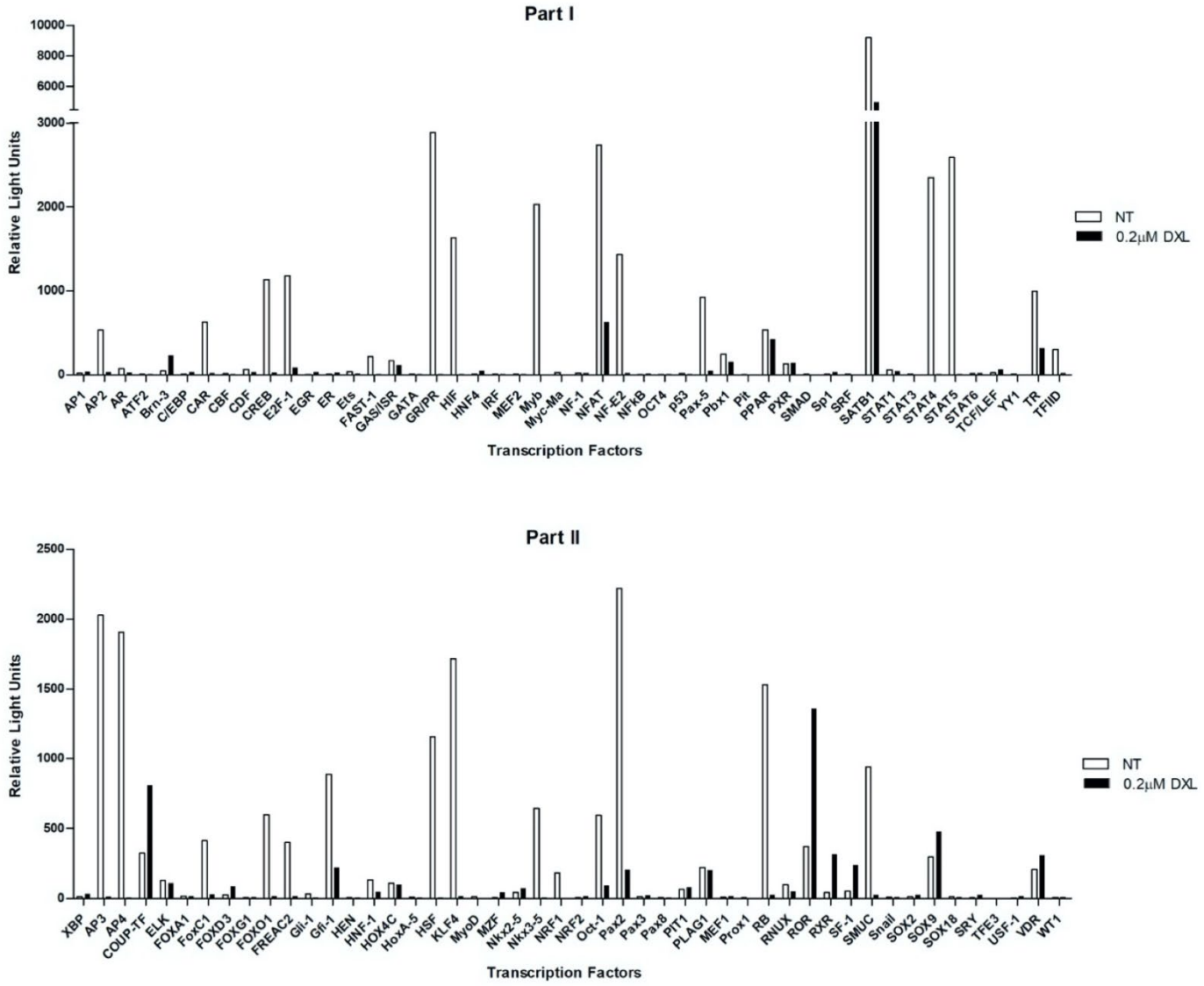
Part I
Relative Light Units
10000
8000
6000
3000
2000
1000
0
NT
0.2μM DXL
AP1 AP2 AR ATF2 Brn-3 C/EBP CAR CBF CDF CREB E2F-1 EGR ER Ets FAST-1 GAS/ISR GATA GR/PR HIF HNF4 IRF MEF2 Myb Myc-Ma NF-1 NFAT NF-E2 NFkB OCT4 p53 Pax-5 Pbx1 Pit PPAR PXR SMAD Sp1 SRF SATB1 STAT1 STAT3 STAT4 STAT5 STAT6 TCF/LEF YY1 TR TFIID
Transcription Factors
Part II
Relative Light Units
2500
2000
1500
1000
500
0
NT
0.2μM DXL
XBP AP3 AP4 COUP-TF ELK FOXA1 FoxC1 FOXD3 FOXG1 FOXO1 FREAC2 Gli-1 Gfi-1 HEN HNF-1 HOX4C HoxA-5 HSF KLF4 MyoD MZF Nkx2-5 Nkx3-5 NRF1 NRF2 Oct-1 Pax2 Pax3 Pax8 PIT1 PLAG1 MEF1 Prox1 RB RNUX ROR RXR SF-1 SMUC Snail SOX2 SOX9 SOX18 SRY TFE3 USF-1 VDR WT1
Transcription Factors

C)

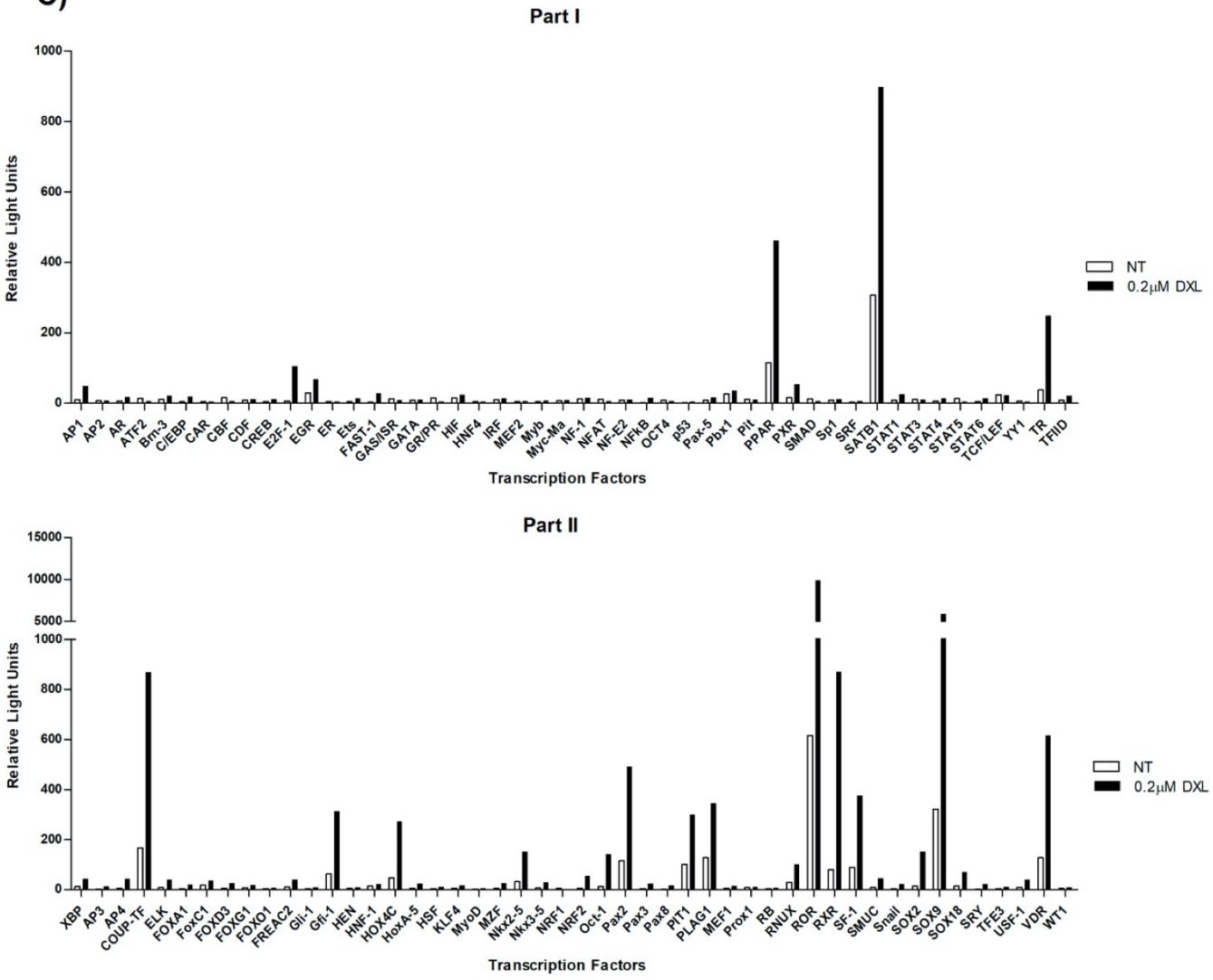
Part I
Relative Light Units
1000
800
600
400
200
0
AP1 AP2 AR ATF2 Brn-3 C/EBP CAR CBF CDF CREB E2F-1 EGR ER Ets FAST-1 GAS/ISR GATA GR/PR HIF HNF4 IRF MEF2 Myb Myc-Ma NF-1 NFAT NF-E2 NFkB OCT4 p53 Pax-5 Pbx1 Pit PPAR PXR SMAD Sp1 SRF SATB1 STAT1 STAT3 STAT4 STAT5 STAT6 TCF/LEF YY1 TR TFIID
Transcription Factors
NT
0.2μM DXL
Part II
Relative Light Units
15000
10000
5000
1000
800
600
400
200
0
XBP AP3 AP4 COUP-TF ELK FOXA1 FoxC1 FOXD3 FOXG1 FOXO1 FREAC2 Gli-1 Gfi-1 HEN HNF-1 HOX4C HoxA-5 HSF KLF4 MyoD MZF Nkx2-5 Nkx3-5 NRF1 NRF2 Oct-1 Pax2 Pax3 Pax8 PIT1 PLAG1 MEF1 Prox1 RB RNUX ROR RXR SF-1 SMUC Snail SOX2 SOX9 SOX18 SRY TFE3 USF-1 VDR WT1
Transcription Factors
NT
0.2μM DXL

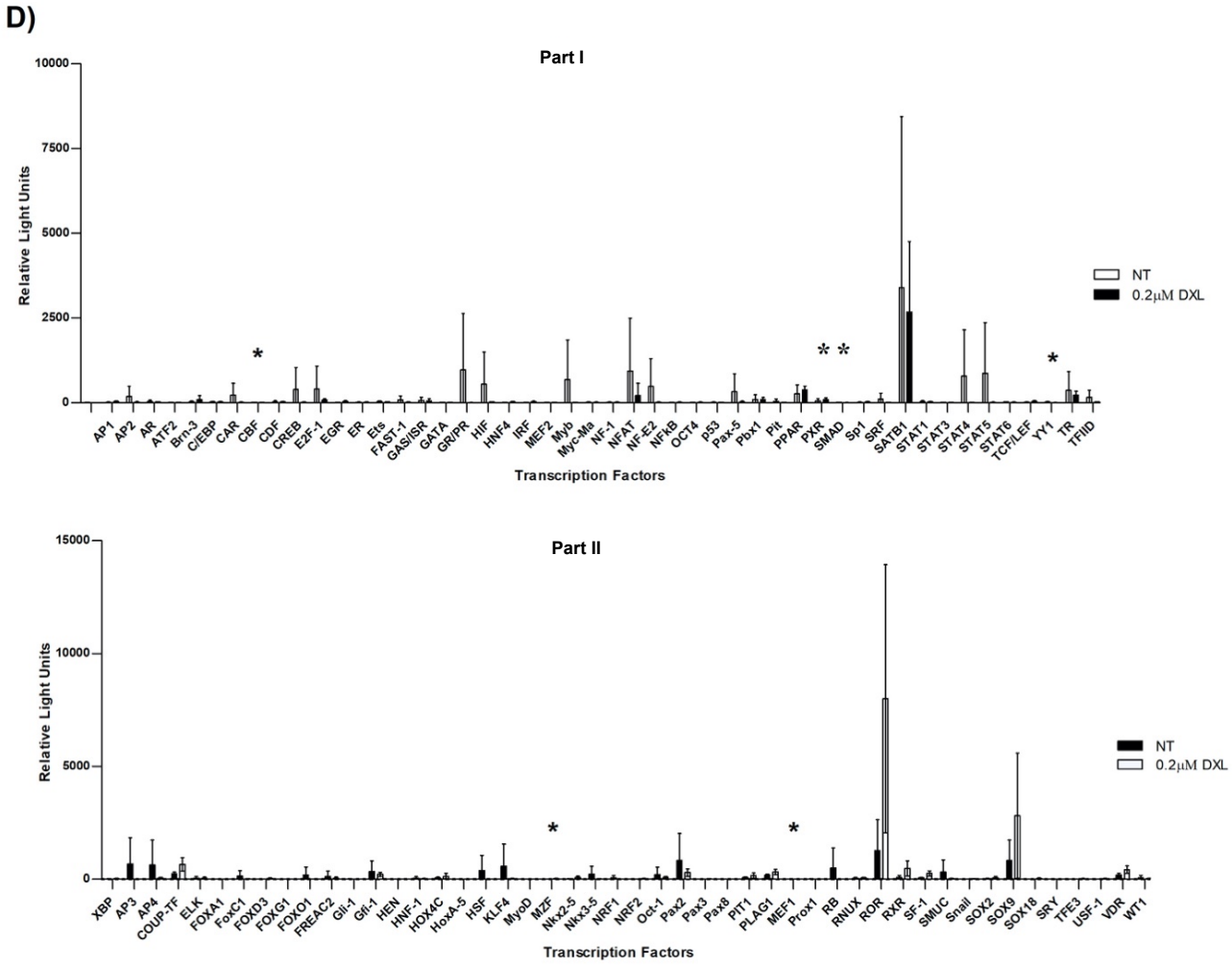

Figure 5. Comparison of activated transcription factors in A2780 cells either treated with 0.2μM DXL or untreated for 8 hours measured in relative light units (RLUs). There were 96 transcription factors on each TFII Profiling Array plate with a no treatment control plate. Three technical replicates were performed using biological Nuclear Extract 1. A) Technical replicate 1 using nuclear extract 1. The first 48 transcription factors are on the top, and the last 48 transcription factors are on the bottom. B) Technical replicate 2 using nuclear extract 1. The first 48 transcription factors are on the top, and the last 48 transcription factors are on the bottom. C) Technical replicate 3 using nuclear extract 1. The first 48 transcription factors are on the top, and the last 48 transcription factors are on the bottom. D) Mean of all three technical replicates. T-test with a Wilcoxon Signed Rank test was performed on the three technical replicates. The transcription factors CBF, YY1, MZF, MEF1, PXR, and SMAD had a p value <0.05 denoted by *.

There were seven transcription factors that were the same between the Mitochondrial UPR plate array and the TFII plate array: C/EBP, E2F1, HIF, HSF, MEF2, Nrf1, and SATB (Figure 3 and 5). The transcription factor C/EBP produced consistently weak signals (<200 RLU) in the TFII array plates, and one moderate signal (>1000 RLU) in the mitochondrial stress plate (Figure 3D). The transcription factor HIF produced one strong signal (>1000 RLUs) in the TFII array plate in technical replicate 2 (Figure 5B), and weak signals (<1000 RLU) in mitochondrial stress array plates (Figure 3). The transcription factor HSF produced weak signals (<200 RLUs) in the TFII plates except for technical replicate 2 which had a moderate signal (<1000 RLUs) (Figure 5B) and produced weak signals (<1000 RLUs) in mitochondrial stress array plates (Figure 3). The transcription factor MEF2 produced weak signals (<200 RLUs) in the TF II array plates (Figure 5) and produced weak signals (<1000 RLUs) in the mitochondrial stress array plates (Figure 3). The transcription factor SATB1 produced strong signals in both the TFII (>1000 RLUs) and mitochondrial stress (>20,000 RLUs) plate arrays (Figure 3 and 5). Statistical analyses performed on the technical replicates and biological replicates across the plates found no significant differences between the DXL treated and untreated samples.

There were five transcription factors that were on both the ER stress plate array and the TFII plate arrays: YY1, CBF, FOXO1, IRF, and HNF4 (Figure 4 and 5). The transcription factor YY1 produced extremely weak signals (<10 RLU) on the TFII array plate (Figure 5); and produced weak (<1000 RLUs) and moderate (>1000 RLUs) signals on the ER stress plates (Figure 4), while the transcription factor CBF produced weak (<1000 RLUs) to moderate (>1000 RLUs) signals on the ER stress plates (Figure 4); and weak signals (<200 RLUs) on the TFII array plates (Figure 5). The transcription factor FOXO1 produced weak (<200 RLUs) to moderate (<1000 RLUs) signals in the TFII array plates (Figure 5), and weak (<1000 RLUs) to

moderate (>1000 RLUs) signals in the ER stress plates (Figure 4). The transcription factor IRF produced weak signals (<200 RLUs) in the TFII plate (Figure 5), and weak (<1000 RLUs) to moderate signals (>1000 RLUs) in the ER stress plate array (Figure 4). The transcription factor HNF4 produced weak signals (<200 RLUs) in TFII (Figure 5), and weak signals (<1000 RLUs) in the ER stress arrays (Figure 4). Statistical analyses performed on the technical replicates and biological replicates between the plates found a significant difference in the expression of the transcription factor YY1 between the DXL treated and untreated samples ($p<0.05$).

There were five transcription factors that were on all three array plates: XBP, AP1, p53, NFκB, and Nrf2 (Figure 3, 4 and 5). The transcription factor XBP produced weak signals (<200 RLUs) in the TFII plate arrays (Figure 5); produced moderate (>1000 RLUs) and weak signals (<1000 RLUs) on the ER stress plate (Figure 4); and produced moderate (>1000 RLUs) and strong signals (>20,000 RLUs) on the Mitochondrial stress plate arrays (Figure 3). The transcription factor AP1 produced weak signals (<200 RLUs) in the TFII array plate (Figure 5); produced weak (<1000 RLUs) and strong signals (>20,000 RLUs) in the ER stress plate (Figure 4); and produced weak (<1000 RLUs) and moderate (>1000 RLUs) on the mitochondrial stress plate (Figure 3). In the TFII array plate, p53 produced weak signals (<200 RLUs) (Figure 5); produced moderate signals (>1,000 RLUs) in the ER stress array plate (Figure 4); and weak signals (<1000 RLUs) in the mitochondrial stress plate (Figure 3). The transcription factor NFκB produced weak signals (<200 RLUs) in the TFII array plates (Figure 5); produced moderate (>1000 RLUs) and strong signals (>20,000 RLUs) in the ER stress array plates (Figure 4); and produced weak signals (<1000 RLUs) in the mitochondrial stress array plates (Figure 3). Nrf2 produced weak signals (<200 RLUs) in the TFII array plates (Figure 5); produced strong signals (>20,000 RLUs) in the ER stress plates (Figure 4); and produced weak (<1000 RLUs) and

moderate (>20,000 RLUs) on the mitochondrial stress plate, but in the second technical replicate all the signals were moderate (Figure 3). Statistical analyses performed on the technical replicates and biological replicates across the plates found no significant differences between the DXL treated and untreated samples.

3.1.3 Selection Criteria for transcription factors for further study

In order to determine which stress-related transcription factors merited further study, a set of criteria were established (Table 3). The first criterion was statistical significance, which was the highest power criterion. The results of the profiling arrays were analyzed using a paired T-test and/or Wilcoxon Signed Rank (non-parametric) between the DXL extract and the untreated extract. Treatment-induced differences in transcription factor activity were considered significant, if the differences met a p value of <0.05. There were six changes in activity that reached statistical significance for the transcription factors CBF, YY1, MZF, SMAD, MEF1, and PXR (Table 4). These changes were statistically significant using the T-test on the samples from the TFII plate, which only had technical replicates for the first nuclear extract. However, treatment-induced differences in YY1 activity were also found to be statistically significant when compared on the ER stress array and the TFII array.

The second criterion looked at reproducible changes in the upregulation or downregulation of the transcription factor in the treated sample compared to the untreated control. Upregulation and downregulation were defined as the increase or decrease in DNA binding activity compared to the no treatment control. Whether an upregulation or downregulation, the second criterion stipulated that the change in DNA binding activity had to occur in all the replicates (biological or technical, as in the case of the TFII plates) (Table 3). There were 26 transcription factors that fit this criterion. Reproducibly upregulated genes

included MZF, ROR, NRF2, MEF1, PXR, MEF2, RXR, SOX9, TFE3, USF1, GR/PR, Brn-3, IRF, Nkx2-5, Pax3, PIT1, SF-1, Snail, SRY, VDR, and COUP-TF (Table 4). Reproducibly downregulated genes included YY1, SMAD, STAT3, and NRF1 (Table 4).

The next criterion was a minimum 2-fold change up or down in transcription factor binding activity upon DXL treatment compared to the untreated control. This applied to all replicates, whether biological or technical (Table 3). There were 21 transcription factors that met this criterion: AP1, ATF4, MEF2, Nrf2, p53, XBP1, CHOP, SREBP1, NFκB, AR, C/EBP, E2F1, GR/PR, AP4, FREAC2, MZF, RNUX, ROR, SOX2, TFE3, and USF1 (Table 4).

The final quantitative selection criterion was the magnitude of luminescence generated for each transcription factor in the probe binding assay, expressed as relative light units (RLUs). The minimum strength of signal was 1000 RLUs, regardless of whether the signal was generated from nuclear extracts of treated or untreated cells (Table 3). There were 19 transcription factors that fell within this criterion: FOXO3, TFEB, C/EBP, NRF2, AP1, XBP1, SATB1, ATF4, ATF6, CBF/NFY, SREBP1, YY1, PG1-1α, ATF3, p53, NFκB, E2F1, ROR, and SOX9 (Table 4).

The ability of the various transcription factors to meet the above criteria are organized in Table 5. No transcription factor met all four quantitative criteria. There were 5 transcription factors that met 3 criteria; 19 that met 2 criteria; and 31 that met only 1 criterion (Table 4). Of the 104 transcription factors studied, 55 met one or more of the above criteria.

Table 3. Selection criteria for transcription factors to study in descending order of importance

Criteria	Description
Statistically Significant	Described as a transcription factor that is statistically significantly different in the treated (DXL) extract compared to the no treatment control in any of the plates individually and across all plates where there are common transcription factors using a paired T-test and/or Wilcoxon Signed Rank
Reproducible Changes	Described as a transcription factor that has increased or decreased binding activity in the treated (DXL) extract compared to no treatment control, in all plate replicates, whether technical or biological
Fold-Change	Described as a transcription factor that has a minimum 2-fold change upwards or downwards, as compared to the no treatment control, in all replicates, whether technical or biological
Signal Strength	Described as a transcription factor with a mean strength of signal of 1000 RLUs in either the no treatment or treated (DXL) extracts
Relevance to Stress in Literature	Described as a transcription factor that is described in peer-reviewed literature as a protein involved in stress response in mammalian cells
Interest	Described as a transcription factor that despite any other criteria was of interest to study

Five transcription factors met 3 of the 4 criteria and were chosen for further investigation: CBF, YY1, MZF, ROR, and Nrf2. In addition, SMAD, MEF1, and PXR were chosen since they reached statistical significance and showed reproducible changes (the two highest ranking criteria). Finally, TFEB and TFE3 were selected for further consideration, since they are known transcription factors activated by cellular stressors and they met 2 of the previously outlined criteria.

As stated above, qualitative criteria were used to finalize the transcription factors that would be investigated in this study. These included an inclusion criterion based on relevance to known cellular stress pathways, and an exclusion criterion based on the lack of reliable antibodies to assess the effects of stress on transcription factor expression or subcellular

localization. Thus, the above criteria narrowed the investigation to four transcription factors: YY1, Nrf2, TFEB, and TFE3.

Table 4. Organization of any transcription factors that met the quantitative selection criteria and from which plate they met those criteria

Statistically Significant ($p<0.05$)	Reproducible Change	Fold-Change	Strength of Signal >1000RLUs	Interest
YY1[3,4]	Nrf2[1] (up)	AP1[1,2,3]	FOXO3[1]	TFEB[1]
CBF[3]	YY1[2,3] (down)	ATF4[1,2]	TFEB[1]	TFE3[3]
SMAD[3]	Brn-3[3] (up)	MEF2[1]	C/EBP[1]	
MZF[3]	CBF[3] (down)	Nrf2[1]	Nrf2[1,2]	
MEF1[3]	GR/PR[3] (down)	p53[1]	AP1[1,2]	
PXR[3]	IRF[3] (up)	XBP1[2]	XBP1[1,2]	
	MEF2[3] (up)	CHOP[2]	SATB1[1,3]	
	PXR[3] (up)	SREBP1[2]	ATF4[2]	
	SMAD[3] (down)	NFkB[2,3]	ATF6[2]	
	STAT3[3] (down)	AR[3]	CBF/NFY[2]	
	COUP-TF[3] (up)	C/EBP[3]	SREBP1[2]	
	MZF[3] (up)	E2F-1[3]	YY1[2]	
	Nkx2-5[3] (up)	GR/PR[3]	PGC-1α[2]	
	NRF1[3] (down)	AP4[3]	ATF3[2]	
	Pax3[3](up)	FREAC2[3]	p53[2]	
	PIT1[3] (up)	MZF[3]	NFκB[2]	
	MEF1[3] (up)	RNUX[3]	E2F1[1,3]	
	ROR[3] (up)	ROR[3]	ROR[3]	
	RXR[3] (up)	SOX2[3]	SOX9[3]	
	SF-1[3] (up)	TFE3[3]		
	Snail[3] (up)	USF-1[3]		
	SOX9[3] (up)			
	SRY[3](up)			
	TFE3[3] (up)			
	USF-1[3] (up)			
	VDR[3] (up)			

[1]Mitochondrial UPR
[2]ER Stress
[3]TFII
[4]ER Stress and TFII

Table 5. The number of quantitative selection criteria that transcription factors met

Number of Criteria	4 Criteria	3 Criteria	2 Criteria	1 Criterion
Transcription Factors		CBF[1,2,4]	SMAD[1,2]	Brn-3[2]
		YY1[1,2,4]	MEF1[1,2]	IRF[2]
		MZF[1,2,3]	PXR[1,2]	STAT3[2]
		ROR[2,3,4]	MEF2[2,3]	Nkx2-5[2]
		NRF2[2,3,4]	RXR[2,3]	NRF1[2]
			SOX9[2,4]	Pax3[2]
			TFE3[2,3]	PIT1[2]
			USF1[2,3]	SF-1[2]
			GR/PR[2,3]	Snail[2]
			AP1[3,4]	SRY[2]
			C/EBP1[3,4]	VDR[2]
			E2F1[3,4]	COUP-TF[2]
			NFκB[3,4]	EGR[3]
			SATB1[3,4]	Ets[3]
			TFEB[3,4]	NFAT[3]
			XBP1[3,4]	AP4[3]
			SREBP1[3,4]	FRAC2[3]
			p53[3,4]	Gli-1[3]
			ATF4[3,4]	HSF[3]
				KLF2[3]
				Nkx3-5[3]
				RNUX[3]
				SOX2[3]
				CHOP[3]
				STAT5[3]
				AR[3]
				CREB[3]
				ATF6[4]
				PGC-1α[4]
				ATF3[4]
				FOXO3[4]

[1]Statistically Significant
[2]Reproducible Change
[3]Mean Fold-Change
[4]Strength of Signal

3.2 Optimization of nuclear extraction protocols

After the previous experiments, a mycoplasma contamination was found in the A2780 ovarian cancer cell line that was being used to conduct these experiments. Earlier vials of A2780 cells in the lab cryorepository were found to be free of mycoplasma and, consequently, new cultures of A2780 cells were used in all subsequent experiments. All future stock cultures were regularly monitored for mycoplasma infection and no additional contaminations were detected in remaining experiments.

Additionally, the nuclear extracts made using the Signosis kits were found not to be enriched for nuclear proteins (i.e. there was contamination of cytoplasmic proteins in the nuclear extracts) (See Appendix Figure 13). In order to study the translocation of transcription factors from the cytoplasm to the nucleus, the nuclear extracts would need to be reasonably free of cytoplasmic proteins. Therefore, a few additional protocols were tested, including one from Schreiber *et al.* (1989) (Figure 6) and one from Rockland Immunochemicals Inc. (not shown) [113]. Figure 6 shows the contamination of a cytoplasmic protein (GAPDH) in the nuclear extracts using the Schreiber *et al.* (1989) protocol. Histone H3 was seen only in the nuclear extracts but was completely absent from the whole cell extracts, indicating some inconsistency (Figure 6). Thus, this protocol was not used.

We observed that a nuclear fractionation protocol recommended by Abcam Inc. worked the best. The protocol was optimized to include extra wash and centrifugation steps during the generation of cytoplasmic and nuclear extracts (Figure 7). Given the strong nuclear localization of YY1, we used YY1 as an additional loading control, which also happened to be a transcription factor that met our selection criteria: YY1.

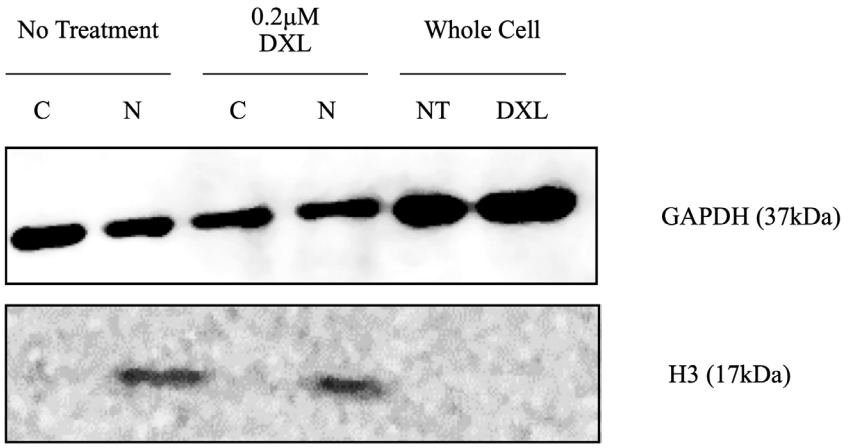

Figure 6. Schreiber *et al.* (1989) nuclear extraction protocol results using a whole cell lysate for comparison. Cells plated for a nuclear extraction were treated for 1 hour with 0.2μM DXL with an untreated control (NT) to determine localization of cytoplasmic (C) and nuclear (N) proteins. Whole cell lysates were treated for 16 hours with 0.2μM DXL with an untreated control. GAPDH (cytoplasmic control) is present in the nuclear fraction, and histone H3 (nuclear control) is absent in the whole cell lysate.

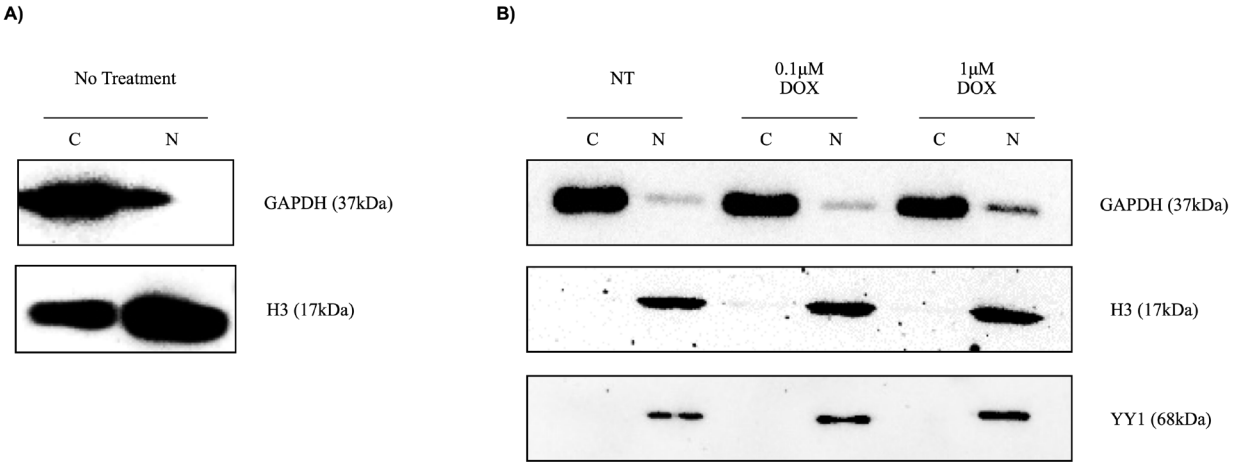

Figure 7. Before and after the addition of wash step and extra centrifugation in the Abcam nuclear fractionation protocol at 0 hours. A) Before adding a wash step and extra centrifugation between the removal of the cytoplasmic fraction (C) and lysing the nuclear fraction (N). B) After adding a wash step and extra centrifugation between the removal of the cytoplasmic fraction and lysing the nuclear fraction.

3.3 Determining translocation kinetics of selected transcription factors by treatment with cellular stressors and chemotherapy

Once a nuclear extraction protocol has been identified that resulted in highly enriched cytoplasmic and nuclear extracts, the selected transcription factors from the transcription factor profiling arrays could be tested. The chosen treatments were known, distinct cellular stressors, including the chemotherapy agents DXL (0.2μM) and DOX (0.5μM), the ER stressor Tpg (0.5μM), and nutrient/growth factor starvation (15% media; 85% PBS). The chosen treatment lengths were 0, 2, 16, and 24 hours.

To ensure the utility of the nuclear and cytoplasmic extracts for monitoring changes in transcription factor localization, both YY1 and histone H3 were used as nucleus-specific biomarkers.

Translocation was determined by visual inspection of western blots, as well as quantitatively, using densitometry values obtained for bands on the blots. When no band was evident in a particular lane on the western blots, a densitometry reading was taken to quantify background levels of the various transcription factors. The ratio of the densitometry value for the nuclear extract divided by the densitometry value for the cytoplasmic extract was used to determine where a specific transcription factor was localized. In this instance, any value above 1 indicated there was more transcription factor in the nucleus, but a value below 1 indicated there was more transcription factor located in the cytoplasm. Finally, baseline was defined as the amount of transcription factor in the untreated sample at 0 hours, whether cytoplasmic or nuclear.

Unfortunately, due to the advent of the COVID-19 pandemic, quantification data could only be obtained for the Nrf2, TFEB, and TFE3 transcription factors and only for one

experiment. Thus, statistical analyses to assess the significance of time- or stressor-specific differences in transcription factor localization were not possible.

3.3.1 Treatment with DXL and DOX

3.3.1.1 DXL and DOX-treated cells result in RNA disruption

Cells free of mycoplasma were plated for cytoplasmic and nuclear extracts and treated with DXL (0.2μM) and DOX (0.5μM) for 0, 16, and 24 hours. Identical cells with identical treatments were also plated for RNA extractions, except that treatments were 72 hours, which was previously determined to be optimal for detection of RNA disruption (Figure 8). The above concentrations of DXL and DOX were able to cause RNA disruption in A2780 cells (Figure 8A and B). The cells treated with DXL had an RDI value significantly higher than untreated cells ($p<0.01$) (Figure 8C). The cells treated with DOX also had significantly higher RDI values than untreated cells ($p<0.001$) (Figure 8C).

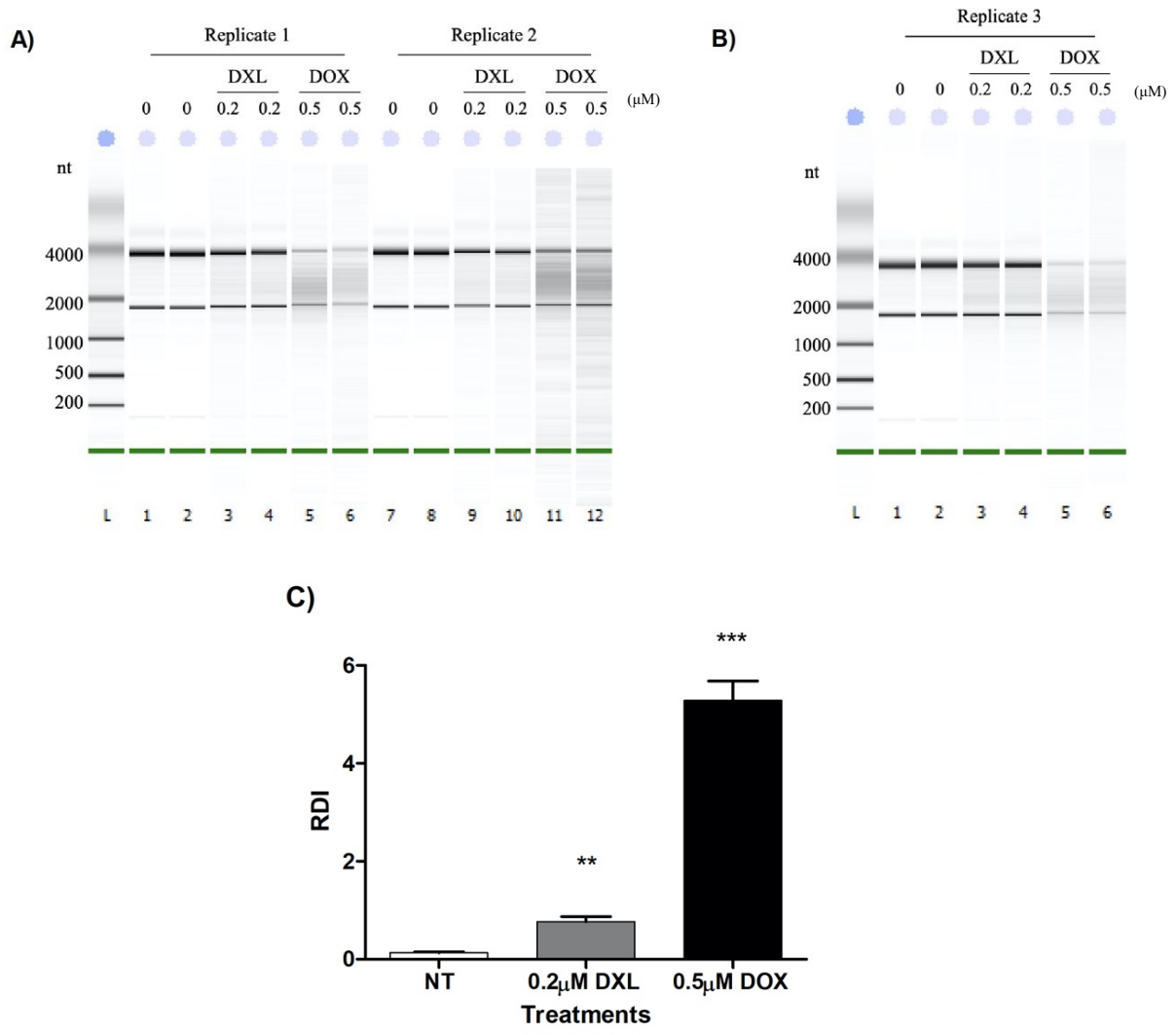

Figure 8. Effect of treatment with 0.2μM DXL or 0.5μM DOX compared to no treatment (NT) control on RNA disruption in A2780 cells at 72h. (A) RNA gel image of biological replicates 1 and 2, with two technical replicates of each treatment. (B) RNA gel image of biological replicate 3, with two technical replicates of each treatment. (C) RDI analysis of three independent replicates. T-test, one-tailed (**p <0.01 and ***p<0.001, n=3)

3.3.1.2 Nrf2 is localized primarily in the nucleus

Despite variations in expression amongst nuclear extracts, Nrf2 localization was found to be predominately in the nucleus, even for untreated cells. Treatment of A2780 cells with DXL, DOX, or Tpg and starvation of cells did not appear to alter Nrf2 expression or subcellular localization (Figure 9A). However, densitometry values were obtained from the cytoplasmic lanes for background and further calculations. The densitometry values from the cytoplasm lanes suggested that there is some Nrf2 localized in the cytoplasm, although no clear Nrf2 bands were evident on immunoblots (Figure 9A).

When normalized to GAPDH, there was 5-fold more Nrf2 localized in the cytoplasm of the DXL treated sample compared to the untreated cytoplasmic sample at 0 hours. The localization of Nrf2 in the cytoplasm of the DOX treated sample was about the same as the untreated sample at 0 hours, which was the baseline amount of Nrf2 in the cytoplasm (Figure 9B). However, without replicate experiments, it is unclear whether these differences may simply represent variations in the localization of Nrf2 and GAPDH in nuclear and cytoplasmic extracts. At 16 hours, there is about 4-fold more Nrf2 localized in the cytoplasm of the untreated sample, 2-fold more Nrf2 localized in the cytoplasm of the DXL treated sample, and 2-fold less Nrf2 localized in the cytoplasm of the DOX treated sample, when compared to the baseline (Figure 9B). Both the DXL and DOX treated samples showed a decrease in the amount of the Nrf2 localized in the cytoplasm of these samples when compared to their respective treatments at 0 hours. Finally, at 24 hours, there was 3-fold more Nrf2 localized in the cytoplasm of the untreated sample compared to baseline; 2-fold more Nrf2 localized in the cytoplasm of the DXL treated sample, and 2-fold more Nrf2 localized in the cytoplasm of the DOX treated sample when compared to the baseline (Figure 9B). There was a decrease in the localization of Nrf2 in

the cytoplasm of the untreated sample between 16 and 24 hours, but it did not return to baseline. The DXL treated sample did not decrease localization in the cytoplasm between 16 and 24 hours, but the DOX treated sample increased localization of Nrf2 above baseline (Figure 9B). While the above findings could represent treatment related changes in Nrf2 localization, such conclusions need to be tempered by determining whether such changes are reproducible and statistically significant.

When normalized to the YY1 nuclear loading control, there was about 2-fold more Nrf2 localized in the nucleus of the DXL treated sample at 0 hours, and about 5-fold more Nrf2 localized in the nucleus of the DOX treated sample at 0 hours compared to the nuclear baseline, which was the untreated nuclear sample at 0 hours (Figure 9C). At 16 hours, there was greater than 2-fold less Nrf2 localized in the nucleus of the untreated sample, 3-fold more Nrf2 localized in the nucleus of the DXL treated sample, and about 2-fold more Nrf2 localized in the nucleus of the DOX treated sample when compared to baseline (Figure 9C). Finally, at 24 hours, there was about 2-fold less Nrf2 localized in the nucleus of the untreated sample, about the same amount of Nrf2 localized in the nucleus of the DXL treated sample, and 3-fold more Nrf2 localized in the nucleus of the DOX treated sample, when compared to baseline (Figure 9B). The untreated sample had an increase in the amount of Nrf2 localized in the nucleus from 16 to 24 hours but did not return to baseline levels from the decrease between 0 and 16 hours. Again, it is not clear whether such findings would be supported in replicate experiments, and, with only one experiment, the significance of these findings could not be assessed. The above differences may simply represent variation in the levels of the Nrf2 and YY1 with nuclear extracts.

The histone H3 western blots showed low to no histone expression data in the nuclear and cytoplasmic extracts (Figure 9A). Nevertheless, there are a few trends that were similar

when normalizing to either of the two nuclear protein biomarkers YY1 and Histone H3. Normalization to both H3 and YY1 showed both treated samples had more Nrf2 in the nucleus than the untreated sample at 0 hours (Figure 9B and C). As well, in both controls, the amount of Nrf2 in the nucleus of the DXL treated sample returned to baseline levels at 24 hours, which was lower than the starting amounts (Figure 9B and C). Finally, there was an increase in the amount of Nrf2 in the nucleus of the DOX treated samples between 16 and 24 hours, even if only slight compared to the H3 control (Figure 9B and C).

Using the densitometry values obtained when normalized to the YY1 nuclear loading control instead of the GAPDH cytoplasmic loading control, the localization of Nrf2 appeared to be mostly cytoplasmic at all timepoints and treatments, since all of the values are below 1 with the exception of the DOX treated sample at 0 hours (Figure 9E). Visually, this does not seem correct when compared to the western blot (Figure 9A). However, using the densitometry values obtained from histone H3 taken over GAPDH, there is a stronger localization of Nrf2 in the nucleus (Figure 9F). There was more Nrf2 localized in the nucleus of the untreated samples across all the timepoints; there was more Nrf2 localized in the nucleus of the DXL treated sample at 0 and 24 hours with an almost even distribution between cytoplasm and nuclear at 16 hours; and an equal localization of Nrf2 in the cytoplasm and nucleus of the DOX treated sample at 0 hour and a strong nuclear localization at 16 and 24 hours (Figure 9F). This data seems to more accurately represent the localization of Nrf2 in the nucleus, as seen visually on the western blot.

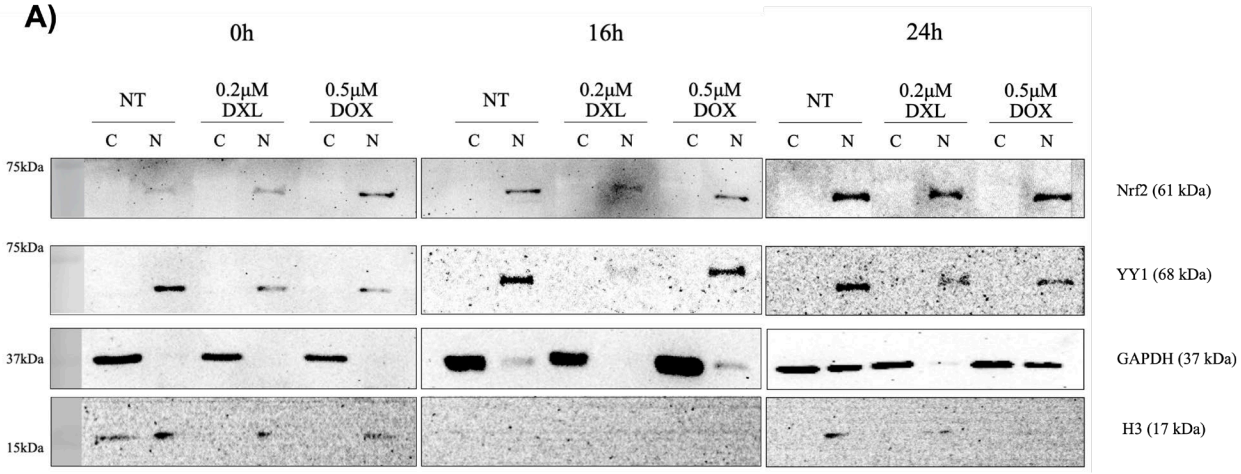
A)
0h
16h
24h
NT
0.2μM DXL
0.5μM DOX
C N
75kDa
75kDa
37kDa
15kDa
Nrf2 (61 kDa)
YY1 (68 kDa)
GAPDH (37 kDa)
H3 (17 kDa)

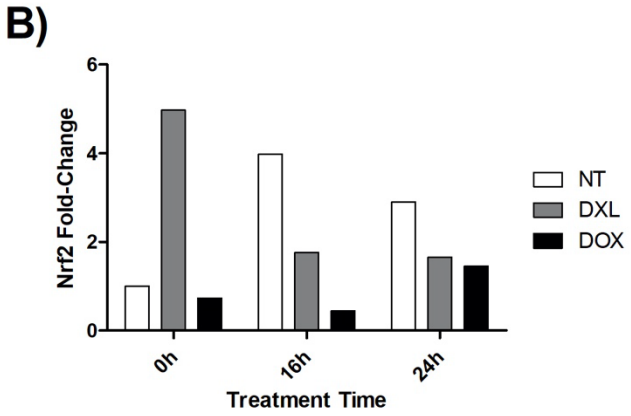
B)
Nrf2 Fold-Change
Treatment Time
0h
16h
24h
NT
DXL
DOX

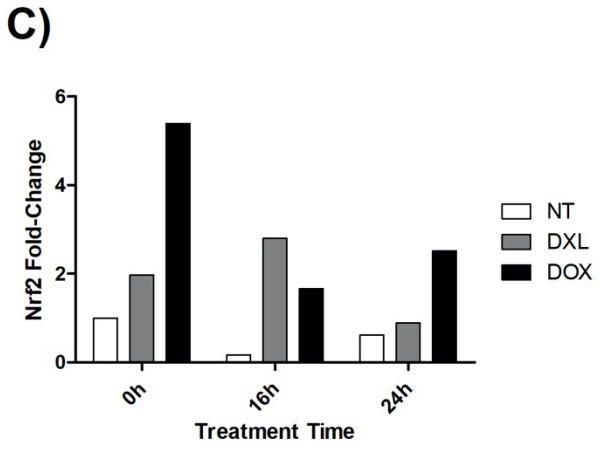
C)
Nrf2 Fold-Change
Treatment Time
0h
16h
24h
NT
DXL
DOX

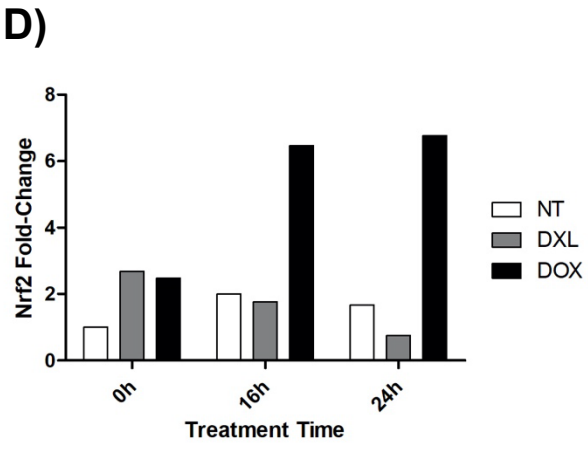
D)
Nrf2 Fold-Change
Treatment Time
0h
16h
24h
NT
DXL
DOX

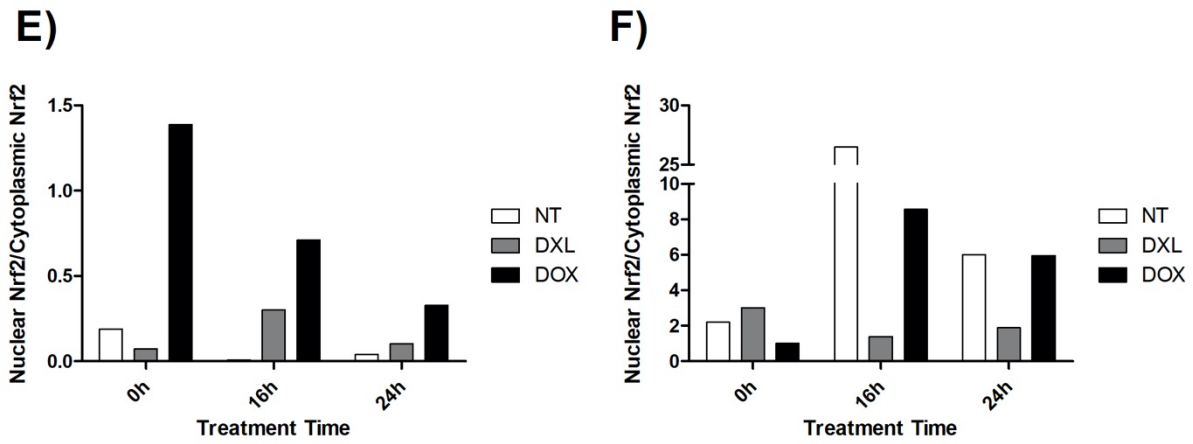

Figure 9. Effect of treatment of A2780 cells with 0.2μM DXL and 0.5μM DOX compared to no treatment (NT) control for 0h, 16h, or 24h on the localization of the transcription factor Nrf2 in cytoplasm (C) or nucleus (N). A) Western blot documenting the localization of Nrf2 with different treatments at different time points. YY1 and H3 are nuclear loading controls, and GAPDH is the cytoplasmic loading control. B) Densitometry values of one biological replicate (replicate 1) normalized to GAPDH cytoplasmic loading control relative to NT at 0 hours (baseline). C) Densitometry values of one biological replicate normalized to YY1 nuclear loading control relative to baseline. D) Densitometry values of one biological replicate compared to H3 nuclear loading control relative to baseline. E) Distribution of Nrf2 between the nucleus (normalized to YY1) and cytoplasm (>1 is nuclear localization, value <1 is cytoplasmic localization). F) Distribution of Nrf2 between the nucleus (normalized to H3) and cytoplasm.

3.3.1.3 TFEB accumulates in the untreated samples beginning at 16 hours

The accumulation of TFEB in the cytoplasm and the nucleus was apparent beginning at 16 hours (Figure 10A).

When normalized to GAPDH, the localization of TFEB in the cytoplasm of the DXL and DOX treated samples was approximately the same as the untreated sample at 0 hours, which was the baseline amount of TFEB in the cytoplasm (Figure 10B). However, there was slightly less TFEB localized in the cytoplasm of the DXL treated sample and slightly more localized in the cytoplasm of the DOX treated sample compared to baseline. At 16 hours, there was 4-fold more TFEB localized in the cytoplasm of the untreated sample, about 2-fold more TFEB localized in the cytoplasm of the DXL treated and about 2-fold less TFEB localized in the cytoplasm of the DOX treated sample, when compared to the baseline (Figure 10B). There was an increase in the amount of TFEB localized in the cytoplasm of the untreated and the DXL treated samples, but a decrease in the amount of TFEB localized in the cytoplasm of the DOX treated sample from 0 to 16 hours. Finally, at 24 hours, there was 6-fold more TFEB localized in the cytoplasm of the untreated sample, a slight decrease in the amount of TFEB localized in the DXL treated sample compared to the baseline, and about 2-fold less TFEB localized in the cytoplasm of the DOX treated sample compared to baseline (Figure 10B). There was an increase in the amount of TFEB localized in the cytoplasm of the untreated sample across all timepoints. The amount of TFEB localized in the cytoplasm of the DXL treated sample was about the same as baseline across all timepoints, which was a slight increase from the amount the DXL sample had at 0 hours. There was no change in the amount of TFEB in the cytoplasm of the DOX treated sample from 16 to 24 hours.

When normalized to YY1 as the nuclear loading control, there was about 3-fold more TFEB localized in the nucleus of the DXL treated sample, and about 5-fold more TFEB localized in the nucleus of the DOX treated sample compared to the untreated sample at 0 hours, which is the baseline amount of TFEB localized in the nucleus (Figure 10C). At 16 hours, there was about 2-fold more TFEB localized in the nucleus of the untreated sample, 8-fold more TFEB localized in the nucleus of the DXL treated sample, and about the same amount of TFEB localized in the nucleus of the DOX treated sample as the baseline, when compared to the baseline (Figure 10C). There was an increase in the amount of TFEB localized in the nucleus of the untreated and DXL treated samples, but a decrease in the amount of TFEB localized in the nucleus of the DOX treated sample from 0 to 16 hours. At 24 hours, there was about 5-fold more TFEB localized in the nucleus of the untreated sample, 5-fold more TFEB localized in the nucleus of the DXL treated sample, and about 2-fold more TFEB localized in the nucleus of the DOX treated sample than the baseline (Figure 10C). There was an increase in the amount of TFEB localized in the nucleus of the untreated sample across all timepoints. There was a decrease in the amount of TFEB localized in the nucleus of the DXL treated sample between 16 and 24 hours. Finally, the amount of TFEB localized in the nucleus in the DOX treated sample increased slightly between 16 and 24 hours.

When normalized to H3, there was more than 4-fold less TFEB localized in the nucleus of the DXL treated sample, and 2-fold less TFEB localized in the nucleus of the DOX treated sample when compared to the untreated sample at 0 hours, which is the baseline (Figure 10D). At 16 hours, there was about 1.5-fold more TFEB localized in the nucleus of the untreated sample, 2-fold less TFEB localized in the nucleus of the DXL treated sample, and about 4-fold less TFEB localized in the nucleus of the DOX treated sample (Figure 10D). There was an

increase in the amount of TFEB localized in the nucleus of the untreated and the DXL treated samples, but a decrease in the amount of TFEB localized in the nucleus of the DOX treated samples from 0 to 16 hours. At 24 hours, there was about 2-fold more TFEB localized in the nucleus of the untreated sample, about 4-fold less TFEB localized in the nucleus of the DXL treated sample, and just over 4-fold less TFEB localized in the nucleus of the DOX treated sample, when compared to baseline (Figure 10D). There was an increase in the amount of TFEB localized in the nucleus of the untreated samples between each timepoint. There was a decrease in the amount of TFEB localized in the nucleus of the DXL treated sample, and an increase in the amount of TFEB localized in the nucleus of the DOX treated sample between 16 and 24 hours. Overall, between the two nuclear loading controls, the trends in the increases and decreases across and between timepoints is the same, just with varying intensities. There was an increase in the localization of TFEB in the nucleus of the untreated sample between 0 and 16 hours, and another increase in localization between 16 and 24 hours (Figure 10C and D). For the DXL treated samples, there was an increase in the amount of TFEB localized in the nucleus between 0 and 16 hours, but a decrease between 16 and 24 hours (Figure 10C and D). Finally, there was a decrease in the amount of TFEB localized in the nucleus in the DOX treated samples between 0 and 16 hours, and an increase between 16 and 24 hours (Figure 10C and D).

Using the densitometry values obtained using the YY1 nuclear loading control taken over the values obtained from the GAPDH cytoplasmic loading control, the distribution of TFEB was strongly localized in the cytoplasm of the untreated samples across all timepoints with all values below 1 (Figure 10E). In the DXL treated samples, there was slightly more TFEB localized in the nucleus of all timepoints; however, most of the values are close to 1, which indicates that there was a slightly even distribution between cytoplasm and nucleus (Figure 10E). Finally, the

DOX treated samples had more TFEB localized in the cytoplasm across all timepoints, however similarly, there was an almost even distribution between cytoplasm and nucleus (Figure 10E). When the values obtained from the H3 nuclear loading control are taken over the GAPDH cytoplasmic loading control values, the distribution of TFEB in the untreated samples showed more of a nuclear localization at 0 hours, and then more of a cytoplasmic localization at 16 and 24 hours, however they were close to an even distribution between cytoplasm and nucleus (Figure 10F). For the DXL treated samples, there was more TFEB localized in the cytoplasm at 0 hours, close to an even distribution at 16 hours however slightly more cytoplasmic, and at 24 hours there was more of a cytoplasmic localization (Figure 10F). Finally, for the DOX treated samples, there was a cytoplasmic localization at 0 hours, followed by an even distribution but slightly more cytoplasmic at 16 hours, and more of a nuclear localization at 24 hours (Figure 10F).

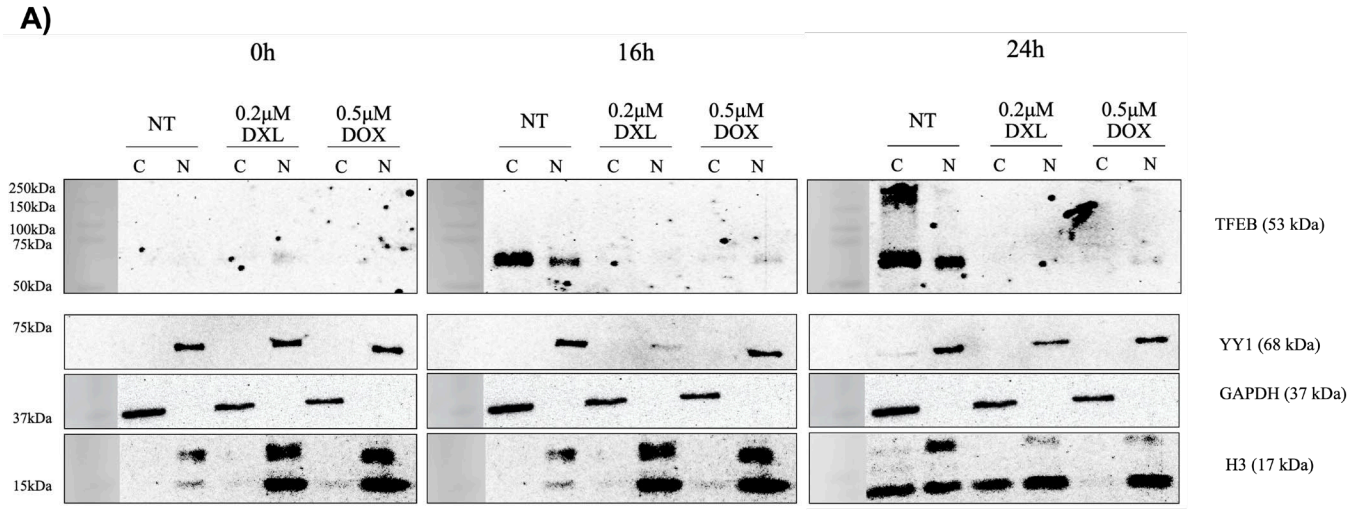
A)
0h
16h
24h
NT
0.2μM DXL
0.5μM DOX
C N C N C N
250kDa
150kDa
100kDa
75kDa
50kDa
75kDa
37kDa
15kDa
TFEB (53 kDa)
YY1 (68 kDa)
GAPDH (37 kDa)
H3 (17 kDa)

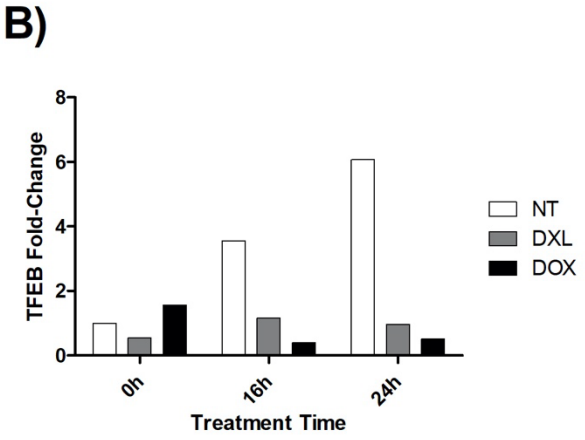
B)
TFEB Fold-Change
Treatment Time
0h
16h
24h
NT
DXL
DOX

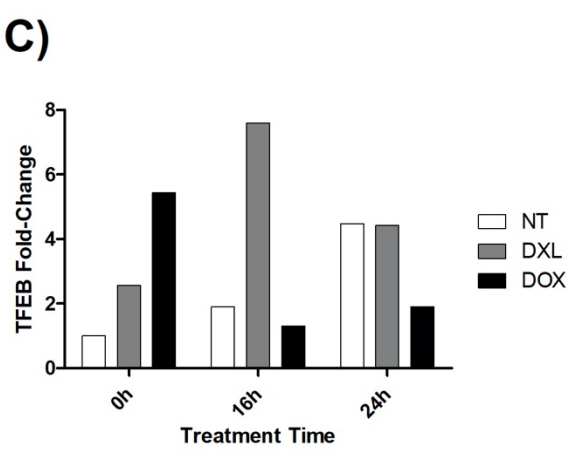
C)
TFEB Fold-Change
Treatment Time
0h
16h
24h
NT
DXL
DOX

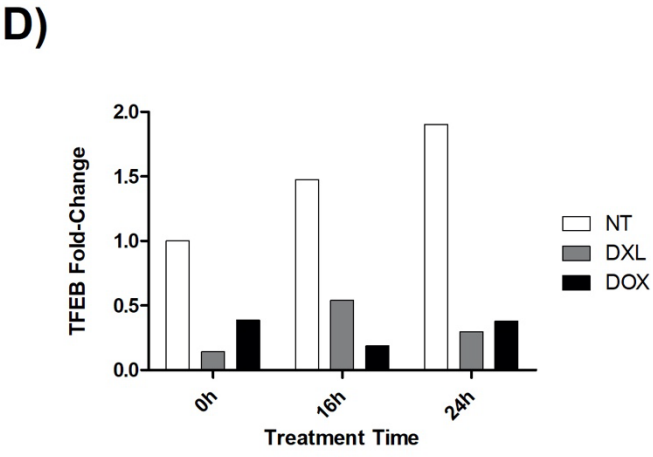
D)
TFEB Fold-Change
Treatment Time
0h
16h
24h
NT
DXL
DOX

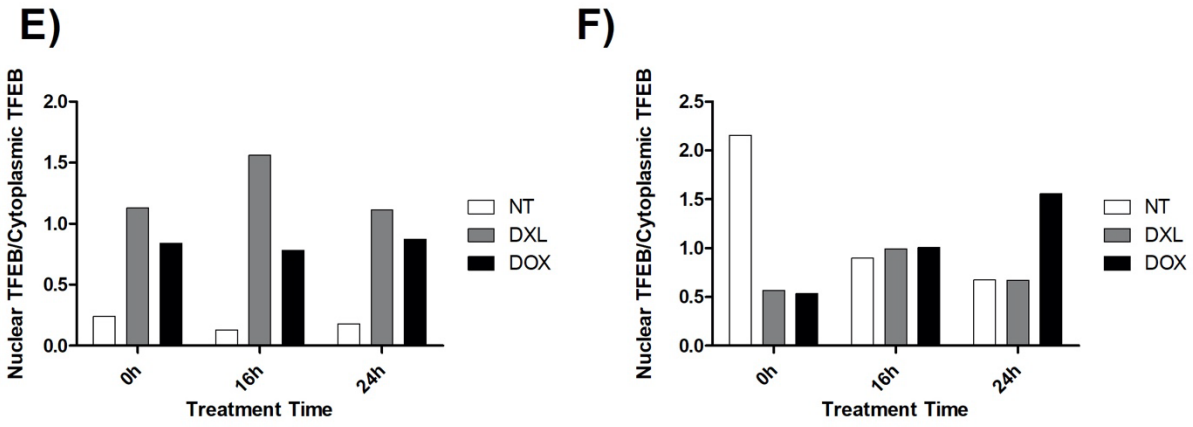

Figure 10. Effect of treatment of A2780 cells with 0.2μM DXL and 0.5μM DOX or no treatment (NT) control for 0h, 16h, or 24h on the localization of the transcription factor TFEB in cytoplasm (C) or nucleus (N). A) Western blot documenting the localization of TFEB with different treatments at different time points. YY1 and H3 are nuclear loading controls, and GAPDH is the cytoplasmic loading control. B) Densitometry values of one biological replicate (replicate 2) for TFEB normalized to GAPDH cytoplasmic loading control relative to NT at 0 hours (baseline). C) Densitometry values for TFEB normalized to YY1 nuclear loading control relative to baseline. D) Densitometry values of TFEB normalized to H3 nuclear loading control relative to baseline. E) Distribution of TFEB between the nucleus (normalized to YY1) and cytoplasm (>1 is nuclear localization, value <1 is cytoplasmic localization). F) Distribution of TFEB between the nucleus (normalized to H3) and cytoplasm.

3.3.2 Treatment with Tpg and starvation

3.3.2.1 Tpg and Starvation treatments result in RNA disruption at 72 hours

Cells plated for cytoplasmic and nuclear extracts that were treated with Tpg (0.5μM) and starved (15% media, 85% PBS) for 0, 2, and 16 hours were also plated for an RNA extraction with the same concentrations for 72 hours (Figure 11). These treatments and concentrations caused RNA disruption in A2780 cells (Figure 11A-C). The cells treated with Tpg had an RDI value significantly different than the untreated and DMSO controls ($p<0.05$) (Figure 11D). The starved cells had an RDI value significantly different than the untreated or PBS Only control ($p<0.001$) (Figure 11D). The DMSO and PBS Only controls were not significantly different from the no treatment control (Figure 11). The PBS sample only generated one RDI value out of the six technical replicates, and five N/A values due to significant RNA disruption. The algorithm used to generate RDI values cannot produce a value if there are not detectable and quantifiable levels of both the 28S and 18S rRNAs to generate an RDI.

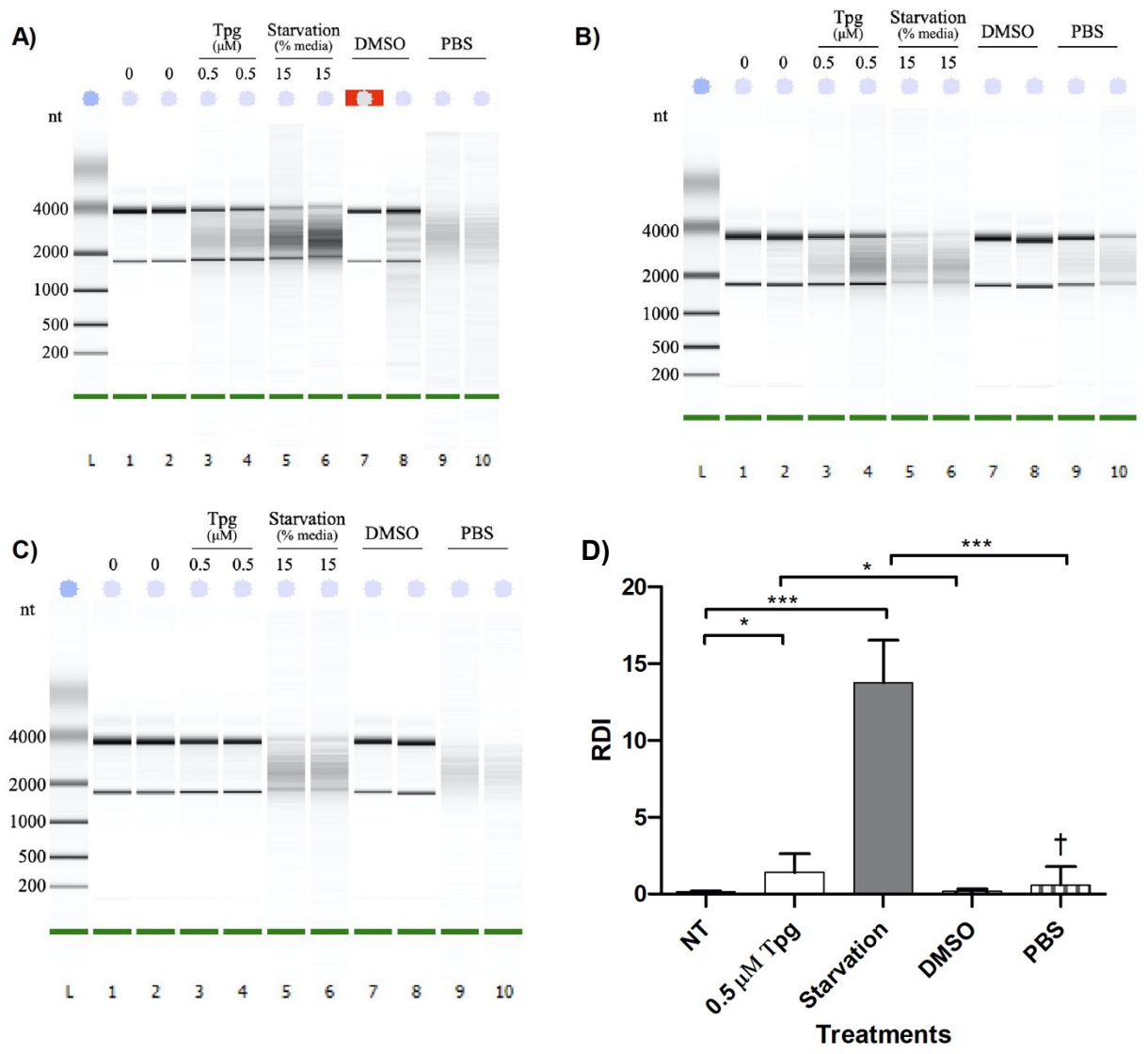

Figure 11. Effect of treatment with 0.5μM thapsigargin (Tpg) and 15% Media (Starvation; 15% media, 85% 1X PBS) with DMSO and no treatment (NT) controls on RNA disruption in A2780 cells at 72h. (A) RNA gel image of biological replicate 1, with two technical replicates of each treatment. (B) RNA gel image of biological replicate 2, with two technical replicates of each treatment. (C) RNA gel image of biological replicate 3, with two technical replicates of each treatment. (D) RDI analysis of three independent replicates. T-test, one-tailed (*p <0.05 Tpg compared to both NT and DMSO controls; ***p<0.001 Starvation compared to NT and PBS control; † denotes that this treatment only generated one RDI value out of all the three replicates because of significant RNA disruption in other two samples generating N/A values)

3.3.2.2 Nrf2 is exclusively present in the nucleus

The localization of Nrf2 appeared to be exclusively in the nucleus at all of the timepoints regardless of treatment or no treatment (Figure 12A). Despite no visible Nrf2 localized in the cytoplasm, the densitometry values of the area were obtained as a background for further calculations. At 0 hours, there was about the same amount of Nrf2 localized in the cytoplasm of the treated samples as the untreated control at 0 hours, which is the baseline for the amount of cytoplasmic Nrf2 (Figure 12B). At 2 hours, there was about 1.5-fold more Nrf2 localized in the cytoplasm of the untreated and DMSO controls, and Tpg treated compared to baseline. There was about 2-fold more Nrf2 localized in the cytoplasm of the starved samples compared to baseline (Figure 12B). There was an increase in the amount of Nrf2 localized in the cytoplasm in all of the samples between 0 and 2 hours. At 16 hours, there was 4-fold more Nrf2 localized in the cytoplasm of the untreated sample than baseline, 1.5-fold more Nrf2 localized in the cytoplasm of the Tpg treated than baseline, 5-fold more Nrf2 localized in the cytoplasm of the starved samples than baseline, and the same amount of Nrf2 localized in the cytoplasm of the DMSO control, when compared to baseline (Figure 12B). There was an increase in the amount of Nrf2 localized in the cytoplasm of the untreated control and the starved sample between 2 and 16 hours. There was no change in the amount of Nrf2 localized in the cytoplasm of the Tpg treated sample, and a slight decrease in the DMSO control between 2 and 16 hours.

When normalized to the YY1 nuclear loading control, there was 6-fold more Nrf2 localized in the nucleus of the Tpg treated, and about 2-fold less Nrf2 localized in the nucleus of the starved sample and the DMSO control, when compared to untreated nuclear sample at 0 hours, which was the baseline amount of nuclear Nrf2 (Figure 12C). However, the large fold-change for the Tpg treated sample can be attributed to the YY1 band to which it was normalized,

which is quite faint (Figure 12A). At 2 hours, there was about 2-fold less Nrf2 localized in the nucleus of all of the treatments and controls, when compared to the baseline (Figure 12C). This was a decrease in the localization of Nrf2 in the nucleus of the untreated and Tpg treated samples from 0 to 2 hours, but the starved and DMSO were unchanged between timepoints. At 16 hours, there was about 4-fold less Nrf2 localized in the nucleus of the untreated and Tpg treated samples compared to baseline, 1.5-fold more Nrf2 localized in the nucleus of the starved sample than baseline, and just over 2-fold less Nrf2 localized in the nucleus of the DMSO control when compared to baseline (Figure 12C). There was a slight decrease in the amount of Nrf2 localized in the nucleus for the untreated and Tpg treated samples between 2 and 16 hours, the starved samples increased between timepoints, and the DMSO control had a slight decrease.

When normalized to H3, there was about 2-fold less Nrf2 localized in the nucleus of the Tpg treated sample, under 2-fold less Nrf2 localized in the nucleus of the starved samples, and 2-fold less Nrf2 localized in the nucleus of the DMSO control, when compared to the untreated nuclear sample at 0 hours, which is the baseline (Figure 12D). At 2 hours, there was 2-fold less Nrf2 localized in the nucleus of the untreated sample, 4-fold less Nrf2 localized in the nucleus of the Tpg treated and starved samples, and 2-fold less Nrf2 localized in the nucleus of the DMSO control when compared to the baseline (Figure 12D). There was a decrease in the localization of Nrf2 in the nucleus of all of the treated samples and the untreated control between 0 and 2 hours, and no change in the DMSO control. At 16 hours, there was 2-fold less Nrf2 localized in the nucleus of the untreated sample, 2-fold less Nrf2 localized in the nucleus of the Tpg treated sample, over 4-fold less Nrf2 localized in the nucleus of the starved sample, and 2-fold less Nrf2 localized in the nucleus of the DMSO control, when compared to baseline at 0 hours (Figure 12D). There was no change in the amount of Nrf2 localized in the nucleus of the untreated

sample between 2 and 16 hours. There was a slight increase in the amount of Nrf2 localized in the nucleus of the Tpg treated and DMSO control between 2 and 16 hours, and a decrease in the starved samples.

Using the densitometry values obtained from the YY1 nuclear loading control and taken over the GAPDH cytoplasmic loading control, the distribution of Nrf2 was more in the nucleus at 0 hours for all of the treatments and controls because the values were above 1 (Figure 12E). At 2 hours, there was a more even distribution of Nrf2 between the cytoplasm and nucleus for all the treatments and the untreated control, except for DMSO (Figure 12E). Although with a value nearing 1, there was more Nrf2 localized in the nucleus of the untreated sample, and more Nrf2 localized in the cytoplasm of the Tpg and starved samples. There was more Nrf2 localized in the nucleus for the DMSO control (Figure 12E). Finally, at 16 hours, there was almost an even distribution of all the treatments and controls between the cytoplasm and the nucleus. However, there was more Nrf2 localized in the cytoplasm of the untreated and Tpg treated samples, and more Nrf2 localized in the nucleus of the starved sample and the DMSO control (Figure 12E).

Using the densitometry values obtained using the histone H3 nuclear loading control and taken over the GAPDH cytoplasmic loading control, the distribution of Nrf2 was strongly localized in the nucleus of the untreated and DMSO controls, and the starved sample at 0 hours with values greater than 1 (Figure 12F). However, the Tpg treated sample was more in the cytoplasm at 0 hours. At 2 hours, there was more Nrf2 localized in the nucleus of all of the treatments and controls (Figure 12F). Finally, at 16 hours, there was a very strong localization of Nrf2 in the nucleus of both controls and the Tpg treated sample, however a stronger localization of Nrf2 in the cytoplasm of the starved sample (Figure 12F).

Figure 12F more accurately describes the localization of Nrf2, which is visually more in the nucleus (Figure 12A).

3.3.2.3 TFE3 is more prominent in the no treatment and DMSO controls

There was a strong TFE3 localization in the cytoplasm of the untreated and DMSO controls beginning at 0 hours (Figure 12A). Unfortunately, at the 2 hour timepoint, there was what is assumed to be a transfer issue with the western blot resulting in a blank blot. The densitometry values were done, but they will not be discussed.

At 0 hours, there was about 2-fold less TFE3 localized in the cytoplasm of the Tpg treated and starved samples than the untreated cytoplasmic control, which was the baseline (Figure 12G). The amount of TFE3 localized in the cytoplasm of the DMSO control was about the same as the baseline, but slightly less (Figure 12G). At 16 hours, there was slightly less TFE3 localized in the cytoplasm of the untreated sample than the baseline, 4-fold less TFE3 localized in the cytoplasm of the Tpg treated than the baseline, slightly more TFE3 localized in the cytoplasm of the starved than the baseline, and about 2-fold more TFE3 localized in the cytoplasm of the DMSO control than compared to baseline (Figure 12G). There was a decrease in the amount of TFE3 localized in the cytoplasm of the untreated and Tpg treated samples between 0 and 16 hours. There was an increase in the amount of TFE3 localized in the cytoplasm of the starved sample and the DMSO control between 0 and 16 hours. However, the increase in the amount of TFE3 localized in the cytoplasm of the starved sample was due to a very weak GAPDH band (Figure 12A).

When normalized to YY1, there was about 10-fold more TFE3 localized in the nucleus of the Tpg treated, the same amount of TFE3 localized in the nucleus of the starved sample, and about 2-fold more TFE3 localized in the DMSO control than the untreated nuclear control at 0

hours, which was the baseline (Figure 12H). There is a weak YY1 band in the nuclear sample of the Tpg treated sample, which resulted in the higher fold change (Figure 12A). At 16 hours, there was about 2-fold more TFE3 localized in the nucleus of the untreated control than the baseline, the same amount of TFE3 localized in the nucleus of the Tpg treated sample as the baseline, about 6-fold more TFE3 localized in the nucleus of the starved sample than the baseline, and about 3-fold more TFE3 localized in the nucleus of the DMSO control, when compared to the baseline (Figure 12H). The YY1 band for the starved sample at 16 hours was slightly weaker than the other bands. Overall, there was an increase in the amount of TFE3 localized in the untreated control, a decrease in the amount of TFE3 in the nucleus of the Tpg treated sample, an increase in the amount of TFE3 localized in the nucleus of the starved sample, and a slight increase in the amount of TFE3 localized in the nucleus of the DMSO control between 0 and 16 hours.

When normalized to H3, there was about same amount of TFE3 localized in the nucleus of the Tpg treated sample as the baseline, 1.5-fold more TFE3 localized in the nucleus of the starved sample than the baseline, and about 1.5-fold more TFE3 localized in the nucleus of the DMSO control when compared to the untreated nuclear control at 0 hours, which was the baseline (Figure 12I). At 16 hours, there was about 3.5-fold more TFE3 localized in the nucleus of the untreated control than the baseline, about the same amount of TFE3 localized in the nucleus of the Tpg treated sample as the baseline, about 2-fold less TFE3 localized in the nucleus of the starved cells than the baseline, and about 4-fold more TFE3 localized in the nucleus of the DMSO control, when compared to the baseline (Figure 12I). Overall, there was an increase in the amount of TFE3 localized in the untreated and DMSO controls between 0 and 16 hours. There was a slight increase in the amount of TFE3 localized in the nucleus of the Tpg treated sample

between 0 and 16 hours, and a slight decrease in the amount of TFE3 localized in the nucleus of the starved samples.

Between the two nuclear loading controls, there were some similarities in trends. There was an increase in the amount of TFE3 localized in the nucleus of the untreated and DMSO controls between 0 and 16 hours (Figure 12H and I). The trends in the Tpg and starved samples are difficult to discern, because both treatments had a weak YY1 band which affected the normalization of densitometry values.

Using the densitometry values obtained using the YY1 nuclear loading control and taken over GAPDH cytoplasmic loading control, the distribution of TFE3 was primarily a cytoplasmic localization for the untreated sample, starved sample and the DMSO control, and nuclear for the Tpg treated sample at 0 hours (Figure 12J). The Tpg distribution should be closer to an even localization between cytoplasmic and nuclear when looking at the western blot, however the densitometry value for the nuclear is incorrect due to the weak YY1 band (Figure 12A). At 16 hours, there was a greater localization of TFE3 in the cytoplasm for all of the samples (Figure 12J). From the western blot, it appears that the distribution is more even between nuclear and cytoplasm (Figure 12A). Overall, there was more cytoplasmic TFE3 in all samples at both 0 and 16 hours, except for the Tpg treated sample (Figure 12J).

Using the densitometry values obtained using the histone H3 nuclear loading control and taken over the GAPDH cytoplasmic loading control, the localization of TFE3 was more nuclear for the untreated control, the starved sample, and the DMSO control at 0 hours. There was more TFE3 localized in the cytoplasm of the Tpg treated sample at 0 hours (Figure 12K). At 16 hours, there was a strong presence of TFE3 localized in the nucleus for all treatments, except for the starved samples which were more cytoplasmic (Figure 12K).

Visually, neither of the distribution figures seems to explain what is happening in the western blot (Figure 12A).

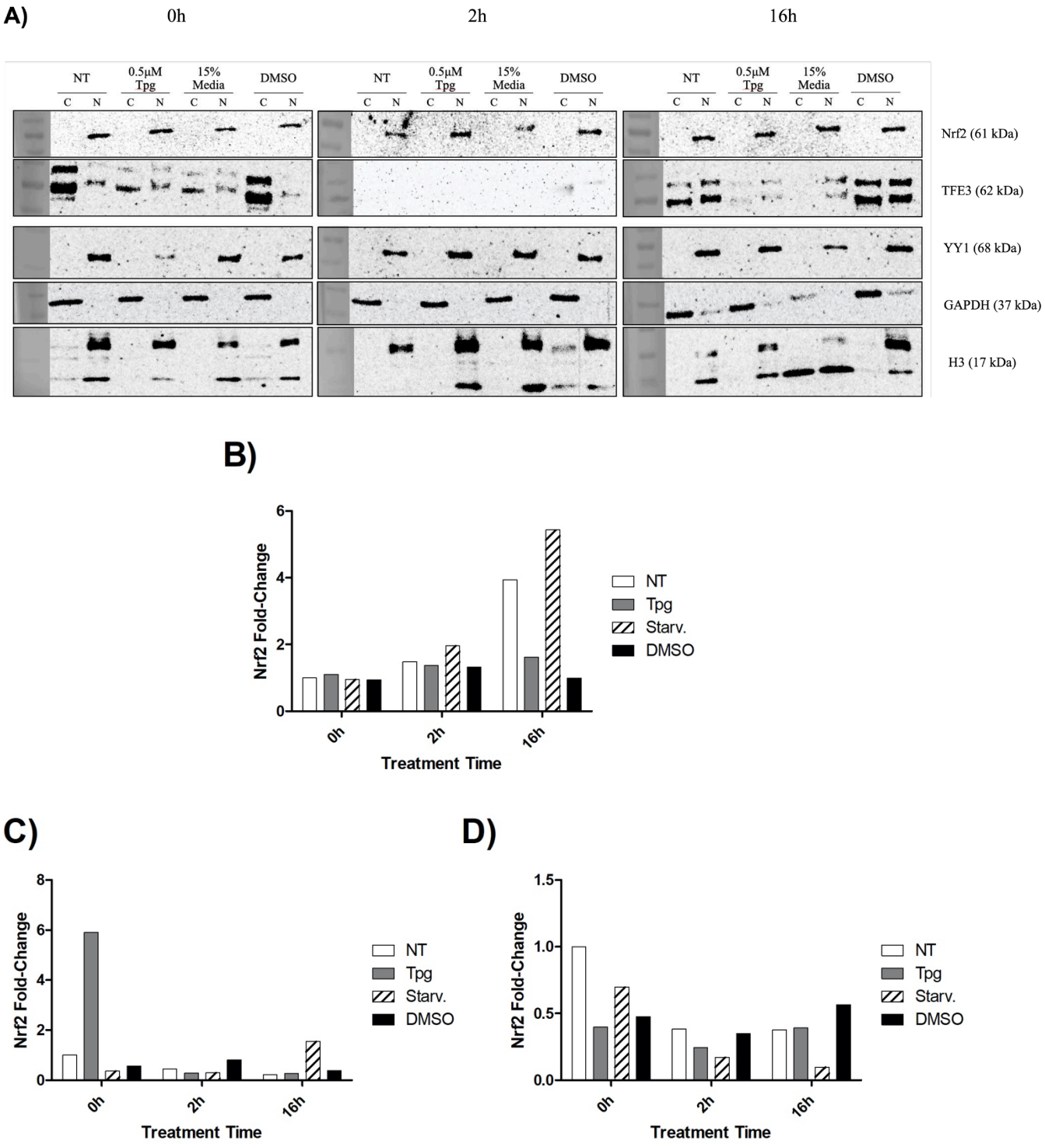
A)
0h
2h
16h
NT
0.5μM Tpg
15% Media
DMSO
C N
Nrf2 (61 kDa)
TFE3 (62 kDa)
YY1 (68 kDa)
GAPDH (37 kDa)
H3 (17 kDa)
B)
Nrf2 Fold-Change
Treatment Time
NT
Tpg
Starv.
DMSO
C)
D)

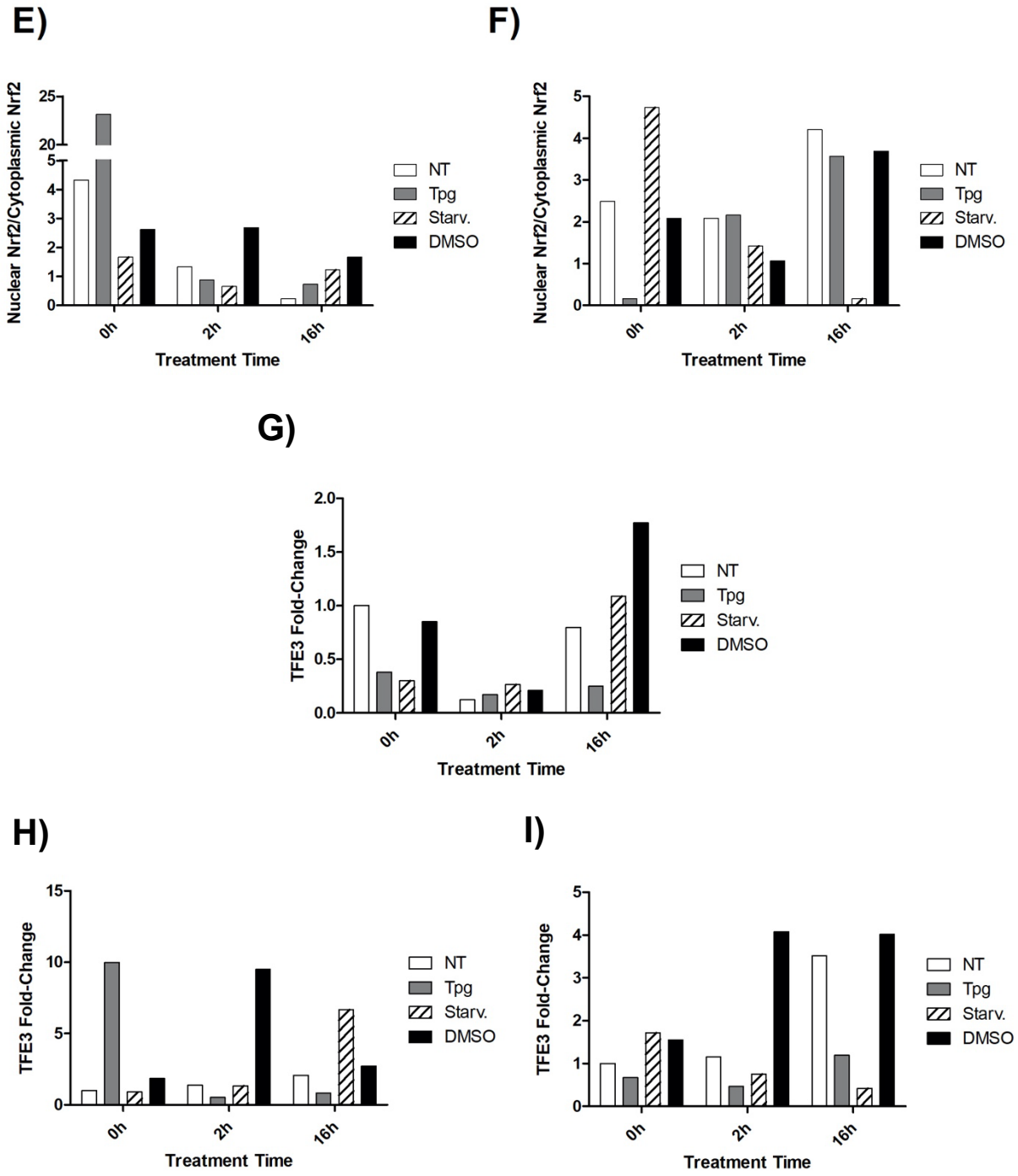
E)
F)
G)
H)
I)
Nuclear Nrf2/Cytoplasmic Nrf2
TFE3 Fold-Change
Treatment Time
0h
2h
16h
NT
Tpg
Starv.
DMSO

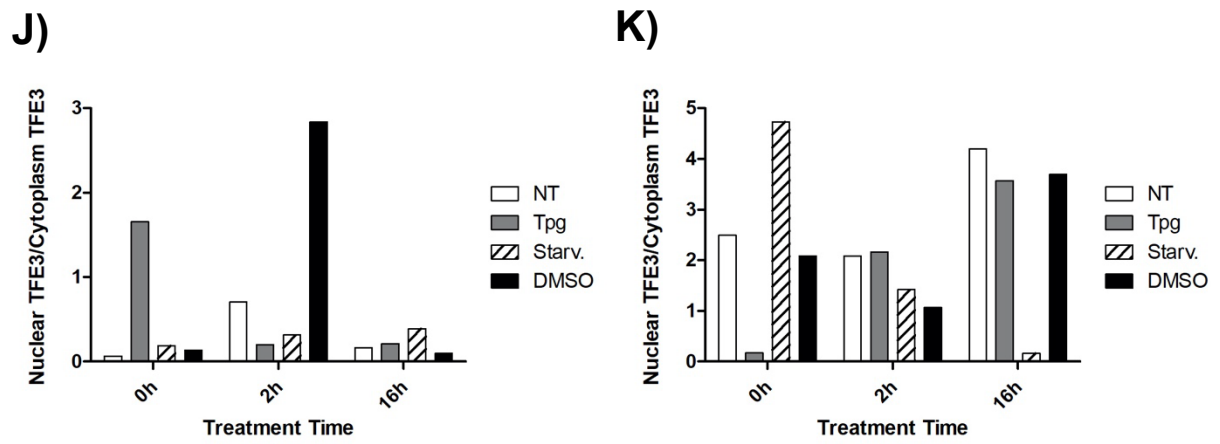

Figure 12. Effect of treatment with 0.5μM Tpg and 15% media (Starvation; 15% media, 85% 1X PBS) with DMSO or no treatment (NT) control for 0h, 2h, or 16h on the localization of the transcription factors Nrf2 and TFE3 in cytoplasm (C) or nucleus (N) in A2780 cells. A) Western blot documenting the localization of Nrf2 and TFE3 with different treatments at different time points. YY1 and H3 are nuclear loading controls, and GAPDH is the cytoplasmic loading control. B) Densitometry values of one biological replicate (replicate 1) for Nrf2 normalized to GAPDH cytoplasmic loading control relative to NT at 0 hours (baseline). C) Densitometry values for Nrf2 normalized to YY1 nuclear loading control relative to baseline. D) Densitometry values for TFEB normalized to H3 nuclear loading control relative to baseline. E) Distribution of Nrf2 between the nucleus (normalized to YY1) and cytoplasm (>1 is nuclear localization, value <1 is cytoplasmic localization). F) Distribution of Nrf2 between the nucleus (normalized to H3) and cytoplasm. G) Densitometry values for TFE3 normalized to GAPDH cytoplasmic loading control relative to NT at 0 hours (baseline). H) Densitometry values for TFE3 normalized to YY1 nuclear loading control relative to baseline. I) Densitometry values for TFE3 normalized to H3 nuclear loading control relative to baseline. J) Distribution of TFE3 between the nucleus (normalized to YY1) and cytoplasm (>1 is nuclear localization, value <1 is cytoplasmic localization). K) Distribution of TFE3 between the nucleus (normalized to H3) and cytoplasm. (n=1)

4.0 Discussion

Cancer remains a significant burden to the Canadian healthcare system as the leading cause of death in Canada, and the cost of care more than doubling between 2005 and 2012 [1]. Ovarian cancer specifically has low incidence rates relative to other cancers, but has one of the highest rate of mortality among gynecologic malignancies, including breast cancers [3]. The reason for this high rate of mortality is the commonly late-stage (including metastatic tumours) at diagnosis [8, 9]. Additionally, recurrence of disease after treatment is common in ovarian cancer patients due to drug resistance and the resultant lack of response to secondary chemotherapy. There is also no consensus amongst doctors on how best to treat recurrent disease [5, 11, 13].

The CAN-NCIC-MA22 clinical trial assessed the integrity of tumour rRNA using RIN, and it was observed that highly degraded rRNA was associated with pCR post-treatment [34, 35, 37]. In fact, when using RIN as a measurement of RNA integrity, highly responding tumours created aberrant bands between the 28S and 18S and resulted in an "n/a" RIN value [35, 37]. This aberrant banding was termed RNA disruption, which can be examined using the RNA disruption assay (RDA) and quantified using RNA disruption index (RDI) [35]. The RDI value increases as the tumour rRNA decreases, however when there is sufficient RNA disruption an "n/a" RDI value can also be generated due to almost complete loss of the 28S and 18S bands used for the algorithm. Within the clinical trial, RDA was able to distinguish patients who responded to chemotherapy treatment from those who did not, by using the RDI values obtained from their tumour rRNA [35, 37]. Furthermore, the RDA has been used *in vitro* to demonstrate that a large variety of mechanistically and structurally distinct chemotherapy drugs and cellular stressors are able to cause RNA disruption in a variety of tumour cell lines. This suggests there could be a common upstream mechanism or pathway that causes RNA disruption. An interesting

target would be transcription factors, which initiate many cellular stress pathways and initiate transcription of proteins that protect the cell or ultimately induce apoptosis if the burden is too great.

Transcription factors are key proteins with DNA-binding regions that bind to specific DNA sequences in the regulatory region of specific genes and regulate their expression through activation or repression of transcription [114]. Gene expression is primarily regulated through gene transcription [39]. Proper regulation of specific genes is essential so that the correct proteins are expressed in the correct tissues in response to appropriate signals at the appropriate time [114]. Cancer is often the result of a change in the expression or activity of specific oncogenes and tumour suppressor genes, which collectively result in enhanced cell survival and replication.

Cancer cells will reprogram to meet energetic and metabolic needs for their survival, and they can do this through multiple mechanisms such as upregulation or downregulation of antiapoptotic or proapoptotic genes, respectively, to survive [115]. Gene mutations or rearrangements that lead to enhanced production or activity of transcription factors can result in the enhanced growth of cancer or the onset of other diseases [114]. Some ways that transcription factors themselves are regulated include protein-protein interactions, ligand binding, and transcription factor phosphorylation [116]. Transcription factors induced by cellular stress usually play a role in the maintenance or return to cellular homeostasis, and the cellular stress can be anything from a xenobiotic agent to redox species. Many different transcription factors can respond at the same time across different pathways or play a role in several overlapping pathways at the same time. By studying specific transcription factors, induced by specific

chemotherapy agents and cellular stressors known to cause RNA disruption, and the role they play in certain stress pathways, a mechanism for RNA disruption may be elucidated.

The objective of this study was to investigate a potential mechanism for RNA disruption through the activation of stress-induced transcription factors. In order to achieve this objective, we needed to:

1) Identify specific stress-induced transcription factors of interest to study by treating A2780 ovarian cancer cells with a concentration of DXL known to cause RNA disruption and identifying which transcription factors became activated using transcription factor activation profiling plate arrays
2) Confirming the activation of specific stress-induced transcription factors by agents that induce cellular stress and RNA disruption by monitoring their translocation from the cytoplasm to the nucleus, where they can regulate gene transcription

4.1 Mycoplasma Contaminated Samples

Mycoplasma are bacteria that do not have a cell wall, and can infect and live off mammalian cells. They are also quite small (0.15-0.3μm) which allows them to go undetected in cell culture media and pass through filters commonly used to sterilize media and other components. Unlike other bacteria, mycoplasma are able to grow in large quantities in the cell culture media without causing turbidity or odour in the medium [117, 118]. These characteristics make it hard to detect mycoplasma contamination.

There are several sources of mycoplasma contamination in laboratory settings, including human, bovine, or swine sources. Human sources are most likely lab personnel, where M. *fermentans* and M. *hominis* can be found in the human oropharyngeal tract, and M. *orale* is most

commonly found in the oral cavity [117]. Bovine sources include from fetal bovine serum (FBS) or newborn bovine serum (NBS) (M. *arginini* and A. *laidlawii*, respectively) [117]. Finally, trypsin from a swine source can be a major source of M. *hyorhinis* [117].

Some side-effects of a mycoplasma contamination in mammalian cell cultures include: inhibition of cell proliferation, increased cell death, fragmentation of DNA, and morphological features of apoptosis [117]. Mycoplasma are able to bind to mammalian cells using special organelles called tips, which contain adhesins that help them to attach and fuse to the host membrane and exchange membrane and cytoplasmic components with the host cell [117]. Altered levels of protein, RNA and DNA synthesis is one general effect on eukaryotic cells [118]. Completely getting rid of mycoplasma is extremely difficult and the process itself can also create a cytotoxic environment for the cell cultures [117]. There are many different parameters that determine the effect of mycoplasma on cell cultures, such as the intensity and duration of infection, cell culture conditions, or the presence of additional infections [118]. Mycoplasma infections can create artefacts and skew results [118].

Unfortunately, when my study began, there was a previously undetected and unidentified mycoplasma infection in the A2780 ovarian cancer cell line cultures in our lab. The nuclear extracts used to study stress-induced transcription factors on the transcription factor activation profiling plate arrays were from the mycoplasma-infected cultures and this infection may have impacted our findings (Figure 1-5; Table 1-5). Likely, the cells used in the transcription factor activation profiling were under some stress caused by the presence of mycoplasma, even in the untreated conditions (although this stress alone was insufficient to induce RNA disruption).

4.1.1Selection of stress-induced transcription factors

In order to determine which transcription factors to study as potential upstream factors contributing to RNA disruption, transcription factor activation profiling plate arrays from Signosis were used. Since there were so many transcription factors, which could be activated at different times and under different conditions, only one timepoint, stressor and concentration of stressor was chosen for the profiling study. Docetaxel was a chemotherapy agent known to induce strong RNA disruption at a concentration of 0.2μM at 48 hours [111]. Thus, DXL was chosen as the stressor. An incubation time of 8 hours was chosen since most transcription factors are upregulated within this time frame. It was expected that the transcription factor would be upregulated before the induction of RNA disruption, which becomes detectable at 24 hours and clearly evident by 48 hours. Thapsigargin was one of the original stressors considered for the arrays, as there was evidence that X-box protein 1 (XBP1) expression was induced by thapsigargin at 8 hours, which was one of the transcription factors on the arrays (see Appendix Figure 14).

RNA disruption was evident at all three concentrations of DXL (0.02, 0.2 and 2μM) at 48 hours (Figure 1). Docetaxel induced RNA disruption at all of the concentrations tested (as seen by reductions in the intensities of the 28S and 18S rRNA bands and the formation of lower molecular weight RNA degradation products). Consistent with this view, RDI values were significantly higher in treated cells at all concentrations compared to untreated cells (Figure 1B). It was previously reported by Narendrula *et al.* (2016) that RNA disruption could be induced by DXL in A2780 cells, as manifested by the generation of very distinct 28S rRNA degradation fragments [111]. We were able to reproduce these findings in these investigations. However, subsequent studies by our research group have revealed that: a) in mycoplasma-free cells, DXL

only induces a small amount of RNA disruption, which appears as a diffuse pattern of rRNA degradation fragments between the 28S and 18S rRNA bands on electropherograms, and b) the presence of mycoplasma in cultures augments DXL-induced RNA disruption, and the RNA degradation fragments appear as a small number of rRNA fragments of very defined molecular weights. This possibly suggests that the mechanism for RNA disruption by DXL may be different in cells infected with mycoplasma.

Since the A2780 cells exhibited RNA disruption, we then assessed whether RNA disruption by known chemotherapy drugs and cellular stressors is preceded or accompanied by increased expression or activation (translocation) of stress-induced transcription factors. The extract protein concentrations of the nuclear and cytoplasmic extracts were quantified (Table 1 and 2), and the Coomassie stained gels were used to confirm the quantification, and to assess differences in the protein banding pattern between nuclear and cytoplasmic extracts (Figure 2). The banding patterns were different between the cytoplasmic and nuclear extracts, as expected due to the different protein compositions of the fractions.

4.1.1.1 Mitochondrial UPR

In our transcription factor activation profiling plate arrays, three collections of transcription factors were assessed for their activation by stressors: transcription factors related to mitochondrial UPR, ER stress-related transcription factors, and a large collection of known transcription factors (TFII). The TFII set included 96 transcription factors, some of which were present on the other profiling plates, which provided more replicates and some new transcription factors that were of interest to the study.

The mitochondria has its own DNA (mtDNA) that encodes roughly 13 mitochondrial proteins [92]. However, the majority of mitochondrial proteins are encoded in the nuclear DNA

and imported into the mitochondria unfolded. Both the mitochondrial- and nuclear-encoded mitochondria proteins are folded in the mitochondria with the help of mitochondrial chaperones [93]. Although not as well established as ER UPR, the mitochondrial UPR can be upregulated after an accumulation of unfolded proteins in the mitochondria, typically as cells undergo stress. Damaged or dysfunctional mitochondria can undergo a mitochondria-specific autophagy called mitophagy [68]. Properly functioning mitochondria are important in the cell, as it is a major site of apoptotic signalling.

The first plate that was tested was the Mitochondrial UPR TF Activation Profiling Plate Array from Signosis. This plate contained 16 different transcription factors that were repeated six times across the plate.

One of the transcription factors that had high levels of DNA binding activity (i.e. high RLUs) across most replicates was SATB. SATB has been described as a "genomic organizer" [119, 120]. SATB was originally identified for its role in differentiation and activation of T cells. However, more recently, SATB has been identified in many human cancers, which may promote development and progression of metastases [119]. SATB had high levels of activity in both the untreated sample and the treated samples (Figure 3B). In the first biological replicate, SATB had an increase in activity compared to the untreated control in both technical replicates. However, in the second and third biological replicates, SATB had an increase in activity in the first technical replicate and a decrease in the second, compared to no treatment (Figure 3C-F). This lack of a clear association between DXL treatment and SATB activation in A2780 cells suggests that the transcription factor is not reproducibly activated in response to DXL treatment. Since RNA disruption does reproducibly occur in response to DXL, this would suggest that SATB1 activation is not associated with RNA disruption. High levels of SATB1 in metastatic ovarian

cancer patients correlated with shorter survival times, and weak or negative SATB1 expression was correlated with patients with longer survival times [119]. Therefore, a higher baseline expression in the untreated samples as well as in the treated samples suggests that the transcription factor may impact on tumorigenesis or disease trajectory for ovarian cancer. There was variability in the upregulation and downregulation of SATB activity between technical replicates, which suggests variability in the data could have been generated by the arrays themselves.

E2 promoter binding factor 1 (E2F1) was another transcription factor that had a high baseline of DNA binding activity across all replicates (Figure 3). E2F1 is a key regulator of cell cycle progression, specifically the progression of cells from G1 to S phase, and its overexpression alone can be enough to drive quiescent cells into S-phase [121, 122]. E2F1 has both tumor promoting and tumor suppressing roles, which appear to be context specific [121, 122]. E2F1 overexpression has been shown to induce apoptosis both dependent and independent of p53 [121]. E2F1 is essential for mitochondrial apoptosis, and many of the factors involved are also involved in ER stress-induced cell death indicating a crosstalk between the two pathways [121]. Due to the enhanced growth of cancer cells, it is possible that the increased expression of E2F1 is conferring an advantage on the cancer cells, promoting transition into S phase. E2F1 had high levels of activity and at least a 2-fold change in all of the replicates on the Mitochondrial UPR array, whether treated or untreated (Figure 3). However, E2F1 exhibited increased activity in all of the first technical replicates of the biological replicates (Figure 3A, C, E), and a decrease in activity in the second technical replicates compared to no treatment (Figure 3B, D, F). This is interesting because all of the first technical replicates are on one array, and the second technical replicates were on another. This suggests that the data variability may be related to the

manufacturer's inability to maintain consistent levels of gene probes across arrays. As for the ability of DXL to activate E2F1, this hypothesis is supported by the first set of technical replicates on the Mitochondrial UPR array, but not in the second set of technical replicates, where E2F1 appears to be downregulated in response to DXL.

FOXO3 is a member of the forkhead box O family of transcription factors that modulates genes involved in development, differentiation, autophagy, apoptosis, metabolism, cell cycle, immune response, stress resistance, and longevity [123-125]. FOXO3 is a substrate of SIRT3, which is a NAD^+ deacetylase specifically found in the mitochondria [125]. Deacetylation of FOXO3 results in reduced levels of cellular ROS through upregulation of antioxidant enzymes [125]. FOXO3 is essential for controlling ROS levels in hematopoietic stem cells, which have high numbers of mitochondria but are relatively inactive metabolically and produce limited ATP [126]. Tseng *et al.* (2013) found that SIRT3-induced-FOXO3 was able to upregulate PGC-1α to promote mitochondrial biogenesis and execute mitophagy under oxidative stress [125]. FOXO3 was another transcription factor that had high levels of baseline activity in all of the experimental replicates (Figure 3). Similar to E2F1, FOXO3 had higher activity in the DXL treated samples in the first technical replicates of the biological replicates (Figure 3A, C, E), and decreased activity in the second technical replicates compared the untreated control cells (Figure 3B, D, F). Again, it is difficult to comment on the implications of FOXO3 activity since there is so much variability between the upregulation and downregulation of the transcription factor between replicate experiments.

4.1.1.2 ER Stress

The second type of array used was the ER Stress (UPR) TF Activation Profiling Plate Array from Signosis (Figure 4). Similar to the Mitochondrial UPR array, there were 16 different transcription factors associated with ER stress on this plate that were repeated six times.

SREBP1 was one of the transcription factors with consistently high DNA binding activity on the ER stress array (Figure 4). SREBP1 is a transcription factor anchored to the ER membrane and plays a role in lipogenesis [127]. SREBs are inactive precursor proteins anchored to the ER membrane, which are activated by proteolytic cleavage to form the transcriptionally active SREBP N-terminal domain, which translocates to the nucleus [127, 128]. SREBP1 has been shown to be upregulated in response to known ER stressors, such as thapsigargin and tunicamycin. It binds to sterol regulatory elements (SRE) which are upstream of genes encoding enzymes involved in fatty acids, lipids, and cholesterol biosynthesis [127, 128]. There have been reports of SREBP1 overexpression in cancer cells to meet the demand for lipids required for cell replication [128]. Huang *et al*. (2012) determined that SREBP1 plays a role in the progression, growth, and survival of prostate cancer cells [127]. This group also showed that overexpression of SREBP1 in prostate cancer cells increased ROS, cell proliferation, migration, and invasion *in vitro* [127]. SREBP1 had a high baseline activity in all replicates, but also had at least a 2-fold change in either direction in all replicates (Figure 4). However, SREBP1 had decreased activity in the first and third replicate but increased activity in the second compared to no treatment (Figure 4). There are several studies linking SREBP1 expression induced by mutant p53 in prostate cancer to DXL resistant tumors [129, 130]. If this were the case, it would be expected that SREBP1 would have increased activity, not decreased in response to DXL treatment in this study, which is the case in two of the three replicates (Figure 4).

XBP1 is a transcription factor originally identified as binding to the promoter region of major histocompatibility complex class II genes [131]. It is now seen as a highly active transcription factor capable of activating UPR in response to ER stress. XBP1 mRNA is induced by ATF6 and then spliced by IRE1 resulting in the active protein [131]. XBP1 binds to the ER stress response element (ERSE) to upregulate ER chaperones [131]. Splicing by IRE1α creates a potent transcription factor, but the unspliced XBP1 protein that exists in low quantities under normal conditions does not have transactivation activity [132]. Interestingly, previous unpublished data from the laboratory indicated that DXL was not able to induce spliced XBP1 in A2780 cells (see Appendix Figure 14). XBP1 had low levels of activity in the first two replicates, but not in the third (Figure 4). It also exhibited a decrease in activity in the first two replicates and an increase in activity in the third compared to no treatment. There was at least a 2-fold change in either direction in all three replicates (Figure 4). The downregulation of XBP1 seen in these first two replicates would align with the unpublished data from the laboratory which showed no visible activation of spliced XBP1 by DXL in immunoblot analysis for up to 72 hours (see Appendix Figure 14).

NFκB can be activated through cytokines, mitogens, chemical agents, oxidants, UV and ionizing radiation, viral and bacterial products, and the accumulation of proteins in the ER [133, 134]. Most of the treatments that induce NFκB also activate AP-1 [135]. NFκB and AP-1 are induced by the intracellular redox state, and regulate the expression of genes involved in oxidative stress and cellular response [134]. NFκB is a member of the Rel family of proteins, which are inactive in the cytoplasm [134]. NFκB is bound to an IκB inhibitory protein which becomes degraded after phosphorylation triggered by stimuli, allowing for the translocation to the nucleus [134]. NFκB regulates genes encoding cytokines, cytokine-receptors, cell adhesion

molecules, and growth factors [134]. High Ca^{2+} contributes to oxidative stress susceptibility, which include proteolytic processes [134]. NFκB had low levels of DNA binding activity in all the treated and untreated sample replicates (Figure 4). There was at least a 2-fold change of the transcription factor in either direction, with a decrease in activity in the first and third replicate and an increase in activity in the second (Figure 4).

AP-1 is an important mediator of tumor promotion and is a dimeric protein composed of Jun and Fos proteins coded by the *c-jun* and *c-fos/ATF* protooncogenes [134]. AP-1 can be induced by growth factors, mitogens, cytokines, neurotransmitters, and cellular stress [136]. It was originally identified as a transcription factor that mediated gene expression in response to 12-*O*-tetradecanoylphorbol-13-acetate (TPA), a common tumor promoter and inducer of ROS [136]. TPA activates c-Jun N-terminal kinases (JNKs), which phosphorylate Jun proteins leading to increased Jun and Fos protein levels and increased transcriptional activity [137]. Each type of AP-1 is differentially expressed and regulated with subtly different functions [137]. Increases in Jun and Fos proteins, as well as JNK activity is reported to accompany apoptosis [137]. When activated, AP-1 bind TPA response elements (TRE), which is in the promoters of many early genes [136]. Some cellular processes regulated by AP-1 include cell proliferation, differentiation, and apoptosis [138]. One study showed a strong increase in AP-1 activity in HepG2 cells after treatment with bortezomib, which resulted in bortezomib-induced apoptosis [138]. The mechanism of action is proposed as activation of JNK, which phosphorylates c-Jun which favours the production of AP-1. The increase in AP-1 results in increased gene expression of c-Jun, FasL, and Bim, which are proapoptotic proteins. FasL induces the activation of caspase-8. Subsequently, the Bim accumulation along with p53 decrease antiapoptotic protein Bcl-2 and increase Bax, which induce the depolarization of the mitochondrial membrane and the release of

cytochrome c and the activation of caspase-3 [138]. AP-1 had low to moderate levels of DNA binding activity, whether in treated or untreated cells (Figure 4). In the first two replicates, there was a decrease in the activity of AP-1 compared to no treatment. However, in the third replicate there was an increase in activity. All of the replicates showed at least 2-fold change in activation in either direction (Figure 4).

PGC-1α is highly expressed in mitochondria and tissues which have higher energy demands [139]. Under normal conditions, PGC-1α is expressed at low-levels and becomes strongly induced in response to increased energy and metabolism demands [115]. PGC-1α responds to energy metabolism, mitochondrial biogenesis, and homeostasis [139]. In cancer, PGC-1α plays a key role in promoting drug resistance through metabolic adaptation, glycolysis, oxidative phosphorylation, fatty acid oxidation, glucose-derived lipogenesis, glutamine-derived lipogenesis, and ROS clearance [139]. Yun *et al.* (2019) found that PGC-1α knockdown in prostate cancer cells resulted in decreased mitochondrial function and resulted in mitochondrial ROS indicating that PGC-1α plays a role in protecting the mitochondria from ROS damage after treatment with chemotherapy which is often a mechanism through which they exert their effects [139]. Mitochondrial ROS production induces ER stress, and PGC-1α expression results in ROS-ER stress-mediated apoptosis [139]. PGC-1α was the transcription factor demonstrating the highest levels of DNA binding activity in both the untreated and treated samples, and only had a minimum 2-fold change in response to DXL treatment in the third replicate (Figure 4). PGC-1α had a slight increase in activity in the first replicate, and a decrease in activity in the second and third replicates (Figure 4). Interestingly, PGC-1α is found highly expressed in the mitochondria but is not on the Signosis Mitochondrial UPR array, and instead found on the ER Stress array. The consistently high expression levels in both the untreated and DXL treated samples could be

a result of meeting the energy demands of the cancer cells. The slight decrease in the activity of PGC-1α in the DXL treated samples could be a result of decreased energy demands as the cell attempts to deal with the suppression of the cell cycle by DXL.

Both CHOP and ATF4 were on the Mitochondrial UPR and ER Stress arrays (Figure 3 and 4). ATF4 is specifically promoted by eIF2α, which is initially phosphorylated by PERK and causes an inhibitory effect on the guanine nucleotide exchange factor eIF2B, resulting in protein synthesis inhibition [128]. ATF4 is able to be upregulated despite protein synthesis inhibition due to an alternate open reading frame allowing for dedicated translation of transcripts with these types of open reading frames [79]. Next, ATF4 induces expression of CHOP, which positively regulates proapoptotic genes in response to ER stress [128]. ATF4 had weak to moderate activity on both arrays (Figure 3 and 4). CHOP is a member of the C/EBP family of transcription factors, which regulate cell differentiation and apoptosis [140]. CHOP is also known as growth arrest and DNA damage-inducible gene 153 (GADD153), which functions as an ER chaperone gene that induces pro-apoptotic functions of prolonged ER stress [140]. CHOP downregulates the anti-apoptotic Bcl-2 protein, while upregulating pro-apoptotic Bim [140]. CHOP can activate death receptor 5 (DR5), which activates apoptosis through caspase 8 activation [140]. CHOP is expressed at low-levels under normal conditions, but can be robustly upregulated during times of stress through all three main activators of ER stress [140]. CHOP produced consistently weak signals on both arrays, which could indicate that the 8-hour DXL treatment was not sufficiently long enough to promote CHOP upregulation. This makes sense, since tunicamycin, a specific ER stressor, causes prolonged ER stress after 16 hours of treatment [51]. It is also possible that CHOP was induced much earlier and returned to low levels within 8 hours. It seems more likely

that it was not yet upregulated, due to the weak and moderate signals of ATF4, which regulates the activation and upregulation of CHOP.

There was a high amount of variability between the technical replicates, as well as biological replicates. Some variability between biological replicates could be expected even when taking care, but presumably not as much as seen. However, knowing now that there was a mycoplasma infection causing the cells stress even if all other factors were accounted for, could account for the variability between biological replicates, but not the technical replicates. Since this was not known at the time, but there was a high amount of variability seen, it was decided that only one biological replicate would be used on the final three sets of plates in 3 technical replicates.

The data from the previous array experiments was used to choose the biological replicate experiment yielding the most consistent findings. This was the first biological replicate and these nuclear extracts were used for the final set of array experiments (TFII).

4.1.1.3 TF II

The last set of transcription factors that were studied were 96 different transcription factors on the TF II Activation Profiling Plate Array from Signosis. These arrays came with two plates, which allowed one set to be used for nuclear extracts from treated cells and one set to be used for nuclear extracts from untreated control cells. Three technical replicates were used from the first biological replicate experiment, which can be seen in Figures 3A&B and 4A.

When the means from the three technical replicates of the first biological replicate experiment were taken, SATB, ROR, and SOX9 met the minimum level of activity (i.e. 1000 RLUs in either the DXL-treated or untreated sample) (Figure 5D). Overall, the TFII array had

less DNA binding activity than the other two array types when compared to the same samples and same transcription factors across arrays. However, there was at least a 2-fold change in either direction seen in AP-1, NFκB, AR, C/EBP, E2F1, GR/PR, AP4, FREAC2, MZF, RNUX, ROR, SOX2, TFE3, and USF-1 (Table 4). Interestingly most of these were not noticeable because their activity was quite low. Finally, there was a reproducible increase or decrease in activity when compared to no treatment seen in many of the transcription factors across replicates including YY1, Brn-3, CBF, GR/PR, IRF, MEF2, PXR, SMAD, STAT3, COUP-TF, MZF, Nkx2-5, NRF1, Pax3, PIT1, MEF1, ROR, RXR, SF-1, Snail, SOX9, SRY, TFE3, USF-1, and VDR (Table 4). Finally, there were statistically significant differences in transcription factor activity between DXL-treated and untreated cells for the following transcription factors: YY1, CBF, SMAD, MZF, MEF1, and PXR (Table 4). While statistical analyses are generally not performed using technical replicates, this was done in order to help focus our efforts on the most relevant transcription factors associated with stress-induced RNA disruption.

4.1.1.4 Selection criteria and process

The variability seen within the plates and between the plates did not allow for definitive and intuitive choices in transcription factors for further study. The variability seen between the technical replicates on different plates, and between the same transcription factors on different plates, can most likely be attributed to inconsistencies in the plates themselves, since there appeared to be great variation in RLU for a given transcription factor across plates, even when using the same nuclear extract. Regardless of the mycoplasma infection, which could cause variability between biological replicates, there should not have been as much variability as there was for technical replicates. In order to remain objective in deciding which transcription factors would be studied further, a set of selection criteria were chosen (Table 3). Ideally, a transcription

factor worth further study would display statistically significant differences in activity between the DXL-treated and untreated cells, reproducible changes in the direction of change in gene expression (upregulation or downregulation) in response to DXL, a minimum 2-fold change in gene expression by DXL, and a signal strength of at least 1000 RLUs for the transcription factor in either the treated or untreated conditions. None of the transcription factors met all four of these criteria, however these criteria did allow for 104 transcription factors to be narrowed down to 55 transcription factors and then finally to 10: YY1, PXR, TFEB, TFE3, Nrf2, MEF1, MZF, ROR, and CBF, and SMAD. They were narrowed down further through a literature review, with particular focus on stress pathways, if there were comparable studies in the literature, and whether there was a reliable antibody on the market for each of the 10 transcription factors.

PXR is a transcription factor involved in xenobiotic response that plays a role in the drug-inducible expression of drug-metabolizing enzymes such as phase I and phase II metabolic enzymes and drug transporters [141, 142]. PXR also plays a role in endobiotic metabolism through expression of genes involved in glucose, lipid, and bile acid metabolism [141]. PXR is largely expressed in hepatocytes, liver, and kidneys but there is a small amount of expression in other tissues including ovaries [141-143]. PXR ligands include drugs (including taxol), endogenous ligands, or products of gut microflora [141]. Some transcription factors that crosstalk with PXR regulation of glucose and lipid homeostasis include: CREB, FOXO1, and SREBP-1. Some other transcription factors that crosstalk with PXR to control cholesterol and bile acid synthesis include: PGC-1α, HNF4α, RXR, and NFκB [141]. PXR has been shown to enhance cancer cell growth and higher levels of expression have been seen in endometrial and other cancers [142, 144]. When bound and activated by its wide variety of ligands, PXR translocates from the cytoplasm to the nucleus and binds as a heterodimer with RXR to

xenobiotic response elements (XRE) [143]. While there is a lot of evidence for PXR involvement in drug metabolism, PXR does not appear to be associated with any of the known stress pathways.

There are eight SMAD proteins in the human genome, and five are substrates of the TGFβ family of receptors [145]. The N-terminal Mad-homology 1 domain (MH1) and the C-terminal MH2 domain are highly conserved in all Smad proteins [145]. The MH1 domain has DNA-binding properties, while the MH2 domain mediates interactions with cytoplasmic retention proteins [145]. Smad proteins accumulate in the nucleus as a result of receptor-mediated phosphorylation which decreases the affinity for cytoplasmic anchors and increases their affinity for nuclear factors [145]. Unfortunately, the Signosis plate did not specify which Smad protein or proteins were included on the array. This limits of the utility of the array to provide insight into the role of Smad protein signalling in stress-induced RNA disruption.

ROR is part of a nuclear receptor superfamily with highly conserved DNA binding domains in the form of two zinc finger structures [146]. This superfamily of nuclear receptors expanded through cloning, but some of the newer members had no known ligand and were referred to as orphan nuclear receptors [146]. Members of the ROR subfamily include RORα, RORβ, and RORγ [146, 147]. Cholesterols are RORα agonists that enhance transcriptional activation, which implicates RORα in lipid metabolism [147]. Although ROR is expressed in many tissues, it is most highly expressed in the brain [147]. There are many studies involving ROR in cellular differentiation and immune cell regulation. There were some studies that indicated RORγ deficiency in mice resulted in higher incidences of thymic lymphomas that metastasize [147]. Increased expression of Th17-associated genes including RORγ has been shown in gastric tumors, and a high incidence of Th17-positive cells are found in ovarian cancers

[147]. RORα is highly induced under hypoxic conditions in a variety of cell types, and can also be induced by H_2O_2, thapsigargin, and tunicamycin [147]. Despite these studies, the role of ROR in these pathways is not well established and there was no clear link in our study between ROR activation and RNA disruption by DXL.

CBF (CCAAT binding transcription factor) is also called NF-Y and CP1 [148]. NFY was first recognized as a protein binding to the major histocompatibility complex (MHC) class II conserved Y box [149]. A CCAAT box is present in approximately 25-30% of eukaryotic promoters, but binds only to some of these CCAAT box-containing promoters, based on the distance of the CCAAT box from other regulatory elements, its position within the promoter, or due to interfering factors [150]. CBF/NF-Y has been shown to regulate many genes that are overexpressed in several types of cancers [149]. Many DNA binding proteins interact with CCAAT but CBF/NFY has been shown to require all 5 nucleotides in order to bind to this sequence [149]. The targets of CBF/NF-Y can be divided into two main categories: cell cycle-related genes and human disease-related genes [149]. CBF/NF-Y controls the expression of topoisomerase IIα and cyclin-dependent kinases (CDKs). There are also reports of CBF/NF-Y regulating mitotic cyclins during p53-dependent G2 arrest due to DNA damage, which suggests a regulatory role at the G2 checkpoint after DNA damage [149]. Knockdown of CBF/NF-Y impairs G2/M progression, induces apoptosis, and activates p53 in the absence of DNA damage [149]. The balance in expression of CBF/NF-Y seems important for cell survival by maintaining transcription of anti-apoptotic genes and preventing p53 activation that triggers the apoptotic cascade [149]. It is not surprising that CBF/NF-Y was induced in our A2780 cancer cells due to its general role in transcriptional activation; however, its role is too general, and no known specific stress pathways appear to be related to CBF/NFY expression or activity.

MZF-1 was originally identified for its role in hematopoiesis, where it regulates cell differentiation and proliferation [151]. It has also been identified to play a role in tumorigenesis and tumor progression, but the mechanism by which this happens is unknown [151]. MEF1 is a transcription factor that has been implicated in tumorogenesis [152]. Many of the citations for both these transcriptions were not recent and there were few of them.

YY1 is a transcription factor with the ability to activate or repress transcription [153]. It is ubiquitously expressed, and regulates the expression of many cellular and viral genes [61]. Additionally, YY1 overexpression has been reported in prostate, breast, and ovarian cancers [4, 154, 155]. Matsumura *et al.* (2009) studied the transcription factor in ovarian cancer and ovarian cancer cell lines, and how its expression may impact on tumour cell response to chemotherapy agents, namely taxanes [4]. They found that increased YY1 expression resulted in increased sensitivity to paclitaxel, but not to cisplatin. They also found that an increased tumour expression of YY1 was associated with improved prognosis in patients treated with paclitaxel [4]. Their study was directly relevant to this study, since this study used docetaxel, a taxane, to treat ovarian cancer cells. Interestingly, YY1 was the only transcription factor that reached statistical significance in our study using biological replicates across arrays.

Nrf2 is a transcription factor involved in the detoxification of xenobiotic agents and is activated as part of an antioxidant response mechanism in cells [156]. Under basal conditions, Nrf2 is kept inactive in the cytoplasm through interaction with Keap1. There are several mechanisms described for the activation of Nrf2 in response to stress, such as conformational changes in Keap1 in response to electrophiles, resulting in the release of Nrf2 or phosphorylation of Nrf2 by different kinases [28]. In fact, PERK is one of the kinases that phosphorylates Nrf2, leading to its dissociation from Keap1 and translocation into the nucleus [28, 59]. Nrf2 binds to

antioxidant response elements (ARE) upstream of genes involved in drug metabolism, apoptosis, and autophagy [55]. Nrf2 was consistently upregulated by at least a factor of 2 compared to the untreated control in our arrays. As a major cellular defense mechanism against toxic compounds, Nrf2 made for an interesting target in this study of stress-induced RNA disruption.

TFEB has been identified as a master regulator of lysosome biosynthesis and autophagy [157]. Interestingly, phosphorylated TFEB and TFE3 are inactive in the cytoplasm through docking to the cytoplasmic chaperone 14-3-3 [47, 157]. TFEB and TFE3 bind to coordinated lysosomal expression and regulation (CLEAR) elements, which are upstream of genes that regulate autophagosomal formation and degradation [45]. TFEB and TFE3 can respond to different types of stress such as starvation, ER stress, mitochondrial infection, and pathogen infection [45]. TFEB and TFE3 were of interest before the study began due to the study by Martina *et al.* (2016), which showed their novel involvement in ER stress through mechanisms different than those used after induction by starvation [51]. This shows that they are able to be induced through multiple stressors, which could be useful since RNA disruption can be induced by multiple types of stressors, as well.

For the above reasons, YY1, Nrf2, TFEB and TFE3 were chosen to be further studied in translocation experiments, and the others were not. Consequently, many of the strongly active transcription factors detected in our transcription factor activity arrays were not pursued for their possible roles in RNA disruption.

4.1.2 Mycoplasma contamination – change of stressors and timepoints

Unfortunately, the specific effects that contaminating mycoplasma had on the transcription factor array studies are not known. It is likely that the presence of mycoplasma induced stresses in the cells even in the absence of treatments – stresses, however, that were not

sufficient to induce RNA disruption. As mentioned, some of the known effects that mycoplasma can have on cell cultures include: altered synthesis of protein, RNA, and DNA; altered cell metabolism; induction or suppression of cytokine expression; interference with biological assays; and influence on signal transduction [118]. We now know that the presence of mycoplasma does affect the banding pattern of RNA electropherograms when cells experience chemotherapy-induced RNA disruption (Butler *et al.* manuscript in preparation). When the A2780 cells are mycoplasma-free, the RNA disruption assay does not show secondary bands of distinct molecular weights below the 28S and 18S rRNAs. Instead, multiple diffuse bands (smearing) are apparent in the inter-region between the 28S and 18S rRNAs and below the 18S rRNA. In addition, unlike our previously published study (Narendrula *et al*. 2016), my findings in this study indicated that DXL does not promote strong RNA disruption [111]. In contrast, doxorubicin (DOX) was found to be a more potent agent of RNA disruption in mycoplasma-free A2780 cells. Additionally, maximum RNA disruption was observed later at 72 hours, as opposed to 48 hours in the mycoplasma-contaminated cells. It is possible that mycoplasma induces cellular stress, which in turn sensitized the cells to earlier RNA disruption by a mechanism distinct from that observed in mycoplasma-free tumour cells. Since mycoplasma can cause DNA and RNA stress and damage through mycoplasma endo- and exonucleases, this could have enhanced RNA disruption by activating a unique RNase, such as RNase L [117].

Although this creates some uncertainty to the validity of the results obtained from the transcription factor activation profiling arrays, in mycoplasma-contaminated cells, the arrays still permitted us to identify active transcription factors that may play a role in RNA disruption. The purpose of the arrays was exploratory and to provide a reference framework for further studies. As well, the data from the arrays, while not definitive, did permit us to objectively select

transcription factors for further study, based on a set of clearly defined selection criteria. Despite the presence of mycoplasma, the activity of these transcription factors was regulated in response to cellular stress induced by DXL and may help promote RNA disruption.

In our subsequent transcription factor localization studies, we continued to use DXL as one cellular stressor, but also made sure to use an agent that was able to potently induce RNA disruption in the absence of a mycoplasma infection (DOX). The RNA disruption assay was done at 72 hours, instead of 48 hours, as higher levels of RNA disruption can be observed at this timepoint in mycoplasma-free cells. Thapsigargin and starvation were also added as stressors, due to their ability to induce ER stress and autophagy, which are two well-established cellular stress pathways.

The initial protocol for preparation of nuclear extract to be used in the Signosis transcription factor arrays was found to be sub-optimal by a prior undergraduate thesis student (see Appendix Figure 15). My studies employed an improved protocol, which generated highly enriched extracts for nuclear or cytoplasmic proteins, as documented in the Results section above.

4.2 Mycoplasma-free Samples

For DOX and DXL, there was not much literature determining when the transcription factors may be activated by the chemotherapy agents. Therefore, the timepoints used were 0, 16, and 24 hours. The study by Martina *et al*. (2016) helped to guide the choices of timepoints for thapsigargin and starvation, where their study used tunicamycin and starvation to induce activation of TFEB and TFE3 in mouse embryonic fibroblasts [51]. They found the induction of TFE3 and TFEB peaked at 30 minutes and lasted up to 2 hours for starvation, but peaked at 16 hours for tunicamycin, another agent known to induce ER stress. Since it was observed that Tpg

induced better RNA disruption than tunicamycin, it was chosen at a concentration that induces RNA disruption. Therefore, the timepoints chosen for these two stressors were 0, 2, and 16 hours.

4.2.1 YY1 as a nuclear localization control as compared to histones

Chromatin is made up of the nucleosomes of core histones, the genomic DNA, and linker histones [150]. DNA wraps around nucleosomal histones, which consist of octamers made up of two H2A-H2B dimers and a tetramer of two H3 and H4 histones [158]. H3 and H4 N-terminals are exposed from the compact core, allowing for easier post-translational modifications such as acetylation, methylation, and phosphorylation [158]. When expression of a gene is required, the DNA for the gene needs to be relaxed or released from the histones. Particularly, acetylation of lysine residues of histone H3 and H4, which neutralizes their positive charges, thereby weakening the interaction between DNA and histones [150]. Further, histones are known to become phosphorylated during chromosome condensation of cell division, beginning during S-phase and peaking during early mitosis [158]. Specifically, histone H3 becomes phosphorylated at Ser10 during G2, peaks at metaphase, and begins to diminish during late anaphase and telophase [158]. Several studies have shown the need for H3 phosphorylation for entry into mitosis [158-161]. Therefore, it would be assumed that a histone would make an ideal nuclear loading control. However, there were some occasional issues with the histone H3 antibody, where the proteins were not detected or were very faint. Interestingly, during the initial experiments used to optimize the Schreiber *et al.* (1989) and Abcam nuclear extract protocols, the transcription factor YY1 was observed exclusively in the nuclear extract (Figure 7). Therefore, having YY1 as another nuclear loading control was helpful. This was also interesting because as a transcription factor and a nuclear loading control, it allowed for direct comparison.

However, YY1 was still identified in the arrays and was the only transcription factor whose activity was significantly elevated in response to DXL in multiple biological replicate experiments (Table 5). The changes in YY1 were not a minimum 2-fold change in either direction in the ER Stress or TF II array; moreover, YY1 only met the ≥1000 RLU criterium in the ER stress arrays (Table 5). Therefore, perhaps the changes were significant but not obvious in our transcription factor localization studies. Matsumura *et al.* (2009) showed differences in the levels of YY1 transcripts, using a more sensitive and quantitative approach [4]. Perhaps the changes in YY1 activation are not large enough to notice visually on a western blot.

To avoid any conflict, both YY1 and histone H3 were used as nuclear loading controls. It is possible the antibody for histone H3 could not bind the phosphorylated H3 in dividing cells which could explain the very faint or absent bands. Only the YY1 results will be discussed.

4.2.2 DXL and DOX treatments results in significant RNA disruption

DXL is a taxane that functions as an anticancer agent by stabilising microtubules, which does not allow for their depolymerization, leading to the inhibition of microtubule dynamics and cell cycle arrest [14]. Taxanes generate low levels of oxidative stress, release of cytochrome c from the mitochondria, diversion of electrons from the electron transport system, and induce apoptosis [162]. It has been shown that DXL can increase autophagic marker LC3-II, as well [163]. DXL was originally used in the transcription factor activation profiling arrays due to its potent induction of RNA disruption in mycoplasma infected A2780 cells. However, as stated above, while DXL still induced RNA disruption in mycoplasma-free cells, the effect was not as strong as previously observed [111].

Anthracyclines generate the highest level of oxidative stress when compared to alkylating agents, platinating agents, and camptothecins [162]. One side effect of doxorubicin is

cardiomyopathy and heart failure, which is due to the diversion of electrons in the cardiac mitochondria, which forms superoxide radicals and ROS at other sites [162]. The cardiac mitochondria have NADH dehydrogenase on the outer membrane, whereas mitochondria in other cells has the NADH dehydrogenase in the inner membrane, which DOX cannot reach because of its hydrophilic nature [162]. Cardiac mitochondrial NADH dehydrogenase reduces DOX, which is essential for the disruption of the electron transport system [162]. Reduced DOX can inhibit membrane ATP-ases, and bind ionic iron, which is a highly toxic complex to membrane lipids, proteins and DNA [164]. DOX has been demonstrated to cause the highest amount of RNA disruption in mycoplasma-free A2780 cells thus far.

A2780 cells were treated with 0.2μM DXL and 0.5μM DOX with an untreated control for 72 hours before RNA isolation. There was a significant increase in RDI for the DXL treated sample, and an even greater increase in the DOX treated sample (Figure 8). This was the expected result due to the known differences in potency as RNA disruption agents. This population of cells was plated for the cytoplasmic and nuclear extractions at the same time, which indicates that the cells used in the cytoplasmic and nuclear extractions were capable of RNA disruption at these concentrations 72 hours later. Therefore, the cells used for the cytoplasmic and nuclear extracts were indicative of the cellular processes occurring before RNA disruption. Since these cells produced significant RNA disruption, the nuclear extracts were tested for clear separation and enrichment of the cytoplasmic and nuclear proteins before proceeding to transcription factor analysis.

4.2.2.1 Localization of Nrf2 exclusively in the nucleus

Reactive oxygen species (ROS) are the natural by-products of different physiological functions and have important roles in intracellular signalling pathways [56]. However, the

overproduction of ROS in the cell creates oxidative stress [56, 57]. Oxidative stress can have deleterious effects promoting inflammatory, metabolic, cardiovascular, and neurodegenerative diseases and cancer [56, 58]. These effects are a result of interactions and damage to DNA, RNA, and proteins by the ROS [57]. As such, oxidative stress is also a well-established risk factor for developing cancer [60]. Spontaneous mutations can be a result of oxidative stress, which can lead to cancer, a disease in a constant state of oxidative stress [57]. The cell has defence mechanisms in place in order to protect against oxidative stress, such as antioxidants, DNA-repair enzymes, and the ER stress response UPR [60].

Nrf2 is the major regulator of antioxidant response within the cell [57]. The antioxidant enzymes that are upregulated by Nrf2 help the cell combat ROS and electrophiles that would otherwise cause genomic instability and an inflammatory response which are conducive to oncogenesis [57]. Nrf2 also modulates the response of other detoxifying and defensive genes, such as anti-inflammatory genes and components of the proteasome to degrade damaged proteins [57].

Even prior to the effects of DXL and DOX (0 hour timepoint), Nrf2 was observed to be exclusively localized in the nucleus, with little to no detection of Nrf2 in cytoplasmic extracts (Figure 9A). While the hypothesis was that all the transcription factors would translocate from the cytoplasm into the nucleus upon treatment, this was not seen with Nrf2. Finding a transcription factor involved in cellular defense mechanisms that is constitutively active in cancer cells is not surprising. Cancer cells are under stress by their very nature and are always adapting to take advantage of the cell's natural defenses for its own survival. They also generate higher levels of ROS than normal cells [165]. Therefore, our observation that Nrf2 is already

localized in the nucleus of A2780 tumour cells makes sense, as it would enable tumour cells to adapt to the ROS production and their damaging effects on cells.

The cytoplasmic densitometry values were done regardless of Nrf2 visually being exclusively localized in the nucleus, in order to obtain a background value. However, there were some bands of slightly higher molecular weight in the cytoplasmic extracts identified by the antibody. They were not used for densitometry because it is unknown if this band was actually Nrf2. The higher molecular weight band could have been due to Nrf2 bound to Keap1 in the cytoplasm; however, it would be expected to be of much higher molecular weight if that were the case. There was some variability in the densitometry of Nrf2 normalized to GAPDH, but there was also quite a bit of background which the densitometry software could have been picking up.

Overexpression of Nrf2 has been shown to lead to resistance of cancer cells to chemotherapy agents, including DOX [156]. This could account for the increase of Nrf2 localized in the nucleus of the A2780 cells treated with DOX across timepoints. While there were some densitometry values that do not make sense when compared visually to the western blot because of inconsistent YY1 bands, they were still present.

4.2.2.2 Localization of TFEB in the cytoplasm of untreated cells

Unlike with Nrf2, there was about the same amount of TFEB localized in the cytoplasm of the treated samples as the untreated at 0 hours (Figure 10B). In the untreated samples, the amount of TFEB localized in the cytoplasm increased at each timepoint. There was no effect on TFEB localization in the cytoplasm with DXL treatment at the different time points, while DOX treatment resulted in a decrease of TFEB localized in the cytoplasm at 16 hours (Figure 10B).

There was an increase in the localization of TFEB in the nucleus of the untreated sample across all timepoints. The amount of TFEB in the nucleus of the DXL treated sample peaked at 16 hours, whereas the amount of TFEB in the nucleus of the DOX treated sample peaked at 24 hours.

At 24 hours, TFEB was localized in the untreated samples compared to almost nothing in the treated extracts, visually (Figure 10A).

When using the values normalized to YY1, there was more TFEB localized in the cytoplasm across all timepoints than in the nucleus of untreated cells; more TFEB was found localized in the nucleus of the DXL treated samples compared to untreated samples across all timepoints; and more TFEB localized in the cytoplasm of the DOX treated samples (Figure 10E). This could indicate a response to the DXL treatment, and an accumulation of TFEB in response to DOX treatment that was not of sufficient length or concentration to cause translocation. However, there was only one biological replicate performed, so this could be individual variation.

4.2.3 Tpg and Starvation treatment causes significant RNA disruption

Tpg is a known ER stressor capable of inhibiting the SERCA pump, which is responsible for pumping Ca^{2+} ions from the cytosol into the intracellular membrane of the ER. This inhibition results in an increase of calcium ions into the cytosol from the ER, which results in ER stress or ultimately apoptosis. Tpg has been shown to cause RNA disruption, and in a more potent manner than tunicamycin. Therefore, it was chosen for this study to show the possible induction of stress-induced transcription factors in response to ER stress.

Starvation is known to induce autophagy through the depletion of nutrients in the cell. Autophagy is a catabolic cell survival pathway which degrades non-essential cellular components into amino acids and fatty acids to be used for maintaining ATP levels or synthesis of components required for cell survival. Starvation through the dilution of cell media has been shown to cause RNA disruption (unpublished data).

A2780 cells were treated with 0.5μM Tpg or starved along with a DMSO, untreated, and 1X PBS only controls for 72 hours before an RNA extraction. The cells were plated for the preparation of nuclear and cytoplasmic extracts and treated for 0, 2, and 16 hours prior to the RNA disruption assay. Treatment of the cells with these concentrations caused RNA disruption (Figure 11A-C). The RDI values of the Tpg treated cells were significantly different from the untreated and DMSO controls. There was an even greater increase in the RDI values of the starvation treatment, which was significantly different from the no treatment and PBS control (Figure 11D). The PBS control only produced one RDI value, while all the other replicates produced "N/A" RDI values. This is due to the RDI algorithm which determines a ratio of the amount of normal 28S and 18S bands to the aberrant degraded RNA between the bands; therefore, if the rRNAs become so highly degraded, no normal 28S or 18S bands can be detected and no RDI value can be calculated, as was the case with the PBS control.

4.2.3.1 Nrf2 is exclusively present in the nucleus despite treatment

As with the DXL and DOX treatments, Nrf2 was present in the nucleus exclusively in all treatments throughout the timepoints beginning at 0 hours in the untreated nuclear sample (Figure 12A). There appears to be an increase of Nrf2 in the cytoplasm of the untreated and starvation samples across all timepoints based on the densitometry values, with the largest

increase in the untreated (4X) and starvation (6X) at 16 hours compared to baseline (Figure 12B).

As for the nuclear content, at 0 hours the stressors are mostly similar to the untreated nuclear control baseline, except for a 6-fold increase in the amount of Nrf2 in the nucleus of the Tpg treated extracts (Figure 12C). However, there is almost no YY1 loading control band to which the Tpg sample is normalized, which would account for this large fold-change.

Overall, not many conclusions can be made from the data of Nrf2 treated with Tpg and starvation, except that Nrf2 is exclusively present in the nucleus of A2780 cells. This was not expected but is corroborated by the studies of another student in the lab (Investigating the Relationship Between the Activation of Transcription Factor Nrf2 and Ribosomal RNA Degradation Upon Exposure to Various Cellular Stressors, Carly Zulich, 2020), who studied Nrf2 using hydrogen peroxide, DXL and DOX in A2780 cells (see Appendix Figure 15). Her experiments found that Nrf2 was exclusively present in the nucleus beginning at 0 hours in the untreated nuclear sample as well. A study by van der Wijst et al. (2015) found that A2780 cancer cells compared to healthy ovarian cancer cells exhibited higher levels of ROS production; therefore to maintain redox balance, cancer cells are more dependent on ROS protective and neutralizing signaling including Nrf2 signaling [60]. This could perhaps account for the constant presence of Nrf2 in the cells. Constitutive activation of Nrf2 has been associated with tumorigenesis and chemoresistance in multiple cancers [156].

4.2.3.2 TFE3 is present most prominently in controls

There was a strong localization of TFE3 in the cytoplasm of the untreated and DMSO controls at 0 hours, which is interesting that it is not localized in the cytoplasm of all samples, only the controls (Figure 12A). This is a similar phenomenon to the localization of TFEB only in

the cytoplasm of the untreated samples, however in that case it did not appear in the cytoplasm of the controls until 24 hours (Figure 10A).

Treatment with Tpg resulted in a slight decrease in the localization of TFEB in the cytoplasm between 0 and 16 hours. Starvation induced more than a 2-fold increase in the localization of TFE3 in the cytoplasm at 16 hours. The DMSO vehicle control had almost 2-fold increase in the amount of TFE3 at 16 hours compared to baseline (Figure 12G).

Unfortunately, at 2 hours, there is no signal on the blot. This could have been a transferring issue, but it is unknown because this is only one replicate. There appears to be some faint bands in the DMSO region of the blot, but these will not be discussed (Figure 12A).

Overall, with the exception of Tpg at 0 hours, there appears to be an increasing trend in the localization of TFE3 in the nucleus over time in the no treatment and DMSO controls (Figure 12G). However, when normalized to H3, Tpg treated samples also showed an increasing trend, though to a lesser extent than no treatment and DMSO (Figure 12H).

This did not match the hypothesis, as it was not expected that TFE3 would be localized prominently in the no treatment and DMSO controls and less so in the treated samples. One hypothesis for the increase is the natural starvation over time from growing cells, as nutrients are depleted and become less available in the media. Perhaps the starvation treatment was too severe to see the phenomenon, but the slower depletion of nutrients in the untreated cells was enough to cause TFE3 induction. The lack of data for the 2 hour timepoint is disappointing as this was one of the timepoints specifically chosen for starvation for TFEB and TFE3.

4.3 Implications of this study

Tumor cells are particularly susceptible to nutrient limitations, such as glucose and oxygen. Due to the fact that tumor cells have a high demand for glucose, while also having the ability to proliferate under nutrient-limiting conditions suggests that they have adapted [59]. Some of these adaptions could include constant upregulation of cellular stress pathways, enabling tumour cells to cope with these metabolic stressors.

Expression of Nrf2 in cancer cells can provide the same protections it provides to normal cells. The role of Nrf2 in carcinogenesis has a dual role as it has been observed as protective, as well as tumour promoting [60]. In human tumours and cancer cell lines, the constitutive activation of Nrf2 increases the expression of genes involved in drug metabolism which can contribute to and sustain resistance to anti-cancer agents [55]. As a regulator of xenobiotic response, Nrf2 regulates the multidrug resistance family genes, including MRP1, MRP2, MRP3, and MRP4 [28, 56]. Increased Nrf2 activity can also increase cell proliferation through redirection towards anabolic pathways [55]. Antiapoptotic proteins Bcl-2 and Bcl-xL have been identified as ARE-controlled target genes of Nrf2, which implicates Nrf2 as a direct contributor to apoptosis [55]. Upregulation of Bcl-2 and Bcl-xL by Nrf2 can confer an anti-apoptotic protection to tumour cells [55]. Nrf2 has been shown to regulate the antiapoptotic protein Bcl-2, which helps the cell evade death [57]. Increased expression of Nrf2 also helps to maintain ROS levels below a toxic threshold to avoid death in the cancer cells [57].

Nrf2 increases the survival of cells challenged with tunicamycin, and the same study showed that Nrf2 deficiency increased apoptosis after tunicamycin treatment [59]. Nrf2 promotes expression of enzymes that mediate the production of glutathione, which in addition to scavenging free radicals, also maintains proper intracellular redox balance and the maintenance

of protein integrity [59]. ER stress rapidly induces transcription of GCLC and NQO1 precursors in the glutathione biosynthetic pathway, and induction is dependent on PERK and Nrf2 [59].

The lysosome has been shown to be part of anticancer drug resistance, through sequestration by lysosomes and increased lysosome biogenesis by TFEB [163]. TFEB can be rapidly activated in response to DXL, and subsequent autophagy and lysosomal levels increased in gastric cancer cells, whereas knockdown of TFEB resulted in increased chemosensitivity to DXL, increased apoptosis, and limited lysosomal activation [163]. In contrast to the study by Martina *et al.* (2016) which used mouse embryonic fibroblasts, our study did not find that TFEB and TFE3 accumulated in the nucleus after treatment with stressors [51].

Some additional characteristics of the microenvironment of tumours are generally are poor vascularization, low oxygen supply, nutrient deprivation, and acidic pH [73]. Nutrient depletion is the most potent physiological inducer of autophagy and can cause autophagy within minutes in mammalian cell cultures [166]. As well, most of these characteristics are inducers of ER stress. UPR has been shown to exert cytoprotective role in tumors by assisting in the increased folding of newly synthesized proteins necessary for tumour growth [73].

In ARPE-19 cells treated with tunicamycin, there was a strong accumulation of TFE3 and TFEB in the nucleus after 16 hours, indicating a response to prolonged ER stress [51]. ATF4 is an essential transcription factor in restoring ER homeostasis, which TFEB and TFE3 can upregulate, and therefore increase the expression of its target genes [51]. After prolonged ER stress, ATF4 can promote cell death through expression of pro-apoptotic genes [45, 46]. Therefore, it is possible that TFEB and TFE3 promote cell death through sustained activation of ATF4 during prolonged ER stress [51]. However, in cells depleted of TFE3 and TFEB, upregulation of autophagic and lysosomal genes was impaired in response to prolonged ER

stress and starvation, and the cells became more resistant to apoptosis [51]. This shows a dual role in TFEB and TFE3 depending on the duration and strength of stress, either as an early pro-survival machinery or late pro-apoptotic [45, 46]. Interestingly, PERK-knockout MEFs treated with tunicamycin showed decreased TFE3 activation, but TFE3 activation was not inhibited in response to starvation [51]. This indicates TFE3 has different mechanisms for different stressors.

5.0 Conclusion

The RDA shows promise as a predictive tumour response tool for patient response to chemotherapy [35]. RNA disruption has been reproducible *in vitro* in a number of different cell lines and in response to structurally and mechanistically distinct cellular stressors, including chemotherapy drugs [111]. This would indicate a common upstream mechanism of RNA disruption. The goal of this study was to identify stress-induced transcription factors activated in response to chemotherapy and cellular stressors known to cause RNA disruption.

This study was unable to identify any transcription factor that is activated in response to known cellular stressors in A2780 ovarian tumour cells, nor was it able to establish a correlation between activation of stress-induced transcription factors and RNA disruption. A wide range of transcription factors were investigated in A2780 cells treated with DXL for 8 hours. The results were extremely variable for a number of reasons including a mycoplasma-infection in the A2780 cell line at the time and inconsistencies in the performance of the Signosis transcription factor activity profiling arrays. However, a set of criteria were created to objectively select a subset of transcription factors for further study, which narrowed down 104 transcription factors to just 4: YY1, Nrf2, TFEB, and TFE3. Unfortunately, we could not provide evidence that activation of these transcription factors by specific cellular stressors precedes or accompanies the onset of RNA disruption by the stressors.

A nuclear extraction protocol was modified and optimized to create robust nuclear and cytoplasmic extracts that could be used to monitor the activation/translocation of stress-induced transcription factors in A2780 cells. GAPDH expression was used to normalize expression of the above transcription in cytoplasmic extracts, while histone H3 and YY1 were used to normalize expression of the above transcription factors in nuclear extracts. These extracts were used to

monitor the localization of the transcription factors after treatment with agents known to induce RNA disruption, including DXL, DOX, Tpg, and starvation alongside untreated and vehicle controls. These experiments and experiments from other students have excluded Nrf2 as a possible transcription factor of interest. These studies have shown Nrf2 localized primarily in the nucleus with and without treatment beginning at 0 hours. Nrf2 is a major regulator of the antioxidant response within the cell, which could explain its constitutive localization in the nucleus of a cancer cell. TFEB was found primarily in the cytoplasm and nucleus of the untreated control beginning at 16 hours. Similarly, TFE3 was found primarily in the cytoplasm of the untreated and DMSO controls beginning at 0 hours and continuing to 16 hours in both the cytoplasm and nucleus of the untreated and DMSO controls. Treatment appears to dramatically reduce TFEB and TFE3 expression in both cytoplasm and nucleus. TFEB and TFE3 have known roles in autophagy and starvation response, which could explain their presence in the nucleus at later timepoints, since there would be a depletion of nutrients in the media over time as cells grow.

Identifying cellular signalling pathways and transcription factors that are activated by agents known to cause RNA disruption prior to RNA disruption could provide some insight into the mechanism involved. Transcription factors provide an interesting target due to their involvement in several cellular stress signalling pathways and the activation of cellular defense mechanisms. By identifying a mechanism for RNA disruption, different and earlier biomarkers could be used to assess chemotherapy response in patients. An earlier assessment of response could improve patient outcome and would improve patient quality of life. Unfortunately, we were unable to identify any transcription factors whose activity as induced by stress and could be responsible for the promotion of RNA disruption.

6.0 Appendix

Table 6. Transcription factors analyzed and which array(s) they were on

Transcription Factor	Profiling Plate Array
AP-1	ER, Mitochondria, TFII
AP-2	TFII
AP-3	TFII
AP-4	TFII
AR	TFII
ATF2	TFII
ATF3	ER
ATF4	ER, Mitochondria
ATF6	ER
Brn-3	TFII
CAR	TFII
CBF/NFY	ER, TFII
CDP	TFII
C/EBP	Mitochondria, TFII
CHOP	ER, Mitochondria
COUP-TF	TFII
CREB	TFII
E2F1	Mitochondria, TFII
EGR	TFII
ELK	TFII
ER	TFII
Ets	TFII
FAST-1	TFII
FOXA1	TFII
FoxC1	TFII
FOXD3	TFII

FOXG1	TFII
FOXO1	ER, TFII
FOXO3	Mitochondria
FREAC2	TFII
GAS/ISR	TFII
GATA	TFII
Gfi-1	TFII
Gli-1	TFII
GR/PR	TFII
HEN	TFII
HIF	Mitochondria, TFII
HNF-1	TFII
HNF4	ER, TFII
HOX4C	TFII
HoxA-5	TFII
HSF	Mitochondria, TFII
IRF	ER, TFII
KLF4	TFII
MEF1	TFII
MEF2	Mitochondria, TFII
Myb	TFII
Myc-Ma	TFII
MyoD	TFII
MZF	TFII
NF-1	TFII
NF-E2	TFII
NFAT	TFII
NFκB	ER, Mitochondria, TFII
Nkx2-5	TFII

Nkx3-5	TFII
NRF1	Mitochondria, TFII
NRF2/ARE	ER, Mitochondria, TFII
Oct-1	TFII
OCT4	TFII
p53	ER, Mitochondria, TFII
Pax-5	TFII
Pax2	TFII
Pax3	TFII
Pax8	TFII
Pbx-1	TFII
PGC-1α	ER
Pit	TFII
PLAG1	TFII
PIT1	TFII
PPAR	TFII
Prox1	TFII
PXR	TFII
Rb	TFII
RUNX	TFII
ROR	TFII
RXR	TFII
SATB	Mitochondria, TFII
SF-1	TFII
SMAD	TFII
SMUC	TFII
Snail	TFII
SOX2	TFII
SOX9	TFII

SOX18	TFII
Sp1	TFII
SREBP1	ER
SRF	TFII
SRY	TFII
STAT1	TFII
STAT3	TFII
STAT4	TFII
STAT5	TFII
STAT6	TFII
TCF/LEF	TFII
TFIID	TFII
TFE3	TFII
TFEB	Mitochondria
TR	TFII
USF-1	TFII
VDR	TFII
WT1	TFII
XBP1	ER, Mitochondria, TFII
YY1	ER, TFII

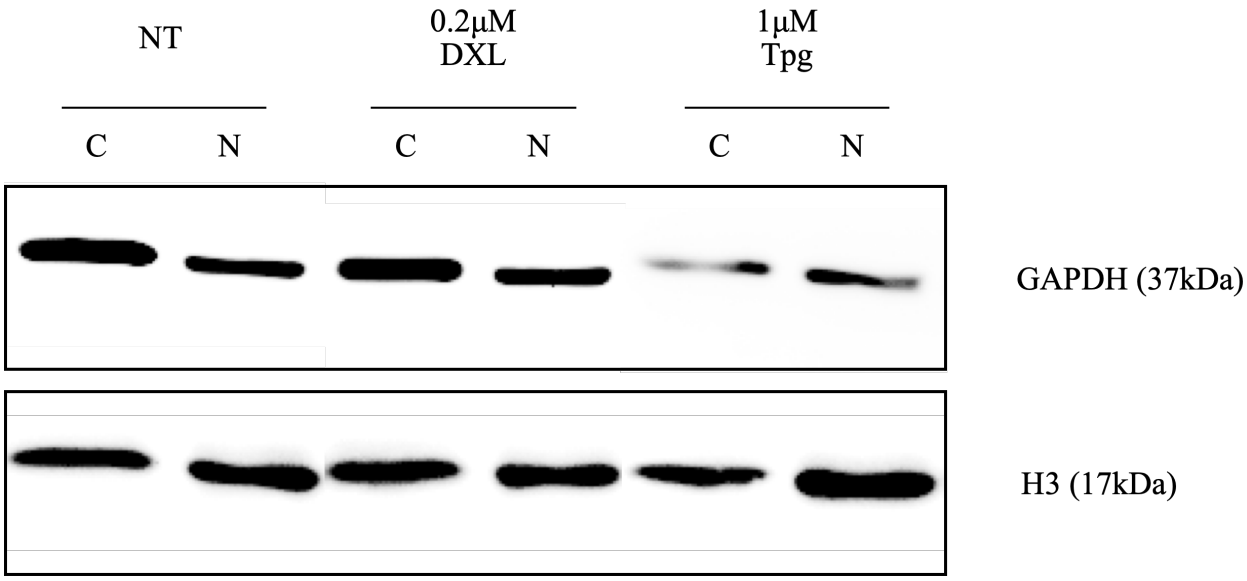

Figure 13. Avery Newman-Simmons' data (not in undergraduate thesis). Cells were treated with 0.2μM DXL and 1μM Tpg for 8 hours with an untreated control. Cytoplasmic (C) and nuclear (N) extracts were made using the Signosis Nuclear Extraction Kit, which shows a lack of enrichment.

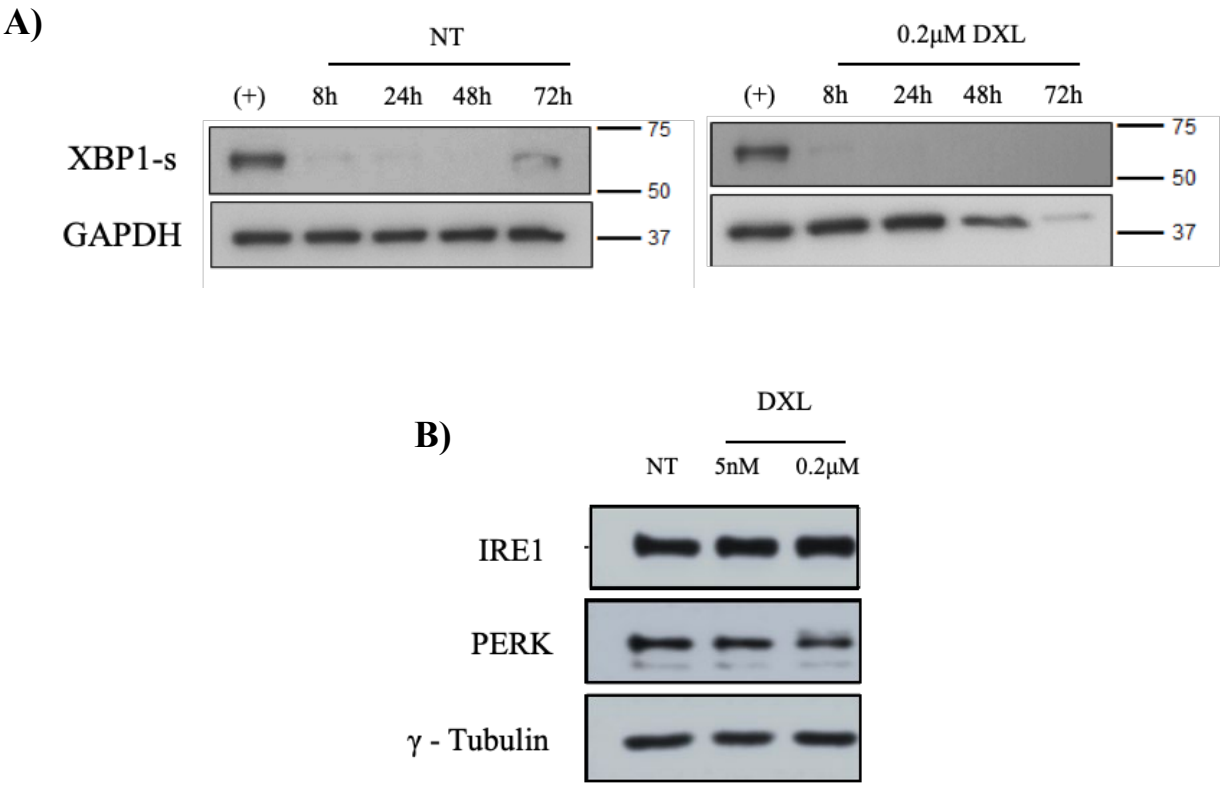

Figure 14. Justin Boudreau's data. (Unpublished data) A) XBP1is not induced by 0.2μM DXL in mycoplasma contaminated A2780 cells after 8 hours, but that B) IRE1 and PERK were activated indicating that ER stress was induced. (+) are Tpg treated A2780 cells of unknown length of time.

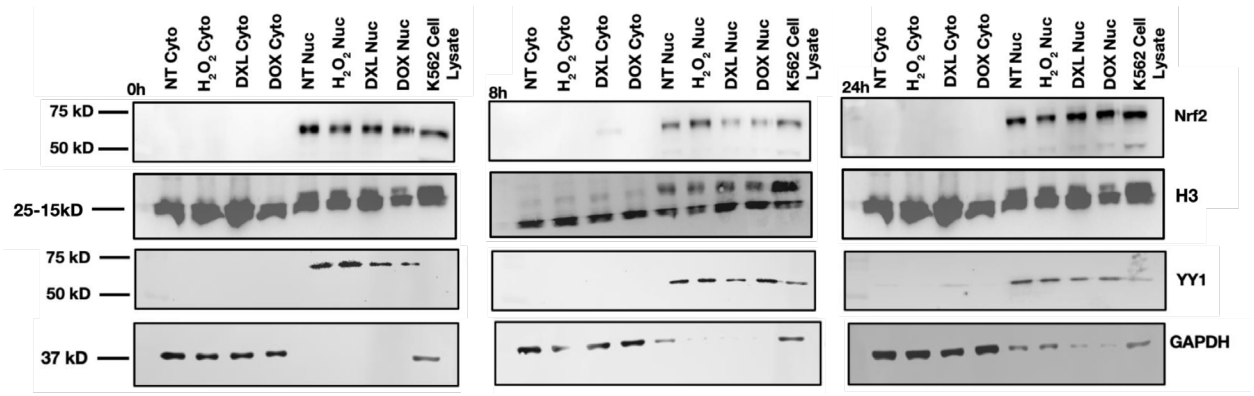

Figure 14. Undergraduate thesis data prepared by Carly Zulich. The transcription factor Nrf2 was found to be present exclusively in the nucleus of the A2780 cells, as well as present in a whole cell lysate of K562 cells as a positive control. Cells were treated with 5µM H_2O_2, 1µM DXL, and 0.5µM DOX along with an untreated control for 0, 8, or 24 hours. This is representative of three independent extracts.

7.0 References

1. Brenner DR, HK Weir, AA Demers, LF Ellison, C Louzado, A Shaw, et al. Projected estimates of cancer in canada in 2020. CMAJ 2020; 192(9): E199-E205.
2. Hanahan D and RA Weinberg. Hallmarks of cancer: The next generation. cell 2011; 144(5): 646-674.
3. Momenimovahed Z, A Tiznobaik, S Taheri, and H Salehiniya. Ovarian cancer in the world: Epidemiology and risk factors. International journal of women's health 2019; 11: 287.
4. Matsumura N, Z Huang, T Baba, PS Lee, JC Barnett, S Mori, et al. Yin yang 1 modulates taxane response in epithelial ovarian cancer. Molecular Cancer Research 2009; 7(2): 210-220.
5. Jayson GC, EC Kohn, HC Kitchener, and JA Ledermann. Ovarian cancer. The Lancet 2014; 384(9951): 1376-1388.
6. Hennessy BT, RL Coleman, and M Markman. Ovarian cancer. The lancet 2009; 374(9698): 1371-1382.
7. Smith LH. Early clinical detection of ovarian cancer: A review of the evidence. Expert review of anticancer therapy 2006; 6(7): 1045-1052.
8. Bast RC, B Hennessy, and GB Mills. The biology of ovarian cancer: New opportunities for translation. Nature Reviews Cancer 2009; 9(6): 415-428.
9. Cho KR and I-M Shih. Ovarian cancer. Annual Review of Pathology: Mechanisms of Disease 2009; 4: 287-313.
10. Visintin I, Z Feng, G Longton, DC Ward, AB Alvero, Y Lai, et al. Diagnostic markers for early detection of ovarian cancer. Clinical cancer research 2008; 14(4): 1065-1072.
11. Yap TA, CP Carden, and SB Kaye. Beyond chemotherapy: Targeted therapies in ovarian cancer. Nature Reviews Cancer 2009; 9(3): 167-181.
12. Lheureux S, M Braunstein, and AM Oza. Epithelial ovarian cancer: Evolution of management in the era of precision medicine. CA: a cancer journal for clinicians 2019; 69(4): 280-304.
13. Lengyel E. Ovarian cancer development and metastasis. The American journal of pathology 2010; 177(3): 1053-1064.
14. Katsumata N. Docetaxel: An alternative taxane in ovarian cancer. British journal of cancer 2003; 89(3): S9.
15. Panday VRN, MT Huizing, WWTB Huinink, JB Vermorken, and JH Beijnen. Hypersensitivity reactions to the taxanes paclitaxel and docetaxel. Clinical drug investigation 1997; 14(5): 418-427.
16. Gligorov J and JP Lotz. Preclinical pharmacology of the taxanes: Implications of the differences. The oncologist 2004; 9: 3-8.
17. Murray S, E Briasoulis, H Linardou, D Bafaloukos, and C Papadimitriou. Taxane resistance in breast cancer: Mechanisms, predictive biomarkers and circumvention strategies. Cancer treatment reviews 2012; 38(7): 890-903.
18. ZHU J, EC BEATTIE, Y Yang, H-J WANG, J-Y SEO, and L-X YANG. Centrosome impairments and consequent cytokinesis defects are possible mechanisms of taxane drugs. Anticancer research 2005; 25(3B): 1919-1925.
19. Crown J and M O'Leary. The taxanes: An update. The Lancet 2000; 355(9210): 1176-1178.

20. Karki R, M Mariani, M Andreoli, S He, G Scambia, S Shahabi, et al. Biii-tubulin: Biomarker of taxane resistance or drug target? Expert opinion on therapeutic targets 2013; 17(4): 461-472.
21. Hagiwara H and Y Sunada. Mechanism of taxane neurotoxicity. Breast cancer 2004; 11(1): 82-85.
22. Fitzpatrick JM and R de Wit. Taxane mechanisms of action: Potential implications for treatment sequencing in metastatic castration-resistant prostate cancer. European urology 2014; 65(6): 1198-1204.
23. Markman M. Managing taxane toxicities. Supportive care in cancer 2003; 11(3): 144-147.
24. Engblom P, V Rantanen, J Kulmala, J Heiskanen, and S Grenman. Taxane sensitivity of ovarian carcinoma in vitro. Anticancer research 1997; 17(4A): 2475-2479.
25. Kelland LR and G Abel. Comparative in vitro cytotoxicity of taxol and taxotere against cisplatin-sensitive and-resistant human ovarian carcinoma cell lines. Cancer chemotherapy and pharmacology 1992; 30(6): 444-450.
26. Zelnak A. Overcoming taxane and anthracycline resistance. The breast journal 2010; 16(3): 309-312.
27. Nielsen D, C Maare, and T Skovsgaard. Cellular resistance to anthracyclines. General Pharmacology: The Vascular System 1996; 27(2): 251-255.
28. Motohashi H and M Yamamoto. Nrf2–keap1 defines a physiologically important stress response mechanism. Trends in molecular medicine 2004; 10(11): 549-557.
29. Sartiano GP, WE Lynch, and WD Bullington. Mechanism of action of the anthracycline anti-tumor antibiotics, doxorubicin, daunomycin and rubidazone: Preferential inhibition of DNA polymerase α. The Journal of antibiotics 1979; 32(10): 1038-1045.
30. Binaschi M, M Bigioni, A Cipollone, C Rossi, C Goso, C Maggi, et al. Anthracyclines: Selected new developments. Current Medicinal Chemistry-Anti-Cancer Agents 2001; 1(2): 113-130.
31. Arai M, A Yoguchi, T Takizawa, T Yokoyama, T Kanda, M Kurabayashi, et al. Mechanism of doxorubicin-induced inhibition of sarcoplasmic reticulum ca2+-atpase gene transcription. Circulation Research 2000; 86(1): 8-14.
32. Peng X, B Chen, CC Lim, and DB Sawyer. The cardiotoxicology of anthracycline chemotherapeutics: Translating molecular mechanism into preventative medicine. Molecular interventions 2005; 5(3): 163.
33. Müller I, A Jenner, G Bruchelt, D Niethammer, and B Halliwell. Effect of concentration on the cytotoxic mechanism of doxorubicin—apoptosis and oxidative DNA damage. Biochemical and biophysical research communications 1997; 230(2): 254-257.
34. Parissenti AM, J-AW Chapman, HJ Kahn, B Guo, L Han, P O'Brien, et al. Association of low tumor rna integrity with response to chemotherapy in breast cancer patients. Breast cancer research and treatment 2010; 119(2): 347.
35. Parissenti AM, B Guo, LB Pritzker, KP Pritzker, X Wang, M Zhu, et al. Tumor rna disruption predicts survival benefit from breast cancer chemotherapy. Breast cancer research and treatment 2015; 153(1): 135-144.
36. Schroeder A, O Mueller, S Stocker, R Salowsky, M Leiber, M Gassmann, et al. The rin: An rna integrity number for assigning integrity values to rna measurements. BMC molecular biology 2006; 7(1): 1-14.

37. Pritzker K, L Pritzker, D Generali, A Bottini, MR Cappelletti, B Guo, et al. Rna disruption and drug response in breast cancer primary systemic therapy. Journal of the National Cancer Institute Monographs 2015; 2015(51): 76-80.
38. Toomey S, AJ Eustace, LB Pritzker, KP Pritzker, J Fay, A O'Grady, et al. Re: Rna disruption assay as a biomarker of pathological complete response in neoadjuvant trastuzumab-treated human epidermal growth factor receptor 2–positive breast cancer. JNCI: Journal of the National Cancer Institute 2016; 108(8).
39. Latchman DS. Transcription factors: An overview. International journal of experimental pathology 1993; 74(5): 417.
40. Gordon S, G Akopyan, H Garban, and B Bonavida. Transcription factor yy1: Structure, function, and therapeutic implications in cancer biology. Oncogene 2006; 25(8): 1125-1142.
41. Latchman DS. Eukaryotic transcription factors. Biochemical journal 1990; 270(2): 281-289.
42. Lambert SA, A Jolma, LF Campitelli, PK Das, Y Yin, M Albu, et al. The human transcription factors. Cell 2018; 172(4): 650-665.
43. Darnell JE. Transcription factors as targets for cancer therapy. Nature Reviews Cancer 2002; 2(10): 740-749.
44. Zhao E and MJ Czaja. Tfeb: A central regulator of both the autophagosome and lysosome. Hepatology (Baltimore, Md) 2012; 55(5): 1632.
45. Raben N and R Puertollano. Tfeb and tfe3: Linking lysosomes to cellular adaptation to stress. Annual review of cell and developmental biology 2016; 32: 255-278.
46. Martina JA and R Puertollano. Tfeb and tfe3: The art of multi-tasking under stress conditions. Transcription 2017; 8(1): 48-54.
47. Napolitano G and A Ballabio. Tfeb at a glance. Journal of cell science 2016; 129(13): 2475-2481.
48. Martina JA, Y Chen, M Gucek, and R Puertollano. Mtorc1 functions as a transcriptional regulator of autophagy by preventing nuclear transport of tfeb. Autophagy 2012; 8(6): 903-914.
49. Settembre C and A Ballabio. Tfeb regulates autophagy: An integrated coordination of cellular degradation and recycling processes. Autophagy 2011; 7(11): 1379-1381.
50. Sardiello M, M Palmieri, A di Ronza, DL Medina, M Valenza, VA Gennarino, et al. A gene network regulating lysosomal biogenesis and function. Science 2009; 325(5939): 473-477.
51. Martina JA, HI Diab, OA Brady, and R Puertollano. Tfeb and tfe3 are novel components of the integrated stress response. The EMBO journal 2016; 35(5): 479-495.
52. Settembre C, C Di Malta, VA Polito, MG Arencibia, F Vetrini, S Erdin, et al. Tfeb links autophagy to lysosomal biogenesis. science 2011; 332(6036): 1429-1433.
53. Peña-Llopis S, S Vega-Rubin-de-Celis, JC Schwartz, NC Wolff, TAT Tran, L Zou, et al. Regulation of tfeb and v-atpases by mtorc1. The EMBO journal 2011; 30(16): 3242-3258.
54. Martina JA, HI Diab, L Lishu, L Jeong-A, S Patange, N Raben, et al. The nutrient-responsive transcription factor tfe3 promotes autophagy, lysosomal biogenesis, and clearance of cellular debris. Sci Signal 2014; 7(309): ra9-ra9.
55. Menegon S, A Columbano, and S Giordano. The dual roles of nrf2 in cancer. Trends in molecular medicine 2016; 22(7): 578-593.

56. Xiang M, A Namani, S Wu, and X Wang. Nrf2: Bane or blessing in cancer? Journal of cancer research and clinical oncology 2014; 140(8): 1251-1259.
57. Shelton P and AK Jaiswal. The transcription factor nf-e2-related factor 2 (nrf2): A protooncogene? The FASEB Journal 2013; 27(2): 414-423.
58. Bryan HK, A Olayanju, CE Goldring, and BK Park. The nrf2 cell defence pathway: Keap1-dependent and-independent mechanisms of regulation. Biochemical pharmacology 2013; 85(6): 705-717.
59. Cullinan SB and JA Diehl. Perk-dependent activation of nrf2 contributes to redox homeostasis and cell survival following endoplasmic reticulum stress. Journal of Biological Chemistry 2004; 279(19): 20108-20117.
60. van der Wijst MG, C Huisman, A Mposhi, G Roelfes, and MG Rots. Targeting nrf2 in healthy and malignant ovarian epithelial cells: Protection versus promotion. Molecular oncology 2015; 9(7): 1259-1273.
61. Castellano G, E Torrisi, G Ligresti, G Malaponte, L Militello, AE Russo, et al. The involvement of the transcription factor yin yang 1 in cancer development and progression. Cell cycle 2009; 8(9): 1367-1372.
62. Kaufhold S, H Garbán, and B Bonavida. Yin yang 1 is associated with cancer stem cell transcription factors (sox2, oct4, bmi1) and clinical implication. Journal of Experimental & Clinical Cancer Research 2016; 35(1): 84.
63. Deng Z, P Cao, MM Wan, and G Sui. Yin yang 1: A multifaceted protein beyond a transcription factor. Transcription 2010; 1(2): 81-84.
64. Fulda S, AM Gorman, O Hori, and A Samali. Cellular stress responses: Cell survival and cell death. International journal of cell biology 2010; 2010.
65. Portt L, G Norman, C Clapp, M Greenwood, and MT Greenwood. Anti-apoptosis and cell survival: A review. Biochimica et Biophysica Acta (BBA)-Molecular Cell Research 2011; 1813(1): 238-259.
66. Mathew R, V Karantza-Wadsworth, and E White. Role of autophagy in cancer. Nature Reviews Cancer 2007; 7(12): 961-967.
67. Kang R, H Zeh, M Lotze, and D Tang. The beclin 1 network regulates autophagy and apoptosis. Cell Death & Differentiation 2011; 18(4): 571-580.
68. Senft D and AR Ze'ev. Upr, autophagy, and mitochondria crosstalk underlies the er stress response. Trends in biochemical sciences 2015; 40(3): 141-148.
69. Levine B. Autophagy and cancer. Nature 2007; 446(7137): 745-747.
70. Mizushima N. Autophagy: Process and function. Genes & development 2007; 21(22): 2861-2873.
71. Yorimitsu T, U Nair, Z Yang, and DJ Klionsky. Endoplasmic reticulum stress triggers autophagy. Journal of Biological Chemistry 2006; 281(40): 30299-30304.
72. Glick D, S Barth, and KF Macleod. Autophagy: Cellular and molecular mechanisms. The Journal of pathology 2010; 221(1): 3-12.
73. Sano R and JC Reed. Er stress-induced cell death mechanisms. Biochimica et Biophysica Acta (BBA)-Molecular Cell Research 2013; 1833(12): 3460-3470.
74. Bernales S, KL McDonald, and P Walter. Autophagy counterbalances endoplasmic reticulum expansion during the unfolded protein response. PLoS biology 2006; 4(12).
75. Wong P-M, C Puente, IG Ganley, and X Jiang. The ulk1 complex: Sensing nutrient signals for autophagy activation. Autophagy 2013; 9(2): 124-137.

76. Song S, J Tan, Y Miao, M Li, and Q Zhang. Crosstalk of autophagy and apoptosis: Involvement of the dual role of autophagy under er stress. Journal of cellular physiology 2017; 232(11): 2977-2984.
77. Tsuru A, Y Imai, M Saito, and K Kohno. Novel mechanism of enhancing ire1α-xbp1 signalling via the perk-atf4 pathway. Scientific reports 2016; 6: 24217.
78. DuRose JB, D Scheuner, RJ Kaufman, LI Rothblum, and M Niwa. Phosphorylation of eukaryotic translation initiation factor 2α coordinates rrna transcription and translation inhibition during endoplasmic reticulum stress. Molecular and cellular biology 2009; 29(15): 4295-4307.
79. Higgins R, JM Gendron, L Rising, R Mak, K Webb, SE Kaiser, et al. The unfolded protein response triggers site-specific regulatory ubiquitylation of 40s ribosomal proteins. Molecular cell 2015; 59(1): 35-49.
80. Tsukumo Y, S Tsukahara, A Furuno, S-i Iemura, T Natsume, and A Tomida. Tbl2 is a novel perk-binding protein that modulates stress-signaling and cell survival during endoplasmic reticulum stress. PloS one 2014; 9(11).
81. Li M, P Baumeister, B Roy, T Phan, D Foti, S Luo, et al. Atf6 as a transcription activator of the endoplasmic reticulum stress element: Thapsigargin stress-induced changes and synergistic interactions with nf-y and yy1. Molecular and cellular biology 2000; 20(14): 5096-5106.
82. Andersen TB, CQ López, T Manczak, K Martinez, and HT Simonsen. Thapsigargin—from thapsia l. To mipsagargin. Molecules 2015; 20(4): 6113-6127.
83. Patkar S, U Rasmussen, and B Diamant. On the mechanism of histamine release induced by thapsigargin fromthapsia garganica l. Agents and actions 1979; 9(1): 53-57.
84. Thastrup O, PJ Cullen, B Drøbak, MR Hanley, and AP Dawson. Thapsigargin, a tumor promoter, discharges intracellular ca2+ stores by specific inhibition of the endoplasmic reticulum ca2 (+)-atpase. Proceedings of the National Academy of Sciences 1990; 87(7): 2466-2470.
85. Lytton J, M Westlin, and M Hanley. Thapsigargin inhibits the sarcoplasmic or endoplasmic reticulum ca-atpase family of calcium pumps. Journal of Biological Chemistry 1991; 266(26): 17067-17071.
86. Thastrup O. Role of ca 2+-atpases in regulation of cellular ca 2+ signalling, as studied with the selective microsomal ca 2+-atpase inhibitor, thapsigargin. Agents and actions 1990; 29(1-2): 8-15.
87. Doan NTQ, ES Paulsen, P Sehgal, JV Møller, P Nissen, SR Denmeade, et al. Targeting thapsigargin towards tumors. Steroids 2015; 97: 2-7.
88. Dubois C, F Vanden Abeele, P Sehgal, C Olesen, S Junker, SB Christensen, et al. Differential effects of thapsigargin analogues on apoptosis of prostate cancer cells: Complex regulation by intracellular calcium. The FEBS journal 2013; 280(21): 5430-5440.
89. Christensen SB, DM Skytte, SR Denmeade, C Dionne, JV Moller, P Nissen, et al. A trojan horse in drug development: Targeting of thapsigargins towards prostate cancer cells. Anti-Cancer Agents in Medicinal Chemistry (Formerly Current Medicinal Chemistry-Anti-Cancer Agents) 2009; 9(3): 276-294.
90. Barbour JA and N Turner. Mitochondrial stress signaling promotes cellular adaptations. International journal of cell biology 2014; 2014.

91. Khan NA, J Nikkanen, S Yatsuga, C Jackson, L Wang, S Pradhan, et al. Mtorc1 regulates mitochondrial integrated stress response and mitochondrial myopathy progression. Cell metabolism 2017; 26(2): 419-428. e5.
92. Zhao Q, J Wang, IV Levichkin, S Stasinopoulos, MT Ryan, and NJ Hoogenraad. A mitochondrial specific stress response in mammalian cells. The EMBO journal 2002; 21(17): 4411-4419.
93. Broadley SA and FU Hartl. Mitochondrial stress signaling: A pathway unfolds. Trends in cell biology 2008; 18(1): 1-4.
94. Guchelaar H, A Vermes, I Vermes, and C Haanen. Apoptosis: Molecular mechanisms and implications for cancer chemotherapy. Pharmacy world & science: PWS 1997; 19(3): 119-125.
95. Cohen GM. Caspases: The executioners of apoptosis. Biochemical Journal 1997; 326(1): 1-16.
96. King K, C Jewell, C Bortner, and J Cidlowski. 28s ribosome degradation in lymphoid cell apoptosis: Evidence for caspase and bcl-2-dependent and-independent pathways. Cell Death & Differentiation 2000; 7(10): 994-1001.
97. Reed JC. Mechanisms of apoptosis. The American journal of pathology 2000; 157(5): 1415-1430.
98. Houge G, B Robaye, T Eikhom, J Golstein, G Mellgren, B Gjertsen, et al. Fine mapping of 28s rrna sites specifically cleaved in cells undergoing apoptosis. Molecular and cellular biology 1995; 15(4): 2051-2062.
99. Kiraz Y, A Adan, MK Yandim, and Y Baran. Major apoptotic mechanisms and genes involved in apoptosis. Tumor Biology 2016; 37(7): 8471-8486.
100. Wen F, R Zhou, A Shen, A Choi, D Uribe, and J Shi. The tumor suppressive role of eif3f and its function in translation inhibition and rrna degradation. PLoS One 2012; 7(3).
101. Allmang C, P Mitchell, E Petfalski, and D Tollervey. Degradation of ribosomal rna precursors by the exosome. Nucleic acids research 2000; 28(8): 1684-1691.
102. Houseley J and D Tollervey. The many pathways of rna degradation. Cell 2009; 136(4): 763-776.
103. Anderson P, N Kedersha, and P Ivanov. Stress granules, p-bodies and cancer. Biochimica et Biophysica Acta (BBA)-Gene Regulatory Mechanisms 2015; 1849(7): 861-870.
104. Anderson P and N Kedersha. Stress granules: The tao of rna triage. Trends in biochemical sciences 2008; 33(3): 141-150.
105. Anderson P and N Kedersha. Rna granules. Journal of Cell Biology 2006; 172(6): 803-808.
106. Van Treeck B, DS Protter, T Matheny, A Khong, CD Link, and R Parker. Rna self-assembly contributes to stress granule formation and defining the stress granule transcriptome. Proceedings of the National Academy of Sciences 2018; 115(11): 2734-2739.
107. LaRiviere FJ, SE Cole, DJ Ferullo, and MJ Moore. A late-acting quality control process for mature eukaryotic rrnas. Molecular cell 2006; 24(4): 619-626.
108. Nishida J, A Shiratsuchi, D Nadano, T-a Sato, and Y Nakanishit. Structural change of ribosomes during apoptosis: Degradation and externalization of ribosomal proteins in doxorubicin-treated jurkat cells. The Journal of Biochemistry 2002; 131(3): 485-493.
109. Nadano D and T-A Sato. Caspase-3-dependent and-independent degradation of 28 s ribosomal rna may be involved in the inhibition of protein synthesis during apoptosis

initiated by death receptor engagement. Journal of Biological Chemistry 2000; 275(18): 13967-13973.
110. Liu Y, W Zou, P Yang, L Wang, Y Ma, H Zhang, et al. Autophagy-dependent ribosomal rna degradation is essential for maintaining nucleotide homeostasis during c. Elegans development. Elife 2018; 7: e36588.
111. Narendrula R, K Mispel-Beyer, B Guo, AM Parissenti, LB Pritzker, K Pritzker, et al. Rna disruption is associated with response to multiple classes of chemotherapy drugs in tumor cell lines. BMC cancer 2016; 16(1): 146.
112. Bradford MM. A rapid and sensitive method for the quantitation of microgram quantities of protein utilizing the principle of protein-dye binding. Analytical biochemistry 1976; 72(1-2): 248-254.
113. Schreiber E, P Matthias, MM Müller, and W Schaffner. Rapid detection of octamer binding proteins with'mini-extracts', prepared from a small number of cells. Nucleic acids research 1989; 17(15): 6419.
114. Latchman DS. Transcription-factor mutations and disease. New England Journal of Medicine 1996; 334(1): 28-33.
115. Vazquez F, J-H Lim, H Chim, K Bhalla, G Girnun, K Pierce, et al. Pgc1α expression defines a subset of human melanoma tumors with increased mitochondrial capacity and resistance to oxidative stress. Cancer cell 2013; 23(3): 287-301.
116. Latchman DS. Transcription factors: An overview. The international journal of biochemistry & cell biology 1997; 29(12): 1305-1312.
117. Nikfarjam L and P Farzaneh. Prevention and detection of mycoplasma contamination in cell culture. Cell Journal (Yakhteh) 2012; 13(4): 203.
118. Drexler HG and CC Uphoff. Mycoplasma contamination of cell cultures: Incidence, sources, effects, detection, elimination, prevention. Cytotechnology 2002; 39(2): 75-90.
119. Xiang J, L Zhou, S Li, X Xi, J Zhang, Y Wang, et al. At-rich sequence binding protein 1: Contribution to tumor progression and metastasis of human ovarian carcinoma. Oncology letters 2012; 3(4): 865-870.
120. Tesone AJ, MR Rutkowski, E Brencicova, N Svoronos, A Perales-Puchalt, TL Stephen, et al. Satb1 overexpression drives tumor-promoting activities in cancer-associated dendritic cells. Cell reports 2016; 14(7): 1774-1786.
121. Hsieh J-K, S Fredersdorf, T Kouzarides, K Martin, and X Lu. E2f1-induced apoptosis requires DNA binding but not transactivation and is inhibited by the retinoblastoma protein through direct interaction. Genes & development 1997; 11(14): 1840-1852.
122. Pagliarini V, P Giglio, P Bernardoni, D De Zio, GM Fimia, M Piacentini, et al. Downregulation of e2f1 during er stress is required to induce apoptosis. Journal of cell science 2015; 128(6): 1166-1179.
123. Hagenbuchner J and MJ Ausserlechner. Mitochondria and foxo3: Breath or die. Frontiers in physiology 2013; 4: 147.
124. Greer EL, PR Oskoui, MR Banko, JM Maniar, MP Gygi, SP Gygi, et al. The energy sensor amp-activated protein kinase directly regulates the mammalian foxo3 transcription factor. Journal of Biological Chemistry 2007; 282(41): 30107-30119.
125. Tseng AH, S-S Shieh, and DL Wang. Sirt3 deacetylates foxo3 to protect mitochondria against oxidative damage. Free Radical Biology and Medicine 2013; 63: 222-234.

126. Liang R and S Ghaffari. Mitochondria and foxo3 in stem cell homeostasis, a window into hematopoietic stem cell fate determination. Journal of bioenergetics and biomembranes 2017; 49(4): 343-346.
127. Huang W-C, X Li, J Liu, J Lin, and LW Chung. Activation of androgen receptor, lipogenesis, and oxidative stress converged by srebp-1 is responsible for regulating growth and progression of prostate cancer cells. Molecular Cancer Research 2012; 10(1): 133-142.
128. Hu Q, Y Mao, M Liu, R Luo, R Jiang, and F Guo. The active nuclear form of srebp1 amplifies er stress and autophagy via regulation of perk. The FEBS journal 2020; 287(11): 2348-2366.
129. Chen J, Z Wu, W Ding, C Xiao, Y Zhang, S Gao, et al. Srebp1 sirna enhance the docetaxel effect based on a bone-cancer dual-targeting biomimetic nanosystem against bone metastatic castration-resistant prostate cancer. Theranostics 2020; 10(4): 1619.
130. Li X, JB Wu, LW Chung, and W-C Huang. Anti-cancer efficacy of srebp inhibitor, alone or in combination with docetaxel, in prostate cancer harboring p53 mutations. Oncotarget 2015; 6(38): 41018.
131. Yoshida H, T Matsui, A Yamamoto, T Okada, and K Mori. Xbp1 mrna is induced by atf6 and spliced by ire1 in response to er stress to produce a highly active transcription factor. Cell 2001; 107(7): 881-891.
132. Sriburi R, S Jackowski, K Mori, and JW Brewer. Xbp1 a link between the unfolded protein response, lipid biosynthesis, and biogenesis of the endoplasmic reticulum. The Journal of cell biology 2004; 167(1): 35-41.
133. Kaneko M, Y Niinuma, and Y Nomura. Activation signal of nuclear factor-κb in response to endoplasmic reticulum stress is transduced via ire1 and tumor necrosis factor receptor-associated factor 2. Biological and Pharmaceutical Bulletin 2003; 26(7): 931-935.
134. Sen CK and L Packer. Antioxidant and redox regulation of gene transcription. The FASEB journal 1996; 10(7): 709-720.
135. Kaneko M, T Takahashi, Y Niinuma, and Y Nomura. Manganese superoxide dismutase is induced by endoplasmic reticulum stress through ire1-mediated nuclear factor (nf)-κb and ap-1 activation. Biological and Pharmaceutical Bulletin 2004; 27(8): 1202-1206.
136. Whitmarsh A and R Davis. Transcription factor ap-1 regulation by mitogen-activated protein kinase signal transduction pathways. Journal of molecular medicine 1996; 74(10): 589-607.
137. Ameyar M, M Wisniewska, and J Weitzman. A role for ap-1 in apoptosis: The case for and against. Biochimie 2003; 85(8): 747-752.
138. Lauricella M, S Emanuele, A D'Anneo, G Calvaruso, B Vassallo, D Carlisi, et al. Jnk and ap-1 mediate apoptosis induced by bortezomib in hepg2 cells via fasl/caspase-8 and mitochondria-dependent pathways. Apoptosis 2006; 11(4): 607-625.
139. Yun CW, Y-S Han, and SH Lee. Pgc-1α controls mitochondrial biogenesis in drug-resistant colorectal cancer cells by regulating endoplasmic reticulum stress. International journal of molecular sciences 2019; 20(7): 1707.
140. Chen X, J Zhong, D Dong, G Liu, and P Yang. Endoplasmic reticulum stress-induced chop inhibits pgc-1α and causes mitochondrial dysfunction in diabetic embryopathy. Toxicological Sciences 2017; 158(2): 275-285.

141. Pavek P. Pregnane x receptor (pxr)-mediated gene repression and cross-talk of pxr with other nuclear receptors via coactivator interactions. Frontiers in pharmacology 2016; 7: 456.
142. Shizu R, T Abe, S Benoki, M Takahashi, S Kodama, M Miayata, et al. Pxr stimulates growth factor-mediated hepatocyte proliferation by cross-talk with the foxo transcription factor. Biochemical Journal 2016; 473(3): 257-266.
143. Ihunnah CA, M Jiang, and W Xie. Nuclear receptor pxr, transcriptional circuits and metabolic relevance. Biochimica et Biophysica Acta (BBA)-Molecular Basis of Disease 2011; 1812(8): 956-963.
144. Masuyama H, Y Hiramatsu, J-i Kodama, and T Kudo. Expression and potential roles of pregnane x receptor in endometrial cancer. The Journal of Clinical Endocrinology & Metabolism 2003; 88(9): 4446-4454.
145. Massagué J, J Seoane, and D Wotton. Smad transcription factors. Genes & development 2005; 19(23): 2783-2810.
146. Wiesenberg I, M Missbach, and C Carlberg. The potential role of the transcription factor rzr/ror as a mediator of nuclear melatonin signaling. Restorative neurology and neuroscience 1998; 12(2, 3): 143-150.
147. Jetten AM. Retinoid-related orphan receptors (rors): Critical roles in development, immunity, circadian rhythm, and cellular metabolism. Nuclear receptor signaling 2009; 7(1): nrs. 07003.
148. Sinha S, SN Maity, J Lu, and B De Crombrugghe. Recombinant rat cbf-c, the third subunit of cbf/nfy, allows formation of a protein-DNA complex with cbf-a and cbf-b and with yeast hap2 and hap3. Proceedings of the National Academy of Sciences 1995; 92(5): 1624-1628.
149. Ly LL, H Yoshida, and M Yamaguchi. Nuclear transcription factor y and its roles in cellular processes related to human disease. American journal of cancer research 2013; 3(4): 339.
150. Matuoka K and KY Chen. Transcriptional regulation of cellular ageing by the ccaat box-binding factor cbf/nf-y. Ageing research reviews 2002; 1(4): 639-651.
151. Chen Y, Z Zhang, K Yang, J Du, Y Xu, and S Liu. Myeloid zinc-finger 1 (mzf-1) suppresses prostate tumor growth through enforcing ferroportin-conducted iron egress. Oncogene 2015; 34(29): 3839-3847.
152. Lacorazza HD, T Yamada, Y Liu, Y Miyata, M Sivina, J Nunes, et al. The transcription factor mef/elf4 regulates the quiescence of primitive hematopoietic cells. Cancer cell 2006; 9(3): 175-187.
153. Shi Y, J-S Lee, and KM Galvin. Everything you have ever wanted to know about yin yang 1. Biochimica et biophysica acta 1997; 1332(2): F49-66.
154. Seligson D, S Horvath, S Huerta-Yepez, S Hanna, H Garban, A Roberts, et al. Expression of transcription factor yin yang 1 in prostate cancer. International journal of oncology 2005; 27(1): 131-141.
155. Allouche A, G Nolens, A Tancredi, L Delacroix, J Mardaga, V Fridman, et al. The combined immunodetection of ap-2α and yy1 transcription factors is associated with erbb2 gene overexpression in primary breast tumors. Breast Cancer Research 2008; 10(1): R9.

156. Bao L-J, MC Jaramillo, Z-B Zhang, Y-X Zheng, M Yao, DD Zhang, et al. Nrf2 induces cisplatin resistance through activation of autophagy in ovarian carcinoma. International journal of clinical and experimental pathology 2014; 7(4): 1502.
157. Medina DL, S Di Paola, I Peluso, A Armani, D De Stefani, R Venditti, et al. Lysosomal calcium signalling regulates autophagy through calcineurin and tfeb. Nature cell biology 2015; 17(3): 288-299.
158. Van Hooser A, DW Goodrich, CD Allis, B Brinkley, and MA Mancini. Histone h3 phosphorylation is required for the initiation, but not maintenance, of mammalian chromosome condensation. Journal of cell science 1998; 111(23): 3497-3506.
159. Th'ng J, X-W Guo, RA Swank, HA Crissman, and E Bradbury. Inhibition of histone phosphorylation by staurosporine leads to chromosome decondensation. Journal of Biological Chemistry 1994; 269(13): 9568-9573.
160. Abe K, M Yoshida, T Usui, S Horinouchi, and T Beppu. Highly synchronous culture of fibroblasts from g2 block caused by staurosporine, a potent inhibitor of protein kinases. Experimental cell research 1991; 192(1): 122-127.
161. Crissman HA, DM Gadbois, RA Tobey, and EM Bradbury. Transformed mammalian cells are deficient in kinase-mediated control of progression through the g1 phase of the cell cycle. Proceedings of the National Academy of Sciences 1991; 88(17): 7580-7584.
162. Conklin KA. Chemotherapy-associated oxidative stress: Impact on chemotherapeutic effectiveness. Integrative cancer therapies 2004; 3(4): 294-300.
163. Zhang J, J Wang, YK Wong, X Sun, Y Chen, L Wang, et al. Docetaxel enhances lysosomal function through tfeb activation. Cell death & disease 2018; 9(6): 1-10.
164. Pieniążek A, J Czepas, J Piasecka-Zelga, K Gwoździński, and A Koceva-Chyła. Oxidative stress induced in rat liver by anticancer drugs doxorubicin, paclitaxel and docetaxel. Advances in medical sciences 2013; 58(1): 104-111.
165. Liou G-Y and P Storz. Reactive oxygen species in cancer. Free radical research 2010; 44(5): 479-496.
166. Kroemer G, G Mariño, and B Levine. Autophagy and the integrated stress response. Molecular cell 2010; 40(2): 280-293.